Team Results Document

SenseNC



SenseNC

University:

North Carolina State University

Team members:

Lauren Mabe
Lily Ro
Ameerah Abazid
Clint Powers
Akshay Balasubramanian
Ebenezer Amare
Nicolas Anzola
Sahiti Mudireddy
Rudhra Unnikrishnan

Supervisor:

Dr. Michael Daniele

Coaches:

Irfan Ismail

August 7th, 2026

SensUs

SensUs 2026
Parkinson's disease

1. Abstract

Parkinson's disease affects over 10 million people worldwide, and levodopa remains the most effective pharmacological treatment for its motor symptoms. However, fluctuating drug response and reliance on subjective, infrequent clinical assessment results in suboptimal dosing and increased side effects, as clinicians lack real-time insight into the relationships between drug concentration, symptom state, and dose timing.

SenseNC presents a wearable, minimally invasive biosensor for continuous levodopa monitoring in interstitial fluid (ISF), built on a multiplexed organic electrochemical transistor (OECT) platform. Three non-biologic polymeric recognition elements, serving as sequential gate electrodes, are engineered to target levodopa's catechol and carboxylate functional groups both independently and in combination. This enables chemistry-resolved, cross-validated detection with enhanced selectivity over structurally related biomolecules such as dopamine. This architecture affords high signal amplification, low-voltage operation, and long-term stability suited to continuous, wearable use.

Stakeholder input from 27 interviews involving patients, caregivers, clinicians, and industry representatives informed the development of a discreet upper-arm microneedle patch, while a 38-respondent stakeholder survey validated the platform's core design assumptions. The proposed translational strategy adopts a B2B commercialization model, positioning the platform for integration into pharmaceutical clinical trials and, ultimately, closed-loop levodopa delivery systems to support individualized, quantitative management of Parkinson's disease.

2. AP award: Biosensor developed for the Eindhoven Testing Event

2.1. Molecular Recognition: Tailored Polymers for Selective Levodopa Binding

Three non-biologic polymeric recognition elements were synthesized to engage distinct functional groups on levodopa in a sequential, multiplexed manner, enhancing selectivity and long-term sensing stability. The first gate, AAPBA-co-AM, incorporates a phenyl-linked boronic acid group that binds levodopa's catechol moiety via reversible boronic ester formation, a mechanism well established for continuous diol sensing (Bian et al., 2020). The second, APTAC-co-AM employs 3-(acrylamidopropyl)trimethylammonium chloride (APTAC), a quaternary ammonium monomer that engages levodopa's carboxylate group through electrostatic interaction (Madhuvilakku & Hong, 2024). The third is a novel hybrid architecture combining both monomers within a single polymer network, AAPBA-APTAC-co-AM, enabling simultaneous catechol and carboxylate recognition. All polymers were synthesized by radical co-polymerization with acrylamide (AM) using an azobisisobutyronitrile (AIBN) thermoinitiator (Section 8.1).

Successful polymerization and functional-monomer incorporation were confirmed by ^{1}H NMR, with characteristic signal intensities scaling with co-monomer-to-AM ratio (Section 8.2). Each polymer was immobilized onto individual gold wafer electrodes via a polyethylenimine (PEI) base layer and glutaraldehyde capping layer, covalently anchoring the recognition elements to the substrate (Section 8.3). These functionalized electrodes constitute the three independent gates of the fabricated multi-gate organic electrochemical transistor (OECT) platform, enabling multiplexed levodopa detection (Fig. 1).

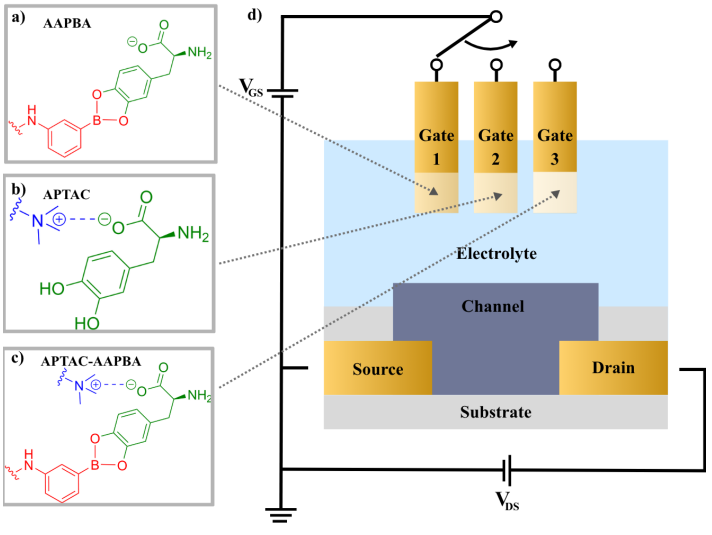


Fig. 1. Schematic of levodopa detection in our biosensor. Molecular interactions of levodopa (green) with gate functionalizations: (a) AAPBA-co-AM, (b) APTAC-co-AM, and (c) AAPBA-co-APTAC-co-AM hybrid polymer. (d) Device schematic and circuit setup. Given an applied drain voltage (V_{DS}) and gate voltage (V_{GS}), the selected gold gate electrode induces doping of the PEDOT:PSS channel, modulating the measured drain current (I_D).

2.2. Physical Transduction: Organic Electrochemical Transistors (OECT)

OECTs are three-terminal devices in which an organic semiconducting channel bridges source and drain electrodes while remaining in direct contact with an electrolyte (Strakosas et al., 2015). A drain voltage (V_{DS}) drives electronic current through the channel,

while an independently applied gate voltage drives ion injection from the electrolyte into the channel bulk. This flux modulates the poly(3,4-ethylenedioxythiophene):poly(styrene sulfonate) (PEDOT:PSS) channel (Friedlein et al., 2018; Rivnay et al., 2018).

Each functionalized gate electrode operates independently, reversibly interacting with levodopa in solution to induce a faradaic current that shifts the effective gate voltage and modulates channel conductivity in proportion to analyte concentration (Friedlein et al., 2018). For each gate, a calibration curve was generated from peak transconductance extracted from transfer sweeps of gate voltage (V_{GS}) across -1 to -0.6 V at a step function of 20 mV every 3 seconds. Gates 1 and 2 are swept at a drain voltage (V_{DS}) of -0.3 V and Gate 3 is swept at a V_{DS} of -0.7 V. As each recognition chemistry exhibits distinct binding kinetics, the resulting calibration curves differ across gates, yielding maximum sensitivities of 0.098, 0.047, and 0.135 mS/decade and limits of detection of 1.43, 25.23, and 1.80 µM for Gates 1, 2, and 3, respectively (Section 3.2.2). Cross-referencing responses across all three gates further enables isolation of levodopa signals from complex serum matrices.

2.3. Cartridge Technology: Microfluidic Sample-Handling

Continuous sensing in interstitial fluid (ISF) is simulated using a modular flow cell (Fig. 2). A commercially available screen-printed gold electrode (Metrohm C220-AT) bearing a PEDOT:PSS channel is mounted in the base holder, with gold traces serving as source and drain contacts. Electrical contact is established using a custom printed circuit board (PCB) equipped with spring-loaded pogo pins. A 100 µL fluid well is secured above the electrode array via a nitrile gasket, with slots for precise placement of functionalized gold electrodes. Finally, an upper compartment with fluidic input and output ports permits continuous fluid exchange through the well.

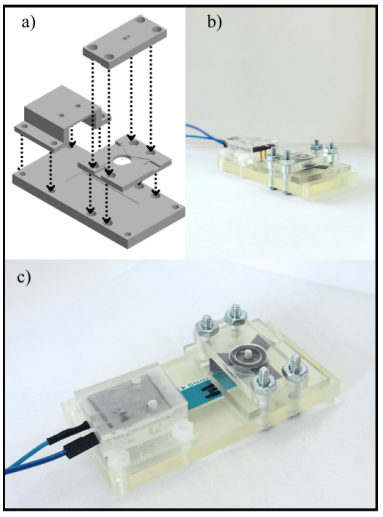


Fig. 2. Flow cell assembly. (a) CAD model showing the 3D-printed components. (b, c) Fully assembled flow cell equipped with integrated electrodes and PCB.

2.4. Reader Instrument and User Interaction: Analog Discovery 3

A Digilent Analog Discovery 3 (AD3) serves as a functional stand-in for the custom printed circuit board (PCB) that will ultimately supply source and gate voltages in the final device. During operation, the AD3 applies the gate-specific bias conditions established for each recognition element (Section 3.2.2), while a custom algorithm extracts the relevant peak transconductance and converts this value to levodopa concentration via the corresponding gate calibration curve (Section 8.4). User interaction is currently limited to cartridge assembly, gate electrode connection to the AD3, and execution of the analysis script, all of which will be fully automated in the final sensor design.

3. IN award: Biosensor innovation

3.1. Wearable Sensor

3.1.1. Technological Novelty of Wearable Sensor

Existing levodopa biosensors are generally unsuited for continuous, wearable deployment or lack sufficient selectivity (Baião et al., 2018; Liu & Zhu, 2019; Özdokur et al., 2018). Enzymatic sensors can achieve high selectivity but are constrained by strict storage requirements and limited long-term stability, precluding practical wearable use (Chokkiveettil et al., 2025). Levodopa's structural similarity to endogenous molecules such as dopamine further complicates selective, reversible detection in interstitial fluid (ISF), a challenge that current sensing strategies have yet to resolve.

To address this limitation, the proposed platform employs a novel recognition strategy. Instead of relying on a single recognition element, three acrylamide (AM)-based recognition polymers were engineered to target complementary chemical features of levodopa, with each polymer assigned to an independent sensing gate: Gate 1 (boronic, AAPBA-co-AM), Gate 2 (cationic, APTAC-co-AM), and Gate 3 (hybrid, AAPBA-APTAC-co-AM) (Fig. 1). Similar to a fingerprinting approach assumed by Nadeem et al. (2026), this three-element recognition strategy paired with multiplexed transduction has not been previously reported for levodopa sensing and confers a selectivity dimension unattainable by single-recognition element approaches. Furthermore, the third gate is composed of a novel hybrid polymer (AAPBA-APTAC-co-AM) currently unreported in literature. Successful polymerization and monomer incorporation were confirmed by ^{1}H NMR for all recognition elements across three co-monomer-to-acrylamide ratios (Fig. 3). The 70:30 ratio was selected for electrochemical testing, as it achieved the highest incorporation of the recognition-element monomer among the ratios synthesized. Additional ^{1}H NMR spectra and ratio discussion are provided in Section 8.2.

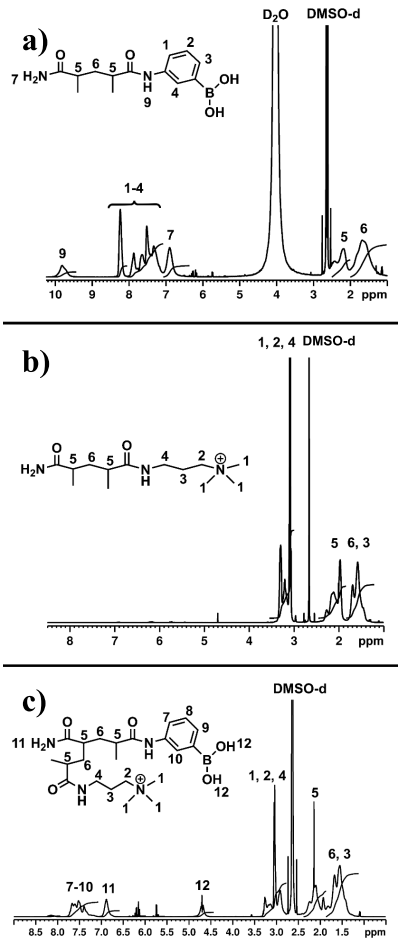


Fig. 3. ^{1}H NMR spectra, chemical structures, and proton assignments for (a) AAPBA, (b) APTAC, and (c) AAPBA-APTAC copolymer at the highest monomer ratio.

The molecular recognition signals were electronically transduced using a three-gate organic electrochemical transistor (OECT). Unlike conventional MOSFETs, which modulate conductivity through a thin interfacial depletion region, OECTs modulate conductivity volumetrically through an electrolyte-permeable organic channel: gate voltage drives ion

exchange into or out of the channel via capacitive coupling, directly modulating source-drain current. This volumetric doping mechanism yields large transconductance at low operating voltages, extending operational lifetime for continuous sensing (Friedlein et al., 2018; Rivnay et al., 2018; Ohayon et al., 2023). By creating a multiplexed system through three sequentially-operated gates, the platform enhances selectivity through dynamic comparison of reaction kinetics across recognition elements.

3.1.2. Technical Feasibility of Wearable Sensor

This multi-gate OECT architecture (Fig. 1) employs each recognition element as a functionalized gold gate electrode. To assess feasibility, modified PEDOT:PSS was spin-coated onto a commercial Metrohm C220-AT electrode at 500 rpm, using the gold working and counter electrodes as source and drain contacts. Vinyl masking defined a consistent 1 mm x 1 mm channel, while spin-coating parameters targeted a consistent channel thickness of 120 nm (Section 8.6).

The resulting OECT was characterized using an unfunctionalized gold wire gate electrode (Fig. 4). Transconductance can be pulled directly from the transfer curves ($\Delta I_D/\Delta V_{GS}$) and corresponds to the effectiveness of the gate electrode in doping the channel. Voltage sweeps beyond ±1 V risk channel overoxidation and electrolysis, leading subsequent operation to be constrained to the ±1 V range. Measurement variability was attributed to gate electrode placement and channel geometry variation. Alternative gate materials were also characterized, but gold was selected for ease of functionalization (Section 8.7).

Similar to a continuous glucose monitor (CGM), this system is amenable to miniaturization onto a microneedle for continuous, low-discomfort ISF access (Fig. 9). Consistent with current benchmarks, the microneedle system targets a 14-day wear period (Olowe et al., 2022). A rechargeable electronic module attaches to the disposable microneedle patch via a twist-lock mechanism with spring-loaded pins contacting the microneedle's pads, transmitting data wirelessly to a patient-facing mobile application.

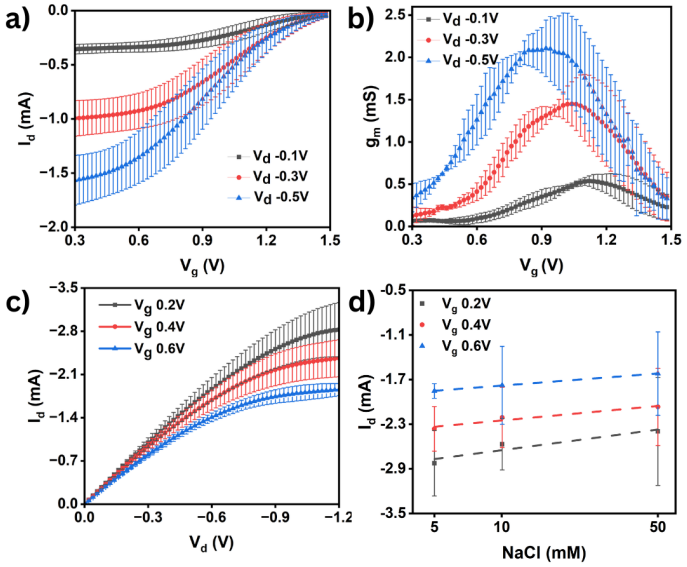


Fig. 4. Characterization of OECT devices with a gold wire gate (n = 3). (*a*) Transfer curves in 5mM NaCl, (*b*) Transconductance curves extracted from the derivative of *a*, (*c*) Output curves in 5mM NaCl, (*d*) Output response over NaCl concentrations at a drain voltage of -1.2V. R^2 values are 0.89, 0.94, and 0.99 for V_g values of 0.2, 0.4, and 0.6V, respectively. Error bars portray standard deviation from mean response.

3.2. Reliability of Sensor Output

3.2.1. Technological Novelty of Reliability Concept

Beyond enhancing selectivity, the three-gate architecture constitutes an intrinsic reliability strategy. As each gate reports an independent, chemistry-specific signal, the system can cross-check gate outputs in real time, exclude a degraded or failing gate, and continue reporting levodopa concentration without interrupting continuous monitoring (Section 8.4). Each gate's recognition element is also reversible by design: in AAPBA, the boron atom accepts electron density from nucleophiles into an empty p-orbital, forming a low-activation-energy B–O bond that favors rapid exchange between bound and free analyte (Bull et al., 2013); in APTAC, the carboxylate interaction is electrostatic, allowing surface charge to rearrange continuously in proportion to analyte concentration under fluid flow (Lee et al., 2010).

Our polymers' reliability was validated through Differential Pulse Voltammetry (DPV) (Section 8.5.1). Gold screen-printed electrodes were functionalized via sequential dropcasting of PEI scaffolding, polymer, and glutaraldehyde crosslinker, validated through cyclic voltammetry (Section 8.3.2) and electrical impedance spectroscopy (Section 8.5.2). Ascending and descending measurements revealed signal changes consistent with concentration-dependent modulation of current, demonstrating that each polymer produces a measurable and reversible electrochemical response with increased levodopa sensitivity in comparison with controls (Fig. 5).

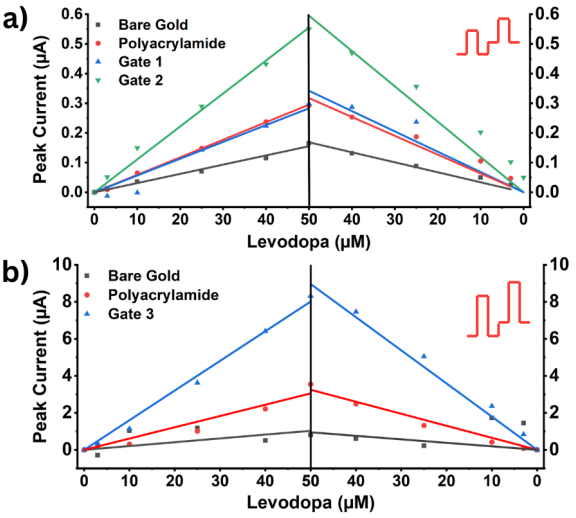


Fig. 5. (a) DPV calibration curve of Gates 1 and 2 with bare gold and pure acrylamide controls taken at a low pulse height (0.02V). (b) DPV calibration curve of Gate 3 with a bare gold and pure acrylamide control taken at a high pulse height (0.2V). See Section 8.5.4 for setting rationale.

To assess the long-term stability of the polymers, the electrochemical response (via DPV) of two identically-fabricated APTAC-functionalized electrodes were tracked to quantify drift in baseline signal, peak position, and sensitivity. One electrode was tested immediately after functionalization while the other was stored in room-temperature conditions for 21 days (Section 8.5.6). A one-tailed paired t-test of the resulting DPV peak currents showed no statistically significant difference ($p = 0.969$), indicating the stored electrode did not exhibit significant signal loss over this period, demonstrating the sensor's potential reliability over extended periods of time.

3.2.2. Technical Feasibility of Reliability Concept

To integrate the recognition chemistry with the OECT platform, gold wafer electrodes were functionalized with PAM, PAM-co-AAPBA, PAM-co-APTAC, and PAM-co-AAPBA-co-APTAC, respectively, and evaluated using a single OECT device (Section 8.7.4). Transfer sweeps were performed across increasing and decreasing levodopa concentrations, yielding drain current and peak transconductance responses for each functionalized electrode. Maximum sensitivities of 0.098, 0.047, and 0.135 mS/decade were obtained for Gates 1, 2, and 3, respectively, with corresponding limits of detection of 1.43, 25.23, and 1.80 µM under optimal conditions, calculated from the minimum logarithmic concentration step where signal change exceeds 3x the standard error of regression (Section 8.7.5).

As each functionalized electrode is designed to interact with levodopa, analyte binding at the polymer surface is expected to modulate peak transconductance by altering double-layer capacitance and gate electrode effectiveness. More broadly, increasing analyte concentration in solution typically decreases peak transconductance, as accumulating analyte near the channel promotes carrier mobility degradation and charge scattering, or forms a physical barrier at the polymer surface that reduces volumetric capacitance. This effect commonly plateaus into a saturation regime at higher concentrations, a hallmark of logarithmic OECT response behavior (Rivnay et al., 2018).

Under identical conditions, the PAM-functionalized control electrode showed the highest peak transconductance, followed by Gate 3, Gate 1, and Gate 2, respectively (Fig. 6). A concentration-dependent decrease is most evident in Gate 2, consistent with its reliance on electrostatic interactions with levodopa, which generate an increasingly restrictive electrostatic barrier at higher concentrations. Gates 1 and 3, by contrast, exhibit a positive trend: increased levodopa binding appears to enhance charge interactions at the electrode surface, increasing volumetric capacitance and yielding higher peak transconductance with concentration. These trends are examined further in Section 8.7.4.

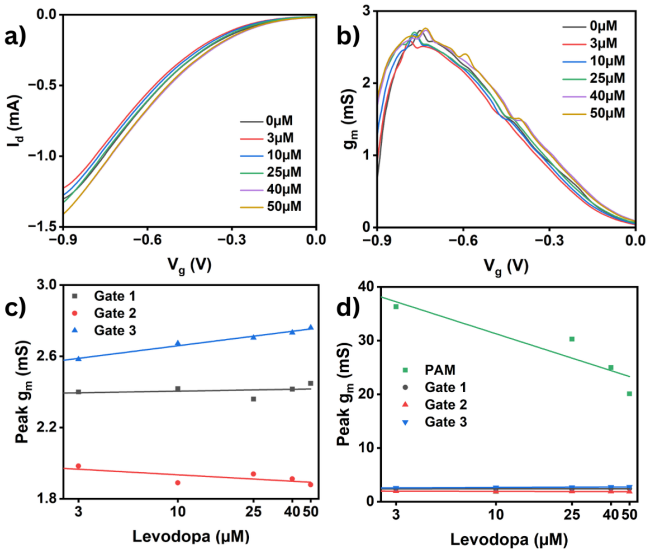


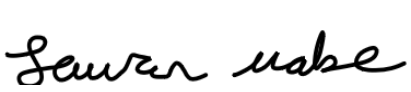
Fig. 6. (*a*) Transfer curves for Gate 3 in increasing levodopa concentrations. (*b*) Transconductance curves extracted from *a*. (*c*) Calibration curves extracted from peak transconductance at a V_d of -0.7V, without PAM. (*d*) Peak transconductance calibration curves, with PAM.

3.3. Original Contributions

3.3.1. Team Captains

The SenseNC biosensor introduces a novel, non-invasive method for continuous levodopa monitoring in patients affected by Parkinson's Disease. By enabling continuous monitoring of ISF levels, it provides quantitative data for personalized therapeutic windows, improving patient outcomes through optimal dosing. Beyond patient use, the biosensor has strong potential in providing quantitative data in pharmaceutical clinical trials or being incorporated into a closed-loop medication system.

The core innovation of SenseNC lies in the multi-gate OECT architecture, with three distinct recognition elements allowing for selective levodopa detection. While the selection of an OECT and polymeric recognition elements was guided by our supervisor, Dr. Daniele, through extensive literature review meetings, the team is solely responsible for the development of these devices. The team wrote up all procedures, gathered the material lists, carried out all testing, and adjusted designs as needed.



Lauren Mabe



Lily Ro

3.3.2. Team Supervisor

The SenseNC team designed and researched a novel electrochemical biosensor for the continuous monitoring of levodopa in interstitial fluid (ISF), designed to optimize therapy management for Parkinson's disease. The core innovation lies in integrating a non-biological polymer recognition element directly onto an organic electrochemical transistor (OECT) architecture. This architecture leverages the high signal amplification inherent to OECTs while the synthetic polymer provides selective, reversible binding to levodopa, enabling real-time tracking of both rising and falling drug concentrations. The student team executed the entire project, synthesizing a recognition element to overcome the stability limitations of biological receptors, optimizing the OECT channel geometry, and engineering the complete microfluidic and hardware system. Advisor involvement was strictly limited to lab safety oversight, facility access, editorial feedback, and fundamental instruction on polymer chemistry, transistor physics, and biosensing. Design choices, fabrication, and experimental validation were driven by the team.



Dr. Michael Daniele

3.4. Bonus Criteria Innovation

Polymeric recognition elements offer key advantages over biological alternatives. Being non-biologic, they are generally robust to environmental fluctuations, improve scalability, and lower production costs (Mo et al., 2024). Their chemical versatility also enables straightforward functionalization, simplifying manufacturing. Organic electrochemical transistors (OECTs) complement these recognition elements as the transduction platform. OECTs operate at low voltage and power, minimize electrolysis-related toxicity, and support long device lifespans (Ohayon et al., 2023). Their compatibility with microfabrication and their high signal amplification at the transduction site yield a strong signal-to-noise ratio, ideal for continuous biosensing. A central innovation of this platform is its multi-gate architecture and incorporation of three polymeric recognition elements. Because each gate exhibits differing reaction kinetics with levodopa, the resulting response profile can generate a unique, multi-dimensional calibration curve specific to the analyte (Section 8.4).

Levodopa therapy is monitored primarily through qualitative patient self-reporting, often resulting in suboptimal dosing and increased side effects. The clinical gold standard for direct quantification, High-Performance Liquid Chromatography (HPLC), requires separating, identifying, and quantifying levodopa in plasma or serum, typically paired with electrochemical or mass spectrometric detection (Karimi et al., 2006). This method is accurate but time-intensive, costly, invasive, and dependent on specialized equipment and trained personnel. As a result, clinical practice commonly relies on the Movement Disorder Society-Unified Parkinson's Disease Rating Scale, which requires 12 hours of medication withdrawal, a baseline motor assessment, and a follow-up evaluation after an elevated levodopa dose (Saranza & Lang, 2021).

Personalized pharmacokinetic modeling can accurately predict blood levodopa concentrations following oral dosing (Othman & Dutta, 2014). The sensor software is designed to incorporate this predictive model, allowing model-predicted values to calibrate initial sensor readings. No validated correlation currently exists between ISF levodopa levels and therapeutic outcome, as effective dosing varies significantly between patients. As such, future work will incorporate an inertial measurement unit (IMU) to directly correlate tremor activity with ISF levodopa levels, enabling patient-specific therapeutic windows and, longer-term, integration into a closed-loop system in partnership with pharmaceutical levodopa pump developers.

4. TP award: Translation potential

4.1. Customer Interviews

4.1.1. Identification of Potential Stakeholders

Levodopa remains the most effective pharmacological treatment for Parkinson's motor symptoms, yet long-term efficacy is frequently compromised by fluctuating drug response: wearing-off phenomena affect 40–50% of patients after five years of therapy, rising to roughly two-thirds over longer durations (Mizuno et al., 2018). This reflects a fundamental visibility problem rather than an issue of patient non-adherence, as clinicians lack real-time insight into the relationship between drug concentration, symptom state, and dose timing in daily life.

To capture perspectives spanning the full continuum of care and anticipated device use, we conducted interviews across five stakeholder groups: patients, caregivers, MedTech and pharmaceutical representatives, movement disorder specialists, and other healthcare professionals. This diversity ensured that clinical, caregiving, and commercial perspectives were each represented, allowing us to triangulate unmet needs across the ecosystem rather than from a single vantage point (Fig. 7).

4.1.2. Interview Approach and Execution

Data were collected through 27 semi-structured stakeholder interviews conducted via Zoom or telephone. For each stakeholder group, a standardized set of five core questions was developed in advance to minimize interviewer bias while preserving flexibility for participants to surface unanticipated insights (Section 8.8). Questions were deliberately broad to elicit candid reflection on existing challenges and unmet needs, consistent with best practices in interview-based qualitative research (E. Marecek, 2015; Robinson, 2014).

With participant consent, interviews were audio-recorded and transcribed in full to eliminate note-taking bias and enable systematic analysis. Participant identities were anonymized using a coding scheme linking each transcript to its stakeholder group and participant number (Section 8.8). At least two research team members were present at each session to ensure consistency in interview conduct. This methodology reflects a human-centered design approach intended to ground subsequent design decisions in stakeholder-derived evidence.

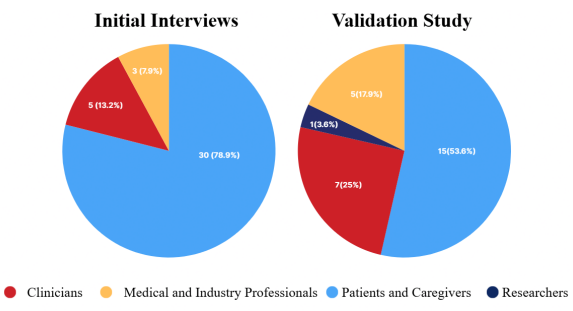


Fig 7. Pie Chart of the interview demographics for (a) initial interviews, and (b) validation study.

4.1.3. Interview Results and Conclusions

Following transcription and anonymization, inductive qualitative coding was conducted in accordance with established methodological practice (Coates et al., 2021; Thomas, 2006): (1) manual coding of raw transcripts to identify recurring themes, (2) synthesis of these codes into higher-order insights across the interview set, and (3) application of conceptual frameworks to translate insights into product and business implications (Fig. 8). The comprehensive findings of the qualitative inductive coding process are depicted in Section 8.8.8.



Fig. 8. Example of the step-by-step qualitative inductive interview coding process

This analysis revealed a clear, unmet need for continuous levodopa monitoring. While clinicians expressed enthusiasm for the concept and agreed it could improve outcomes, they voiced hesitancy toward adopting such a tool directly within their own practice. Patients and caregivers responded strongly to personalized, objective dosing data, citing persistent frustration with the subjectivity of current monitoring. Medical device and pharmaceutical stakeholders likewise expressed strong interest, noting the absence of any comparable continuous, wearable levodopa sensor on the market. Pharmaceutical stakeholders further noted that reliance on subjective levodopa equivalent dose (LED) estimates complicates clinical trial design for related Parkinson's therapies (Julien et al., 2021); a quantitative sensing platform could reduce associated time and cost while improving confidence in outcomes.

Based on these findings, the proposed commercialization strategy adopts a business-to-business (B2B) model targeting MedTech and pharmaceutical partners, aiming to streamline clinical trial infrastructure and establish integration partnerships with oral and intravenous levodopa delivery systems toward a fully closed-loop system. Consistent with patient and caregiver feedback, the wearable component was designed for placement on the upper arm or abdomen, prioritizing a simple form factor compatible with limited motor function (Section 4.2.2).

4.2. Design of Validation Study

4.2.1. Selection of the Problem

Stakeholder interviews (n = 27) revealed that management of Parkinson's disease (PD) is severely constrained by infrequent, subjective, and burdensome symptom tracking. Patients and caregivers consistently described logging fatigue associated with tracking erratic motor and non-motor symptoms between clinical visits, leaving clinicians and researchers with an incomplete, unreliable picture of a patient's levodopa response.

A wearable sensor directly addresses this need by shifting the tracking burden from patient or caregiver to a continuous, automated monitoring system, generating objective, quantitative levodopa metabolism data without added patient effort. This bridges the gap between patient experience and clinical need: greater transparency into fluctuating levodopa levels empowers patients to engage in their own treatment, while providing pharmaceutical and MedTech partners the means to accelerate clinical trials and optimize therapeutic interventions, respectively. In-depth market analysis further evaluated the economic viability of a sensor-based solution and identified the target market share (Section 8.9).

4.2.2. Conceptual Design and Use Case

The proposed device is a minimally invasive, OECT-based biosensor platform for continuous levodopa monitoring in interstitial fluid (ISF). Three gates, each functionalized with a distinct non-biologic recognition element, interact independently and electrochemically with levodopa, improving reliability through cross-gate signal comparison and enabling robust detection in a biologically complex environment. Because these recognition elements are non-biologic, they retain functionality after extended room-temperature storage (Section 8.5.6), simplifying scalability and manufacturing while lowering production costs. The OECT platform's low power consumption further supports long-term in-body operation.

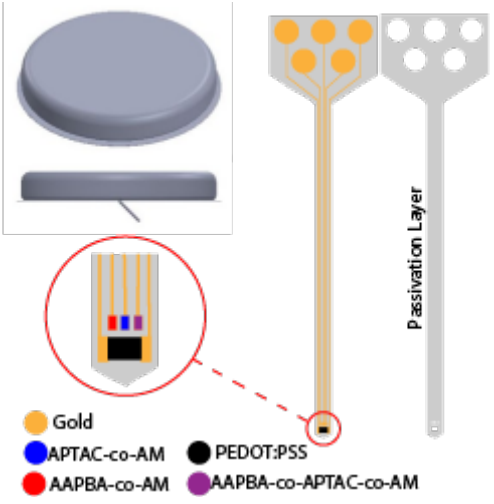


Fig. 9. Layered microneedle design exposing only the channel, functionalized gates, and connection pads (not to scale).

To align with patient preference for discretion, the sensor is designed as an upper-arm patch. A reusable electronic module attaches to the disposable sensing patch and transmits data via Bluetooth to a companion software platform (Section 8.10); a

twist-lock attachment mechanism accommodates patients with limited motor function, minimizing required patient interaction (Fig. 9).

This platform is intended to accelerate PD therapy development and enable individualized medication management through continuous levodopa monitoring. Under a B2B model, pharmaceutical companies serve as primary customers and strategic partners, while patients benefit directly from more individualized dosing and access to personal levodopa profiles. To mitigate commercialization risk independent of an early pharmaceutical joint venture, investigator-led research with neurologists and academic medical centers will be pursued to generate preliminary clinical evidence and accelerate the regulatory pathway.

4.2.3. Validation Study Design

A formative pre-validation study was conducted prior to full technical validation using a structured Stakeholder Concept Validation Survey to quantify problem severity and characterize desired product specifications. A multi-channel outreach strategy ensured representative sampling: the survey was distributed directly to prior interview participants (patients, caregivers, neurologists, and movement disorder specialists), shared with the Rock Steady Boxing of the Carolinas support group network following an in-person presentation, and promoted via LinkedIn by the Southeast Chapter of the Parenteral Drug Association (Fig. 7). In total, 38 structured Likert-scale responses were collected and analyzed (Section 8.11).

Results from this survey confirmed strong demand for continuous levodopa monitoring (Fig. 10). This preliminary validation study also captured stakeholder feedback on software design and key feature priorities (Section 8.11), quantitatively validating core elements of the sensor design while identifying targets for future iteration.

Pharmaceutical and MedTech representatives further emphasized the importance of FDA approval, regardless of joint-venture requirements, noting that as one of the first devices of its kind, rigorous clinical validation and patent protection would be essential to establishing market position; both pathways are addressed in Section 8.12.

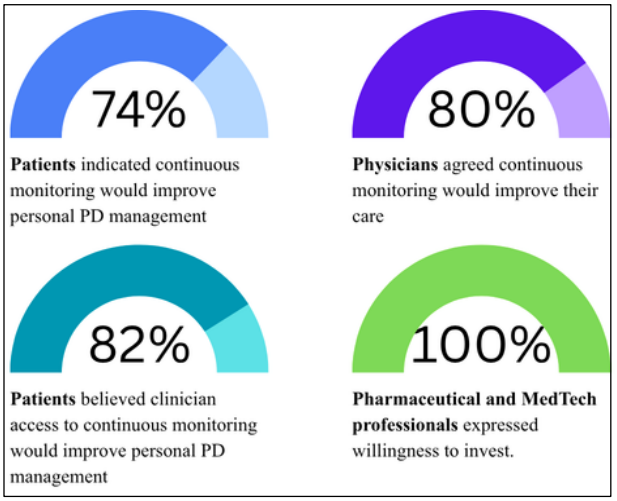


Fig 10. Quantitative survey results evaluating stakeholder demand for continuous levodopa monitoring. Proportions of surveyed patients, physicians, and pharmaceutical/MedTech professionals indicating positive utility across Parkinson's Disease management, clinical care integration, and commercial investment interest.

4.3. Bonus Criteria Translation Potential

Our commercialization strategy employs a B2B model structured around two complementary pathways: pharmaceutical partnerships and independent, investigator-led clinical research collaborations. Initial market entry prioritizes partnership discussions with pharmaceutical companies, while the team concurrently develops validation studies with movement-disorder specialists and academic medical centers, reducing reliance on an early joint venture while pharmaceutical discussions mature. A pharmaceutical partnership pathway would integrate the biosensor directly into drug-development pipelines as a tool for generating continuous, quantitative levodopa concentration-time data, addressing the reliance on subjective levodopa equivalent dose estimates that currently complicates PD drug trials (Section 4.1.3).Given that the global Parkinson's disease therapeutics market is projected to exceed $10 billion annually over the coming decade, this represents a commercially attractive opportunity for technologies that improve therapy development efficiency and support individualized medication optimization.

Each pilot unit would comprise 100 biosensors at an estimated price of $540 per sensor, generating approximately $54,000 in revenue per pilot deployment. Each pilot unit would comprise 100 biosensors at an estimated price of $540 per sensor, generating approximately $54,000 in revenue per pilot deployment. This model incorporates projected pilot sales, cost of goods sold, manufacturing costs, economy-of-scale assumptions, operating expenses, customer acquisition costs, and potential joint-venture revenue-sharing (Section 8.13), providing an early quantitative basis for evaluating manufacturing feasibility and pricing strategy as the platform scales.

The regulatory strategy includes pursuing Class II classification through the FDA's De Novo pathway, given the absence of a substantially equivalent predicate device (Section 8.12), followed by European market expansion within several years of launch (Section 8.14). A consolidated timeline integrating these regulatory, manufacturing, and commercialization milestones is presented in Section 8.15.

Collectively, this work in business model development, financial planning, and regulatory strategy extends meaningfully beyond the interview and validation work in Sections 4.1 and 4.2, demonstrating a proactive, evidence-based pathway toward real-world deployment.

5. Team and Support

5.1. Contributions of the team members

Dr. Michael Daniele and **Irfan Ismail** served as Team Supervisor and Coach, respectively, and were instrumental in providing team support.

The nine-member SenseNC team organized into three subteams to execute this project. The chemistry subteam (**Lily Ro, Akshay Balasubramanian, and Ebenezer Amare**) was responsible for researching, synthesizing, and characterizing the polymeric recognition elements, using NMR spectroscopy and electrochemical techniques to confirm successful polymerization and functional performance. The OECT subteam (**Lauren Mabe, Ameerah Abazid, and Clint Powers**) researched, developed, and optimized the multi-gate organic electrochemical transistor platform, establishing the device architecture central to our sensing approach. The operations subteam (**Nicolas Anzola, Sahiti Mudireddy, and Rudhra Unnikrishnan**) led fabrication of electrodes used throughout experimental testing.

For translation potential, the entire team contributed to researching and shaping our business plan. **Lauren, Clint, and Nicolas** were instrumental in conducting stakeholder interviews and collecting data, while **Clint, Nicolas, and Sahiti** led analysis of the resulting interview data. **Lauren, Clint, Rudhra, and Nicolas** were the primary developers of our business model and commercialization strategy, translating stakeholder insights into an actionable go-to-market plan.

5.2. People who have given support

Jim Marciariello was vital in our translation potential development, giving us valuable insights into the FDA regulatory administration and long-term business planning.

Dr. Zainab Akbar was crucial in guiding our interview analysis and qualitative coding efforts. The **BioInterface Lab Members** gave technical support when needed.

5.3. Sponsors and partners

NC State Institute for Connected Sensor-Systems (IConS), the **NC State Office of Undergraduate Research,** and **DermiSense** provided funding and support.

Rock Steady Boxing provided feedback and outreach from several stakeholders.

NC State College of Engineering and the **NC State/UNC-CH Lampe Joint Department of Biomedical Engineering** provided funding for our competition travel.

PalmSens and **Demcon** provided feedback on our sensor and suggested improvements.

6. Final remarks

We would like to express our sincere gratitude to the patients, clinicians, and industry professionals who generously contributed their time and insights throughout the development of this biosensor. Their lived experiences and professional perspectives were instrumental in shaping a solution that is not only technically robust, but also clinically and emotionally meaningful.

As a student team consisting entirely of undergraduates, we were fortunate to collaborate with mentors and researchers across biomedical engineering, regulatory science, and healthcare delivery. We are especially grateful to the faculty and staff at North Carolina State University and the University of North Carolina at Chapel Hill for providing access to facilities, guidance, and encouragement throughout the SensUs 2026 journey.

Looking ahead, we plan to continue developing our biosensor beyond the competition through institutional support and potential partnerships with clinical and commercial stakeholders. Our immediate goals include refining the hardware for long-term use, expanding validation studies with human-derived ISF, and exploring regulatory submission pathways. We believe that optimizing dosing for Parkinson's Disease has the potential to improve outcomes for millions of patients, and we are committed to translating this vision into clinical reality.

7. References

Baião, V., Tomé, L. I. N., & Brett, C. M. A. (2018). Iron Oxide Nanoparticle and Multiwalled Carbon Nanotube Modified Glassy Carbon Electrodes. Application to Levodopa Detection. *Electroanalysis*, *30*(7), 1342–1348. https://doi.org/10.1002/elan.201700854

Bennett E. Kuhar. (2026, March 26). Before You Share Your Invention: What Public Disclosures Count as Prior Art Under U.S. Patent Law. *IP Tip of the Month*. https://www.tuckerellis.com/ip-tip-of-the-month-blog/before-you-share-your-invention-what-public-disclosures-count-as-prior-art-under-u-s-patent-law/

Bian, Z., Liu, A., Li, Y., Fang, G., Yao, Q., Zhang, G., & Wu, Z. (2020). Boronic acid sensors with double recognition sites: A review. *The Analyst*, *145*(3), 719–744. https://doi.org/10.1039/C9AN00741E

Bull, S. D., Davidson, M. G., Van Den Elsen, J. M. H., Fossey, J. S., Jenkins, A. T. A., Jiang, Y.-B., Kubo, Y., Marken, F., Sakurai, K., Zhao, J., & James, T. D. (2013). Exploiting the Reversible Covalent Bonding of Boronic Acids: Recognition, Sensing, and Assembly. *Accounts of Chemical Research*, *46*(2), 312–326. https://doi.org/10.1021/ar300130w

Ceccardi, F., Mariani, F., Decataldo, F., Vurro, V., Tessarolo, M., Gualandi, I., Fraboni, B., & Scavetta, E. (2025). A point-of-care, label-free OECT sensor for uric acid detection: Validation in human saliva. *Electrochimica Acta*, *519*, 145834. https://doi.org/10.1016/j.electacta.2025.145834

Cetó, X., Céspedes, F., & Del Valle, M. (2013). Comparison of methods for the processing of voltammetric electronic tongues data. *Microchimica Acta*, *180*(5–6), 319–330. https://doi.org/10.1007/s00604-012-0938-7

Chokkiveettil, N., Antherjanam, S., & Rajamani, R. (2025). A Critical Review on Non-Enzymatic Electrochemical Strategies for L-Glutamate Monitoring in Biological Systems. *Critical Reviews in Analytical Chemistry*, 1–14. https://doi.org/10.1080/10408347.2025.2584363

Coates, W. C., Jordan, J., & Clarke, S. O. (2021). A practical guide for conducting qualitative research in medical education: Part 2—Coding and thematic analysis. *AEM Education and Training*, *5*(4), e10645. https://doi.org/10.1002/aet2.10645

E. Magnusson Jeanne Marecek. (2015). *Doing Interview-Based Qualitative Research: A Learner's Guide*. Swarthmore. https://works.swarthmore.edu/fac-psychology/806/

European Commission. (2026a). CE Marking. *European Commission*. https://single-market-economy.ec.europa.eu/single-market/goods/ce-marking_en

European Commission. (2026b). Economic Operators. *European Commission*. https://health.ec.europa.eu/medical-devices-topics-interest/economic-operators_en

European Commission. (2026c). Guidance—MDCG endorsed documents and other guidance. *European Commission*. https://health.ec.europa.eu/medical-devices-sector/new-regulations/guidance-mdcg-endorsed-documents-and-other-guidance_en?utm_source=chatgpt.com

European Commission. (2026d). Medical Devices—EUDAMED. *European Commission*. https://health.ec.europa.eu/medical-devices-eudamed_en

European Commission. (2026e, May 18). Simpler and more effective rules for medical devices – Commission proposal for a targeted revision of the medical devices regulations. *European Commission*. https://health.ec.europa.eu/medical-devices-new-regulations/overview_en?utm_

Friedlein, J. T., McLeod, R. R., & Rivnay, J. (2018). Device physics of organic electrochemical transistors. *Organic Electronics*, *63*, 398–414. https://doi.org/10.1016/j.orgel.2018.09.010

Hassani-Marand, M., Fahimi-Kashani, N., & Hormozi-Nezhad, M. R. (2023). Machine-learning assisted multiplex detection of catecholamine neurotransmitters with a colorimetric sensor array. *Analytical Methods*, *15*(9), 1123–1134. https://doi.org/10.1039/D2AY01797K

Julien, C., Hache, G., Dulac, M., Dubrou, C., Castelnovo, G., Giordana, C., Azulay, J., & Fluchère, F. (2021). The clinical meaning of levodopa equivalent daily dose in Parkinson's disease. *Fundamental & Clinical Pharmacology*, *35*(3), 620–630. https://doi.org/10.1111/fcp.12646

Karimi, M., Carl, J. L., Loftin, S., & Perlmutter, J. S. (2006). Modified high-performance liquid chromatography with electrochemical detection method for plasma measurement of levodopa, 3-O-methyldopa, dopamine, carbidopa and 3,4-dihydroxyphenyl acetic acid. *Journal of Chromatography B*, *836*(1–2), 120–123. https://doi.org/10.1016/j.jchromb.2006.03.027

Lee, I.-H., Gong, M.-S., & Kim, J.-G. (2010). Anchoring of polyelectrolyte membrane containing chalcone group to electrode substrate by [2+2] cycloaddition and its humidity-sensing properties. *Macromolecular Research*, *18*(12), 1218–1225. https://doi.org/10.1007/s13233-010-1212-7

Liu, W., & Zhu, X. (2019). A novel fluorescence “turn off-on” sensor based on N-doped graphene quantum dots in amino acid ionic liquid medium and its application. *Talanta*, *197*, 59–67. https://doi.org/10.1016/j.talanta.2019.01.008

Madhuvilakku, R., & Hong, Y. (2024). Portable Sensing Probe for Real-Time Quantification of Ammonia in Blood Samples. *ACS Applied Materials & Interfaces*, *16*(36), 47242–47256. https://doi.org/10.1021/acsami.4c09573

Mizuno, Y., Shimoda, S., & Origasa, H. (2018). Long-term treatment of Parkinson’s disease with levodopa and other adjunctive drugs. *Journal of Neural Transmission*, *125*(1), 35–43. https://doi.org/10.1007/s00702-016-1671-x

Mo, R., Yu, D., Li, W., Sheng, X., & Zhang, X. (2024). Storage-stable and self-crosslinkable combinations of boronic acid containing polymers and diol containing polymers enabled by the latex system. *Polymer*, *299*, 126977. https://doi.org/10.1016/j.polymer.2024.126977

Nadeem, A., Rahmani, M., Wang, Y., Yari, S., Lopez, R. M., Kim, M., & Roxbury, D. (2026). Spectral Fingerprinting of Engineered Nanomaterials for Precision Biosensing. *ACS Nano*, *20*(5), 3921–3943. https://doi.org/10.1021/acsnano.5c18348

National Library of Medicine. (2026). ClinicalTrials.gov. *National Library of Medicine*. https://clinicaltrials.gov/search?cond=Parkinsons%20Disease&viewType=Card&intr=medication

Norman, G. (2010). Likert scales, levels of measurement and the “laws” of statistics. *Advances in Health Sciences Education*, *15*(5), 625–632. https://doi.org/10.1007/s10459-010-9222-y

Ohayon, D., Druet, V., & Inal, S. (2023). A guide for the characterization of organic electrochemical transistors and channel materials. *Chemical Society Reviews*, *52*(3), 1001–1023. https://doi.org/10.1039/D2CS00920J

Olowe, M., Parupelli, S. K., & Desai, S. (2022). A Review of 3D-Printing of Microneedles. *Pharmaceutics*, *14*(12), 2693. https://doi.org/10.3390/pharmaceutics14122693

Ossila. (2026). *Spin Coating: Complete Guide to Theory and Techniques*. https://www.ossila.com/pages/spin-coating

Othman, A. A., & Dutta, S. (2014). Population pharmacokinetics of levodopa in subjects with advanced P arkinson’s disease: Levodopa-carbidopa intestinal gel infusion *vs.* Oral tablets. *British Journal of Clinical Pharmacology*, *78*(1), 94–105. https://doi.org/10.1111/bcp.12324

Özdokur, K. V., Engin, E., Yengin, Ç., Ertaş, H., & Ertaş, F. N. (2018). Determination of Carbidopa, Levodopa, and Droxidopa by High-Performance Liquid Chromatography–Tandem Mass Spectrometry. *Analytical Letters*, *51*(1–2), 73–82. https://doi.org/10.1080/00032719.2017.1316283

Quintino, M. S. M., Yamashita, M., & Angnes, L. (2006). Voltammetric Studies and Determination of Levodopa and Carbidopa in Pharmaceutical Products. *Electroanalysis*, *18*(7), 655–661. https://doi.org/10.1002/elan.200503445

Rivnay, J., Inal, S., Salleo, A., Owens, R. M., Berggren, M., & Malliaras, G. G. (2018). Organic electrochemical transistors. *Nature Reviews Materials*, *3*(2), 17086. https://doi.org/10.1038/natrevmats.2017.86

Robinson, O. C. (2014). Sampling in Interview-Based Qualitative Research: A Theoretical and Practical Guide. *Qualitative Research in Psychology*, *11*(1), 25–41. https://doi.org/10.1080/14780887.2013.801543

Saranza, G., & Lang, A. E. (2021). Levodopa challenge test: Indications, protocol, and guide. *Journal of Neurology*, *268*(9), 3135–3143. https://doi.org/10.1007/s00415-020-09810-7

Shahdost-Fard, F., Bigdeli, A., & Hormozi-Nezhad, M. R. (2021). A Smartphone-Based Fluorescent Electronic Tongue for Tracing Dopaminergic Agents in Human Urine. *ACS Chemical Neuroscience*, *12*(17), 3157–3166. https://doi.org/10.1021/acschemneuro.1c00160

Strakosas, X., Bongo, M., & Owens, R. M. (2015). The organic electrochemical transistor for biological applications. *Journal of Applied Polymer Science*, *132*(15), app.41735. https://doi.org/10.1002/app.41735

Sullivan, G. M., & Artino, A. R. (2013). Analyzing and Interpreting Data From Likert-Type Scales. *Journal of Graduate Medical Education*, *5*(4), 541–542. https://doi.org/10.4300/JGME-5-4-18

Thomas, D. R. (2006). A General Inductive Approach for Analyzing Qualitative Evaluation Data. *American Journal of Evaluation*, *27*(2), 237–246. https://doi.org/10.1177/1098214005283748

Tumová, Š., Malečková, R., Kubáč, L., Akrman, J., Enev, V., Kalina, L., Vojtková, E., Pešková, M., Víteček, J., Vala, M., & Weiter, M. (2023). Novel highly stable conductive polymer composite PEDOT:DBSA for bioelectronic applications. *Polymer Journal*, *55*(9), 983–995. https://doi.org/10.1038/s41428-023-00784-7

University of Notre Dame. (2026). *How much does a patent cost? Who pays for the patent on my invention?* https://ideacenter.nd.edu/commercialization-engine/for-researchers/learn/inventors-guide-to-commercialization/how-much-does-a-patent-cost-who-pays-for-the-patent-on-my-invention/

Wang, T., Jafar, N. N. A., Al-Rihaymee, A. M. A., Alhameedi, D. Y., Rasen, F. A., Hashim, F. S., Hussein, T. K., Ramadan, M. F., Alasedi, K. K., Suliman, M., & Alawadi, A. H. (2024). Highly efficient electrocatalytic oxidation of levodopa as a Parkinson therapeutic drug based

on modified screen-printed electrode. *Heliyon*, *10*(14), e34689. https://doi.org/10.1016/j.heliyon.2024.e34689

Xie, K., Wang, N., Lin, X., Wang, Z., Zhao, X., Fang, P., Yue, H., Kim, J., Luo, J., Cui, S., Yan, F., & Shi, P. (2020). Organic electrochemical transistor arrays for real-time mapping of evoked neurotransmitter release in vivo. *eLife*, *9*, e50345. https://doi.org/10.7554/eLife.50345

Yao, Y., Alimardani, F., Ren, P., Dong, J., Lee, S., Lee, Y., & Wang, Y. (2025). Dual-Gate Organic Electrochemical Transistors Based on Laser-Scribed Graphene for Detecting Dopamine and Glutamate. *Advanced Materials Technologies*, *10*(9), 2401732. https://doi.org/10.1002/admt.202401732

8. Appendix

8.1. Synthesis of Polymers for Selective Levodopa Sensing

8.1.1 Chemical Materials

3-acrylamidophenyl boronic acid (AAPBA), 75 wt% 3-acrylamidopropyl trimethylammonium chloride solution (APTAC), acrylamide, 2,2'-Azobis(2-methylpropionitrile) (AIBN), and dimethyl sulfoxide were used as purchased from Sigma-Aldrich without further purification. Acetone, ethanol, and acetonitrile solvent were used as purchased from VMR International without further purification.

8.1.2 Polymerization of Boronic Recognition Element (AAPBA-co-AM)

AAPBA monomer , acrylamide monomer, and AIBN were dissolved in a MilliQ-DMSO cosolvent. The solution was sparged with nitrogen gas for 30 minutes while magnetically stirred. After degassing, the solution was heated to 70 ° C to thermoinitiate the polymerization reaction and kept for 6 hours. The solution was then pipetted drop-wise into ice-cold acetone functioning as a non-solvent to 'crash out' the polymer. The polymer was extracted via vacuum filtration and air dried overnight in a dessicator.

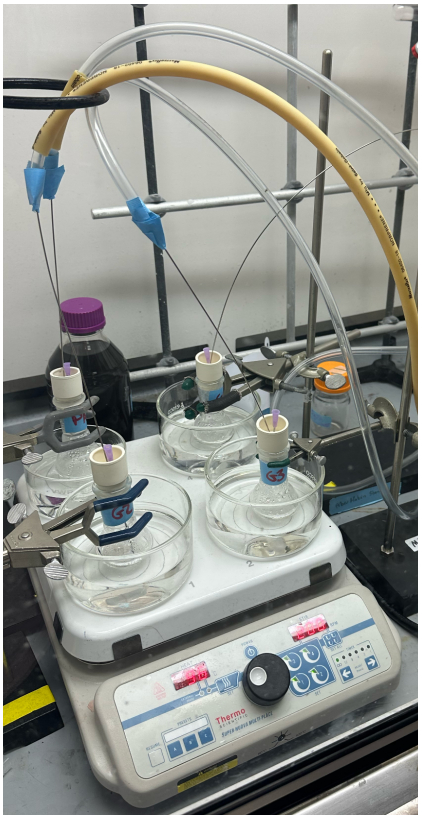


Fig. 11. A picture of synthesis set up where we are synthesizing gates 1, 2, 3, and polyacrylamide.

8.1.3 Polymerization of Cationic Recognition Element (APTAC-co-AM)

APTAC monomer, acrylamide monomer, and AIBN were dissolved in MilliQ-DMSO cosolvent. The solution was sparged with nitrogen gas for 30 minutes while magnetically stirred. After degassing, the solution was heated to 70 ° C to thermoinitiate the polymerization reaction and kept for 6 hours. The solution was then pipetted drop-wise into ice-cold acetonitrile functioning as a non-solvent to 'crash out' the polymer. The polymer was extracted via vacuum filtration and air dried overnight in a dessicator.

8.1.4 Preparation of Dual-Recognition Element (AAPBA-co-APTAC-co-AM)

AAPBA monomer, APTAC monomer, acrylamide monomer, and AIBN were dissolved in a MilliQ-DMSO cosolvent. The solution was sparged with nitrogen gas for 30 minutes while magnetically stirred. After degassing, the solution was heated to 70 °C to initiate the polymerization reaction and kept for 6 hours. The solution was then pipetted drop-wise into ice-cold acetonitrile, functioning as a non-solvent to 'crash out' the polymer. The polymer was extracted via vacuum filtration and air dried overnight in a dessicator.

8.1.5 Polymer Isolation and Purification

Following polymerization, the polymer solutions were added dropwise to the corresponding ice-cold non-solvent to precipitate the synthesized polymer. AAPBA-co-AM was precipitated in acetone, while APTAC-co-AM and AAPBA-co-APTAC- co-AM were precipitated in acetonitrile. The precipitated polymer was collected by vacuum filtration. When necessary, centrifugation was additionally used to separate the polymer from the surrounding solvent, producing a concentrated polymer pellet and supernatant that could be removed. The recovered polymers were then air dried overnight in a desiccator.

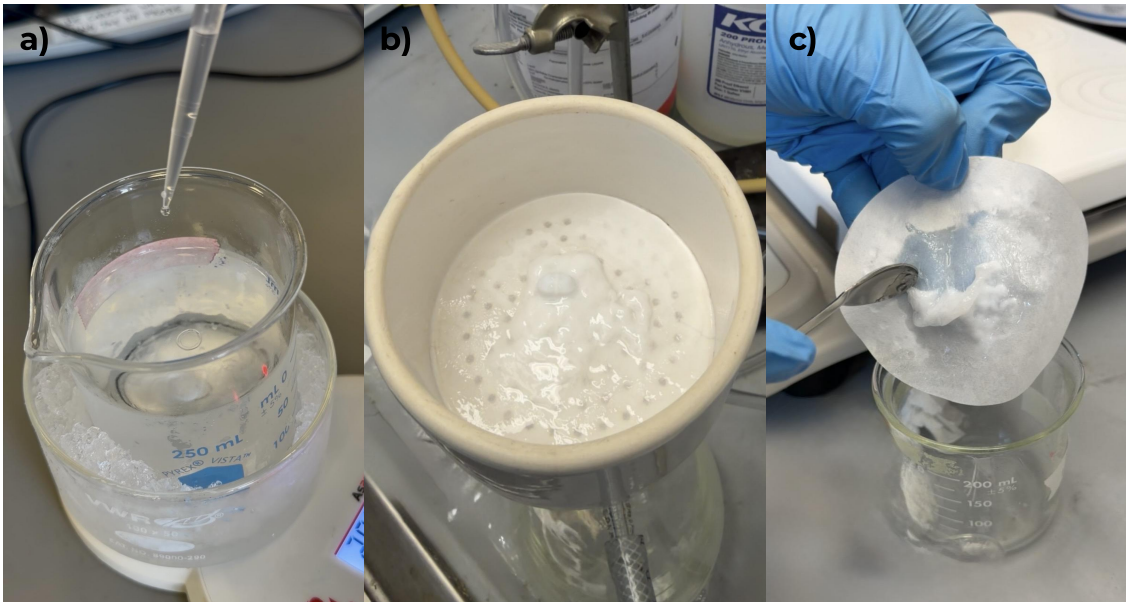


Fig. 12. Polymer precipitation and recovery following synthesis. (a) Polymer precipitation following dropwise addition to ice-cold non-solvent, (b) collection of the precipitated polymer by vacuum filtration, and (c) recovery of the filtered polymer.

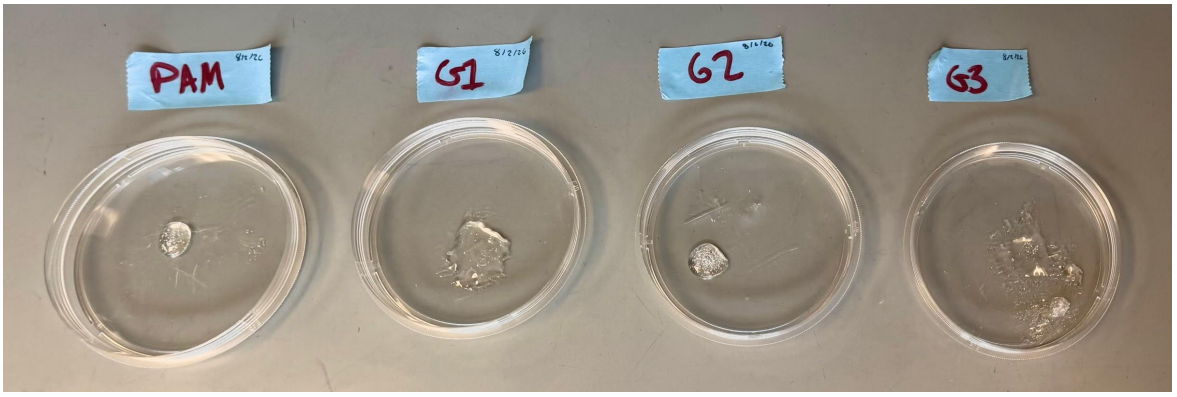


Fig. 13. Synthesized PAM control and Gate 1, Gate 2, and Gate 3 recognition polymers stored in a dessicator after precipitation, vacuum filtration, and drying

8.1.6 Material Quantities & Monomer Ratio Optimization

Each polymer above was synthesized in 3 acrylamide:recognition element ratios to optimize levodopa binding. The ratios are described in the table below, along with the appropriate material quantities. Each synthesis utilized a 10 mL solution volume, 5 solute wt/vol%, and .5 mol% AIBN:total monomer ratio.

Table A1.

Boronic Recognition Element Synthesis Quantities

Acrylamide: Recognition Element (mol %)	AAPBA monomer (g)	APTAC monomer 75 wt% sol (g)	Acrylamide (g)	AIBN (mg)	DMSO-Milli Q cosolvent (mL)
70:30	0.304	0	0.264	4.36	10
85:15	0.183	0	0.386	5.34	10
95:05	0.07	0	0.498	6.06	10

Table A2.

Cationic Recognition Element Synthesis Quantities

Acrylamide: Recognition Element (mol %)	AAPBA monomer (g)	APTAC monomer 75 wt% sol (g)	Acrylamide (g)	AIBN (mg)	DMSO-Milli Q cosolvent (mL)
70:30	0	0.421	0.253	4.18	10
85:15	0	0.257	0.376	5.10	10
95:05	0	0.101	0.493	5.99	10

Table A3.

Hybrid Recognition Element Synthesis Quantities

Acrylamide: Recognition Element (mol %)	AAPBA monomer (g)	APTAC monomer 75 wt% sol (g)	Acrylamide (g)	AIBN (mg)	DMSO-Milli Q cosolvent (mL)
80:10:10	0.113	0.173	0.341	5.52	10
85:7.5:7.5	0.090	0.131	0.386	5.15	10
90:5:5	0.065	0.091	0.437	4.72	10

8.2. Polymer Characterization (^{1}H NMR)

8.2.1 Sample Preparation and NMR Codes

Each polymer ratio was characterized by ^{1}H NMR. Samples containing at least 5 mg of polymer were dissolved in 560 µL of solvent to improve spectral resolution. Spectra were collected at 600 MHz using an Avance NEO spectrometer located within North Carolina State University's Molecular Education, Technology, and Research Innovation Center (METRIC).

8.2.2 AAPBA, APTAC, and Hybrid Gate Spectra

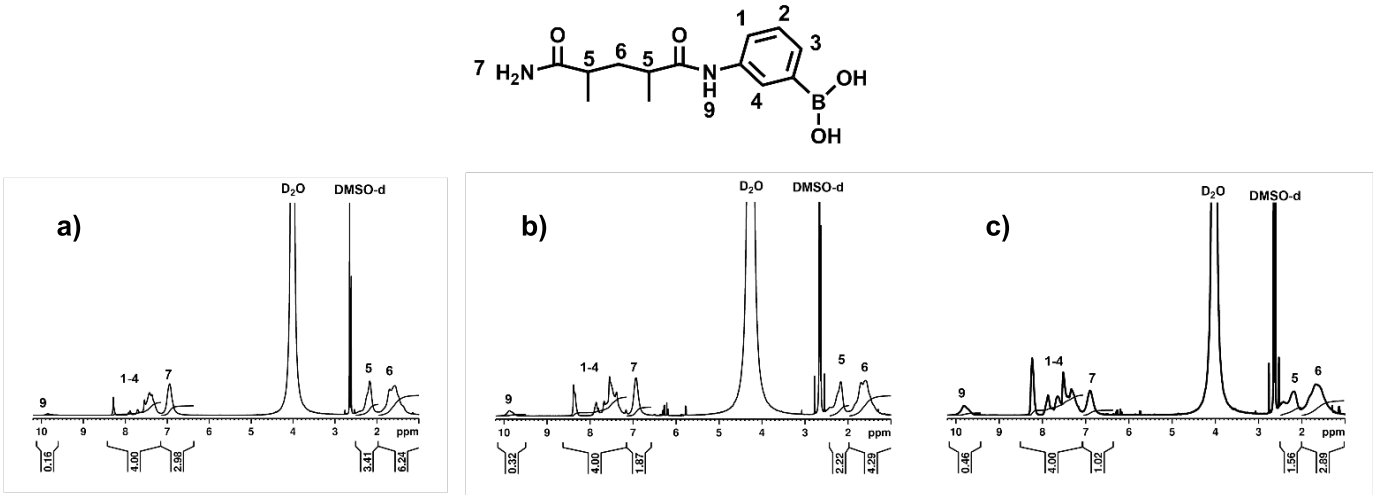


Fig. 14. NMR spectra of Gate 1 at increasing incorporation ratios; a) 95:5 mol% Acrylamide: AAPBA b) 85:15 mol% Acrylamide: AAPBA and c) 70:30 mol% Acrylamide: AAPBA

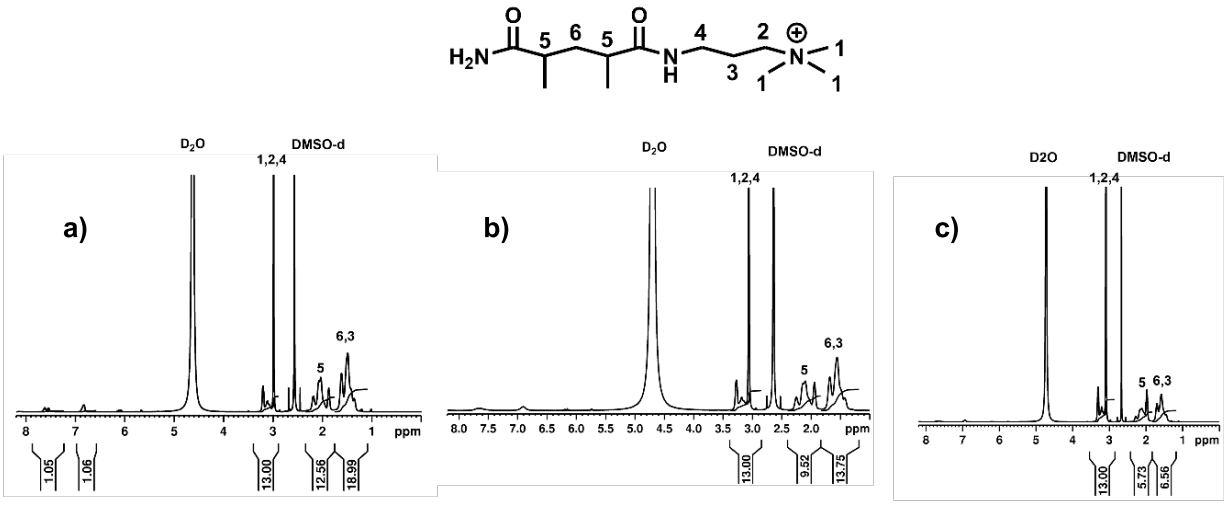


Fig. 15. NMR spectra of Gate 2 at increasing incorporation ratios; a) 95:5 mol% Acrylamide: APTAC b) 85:15 mol% Acrylamide: APTAC and c) 70:30 mol% Acrylamide: APTAC

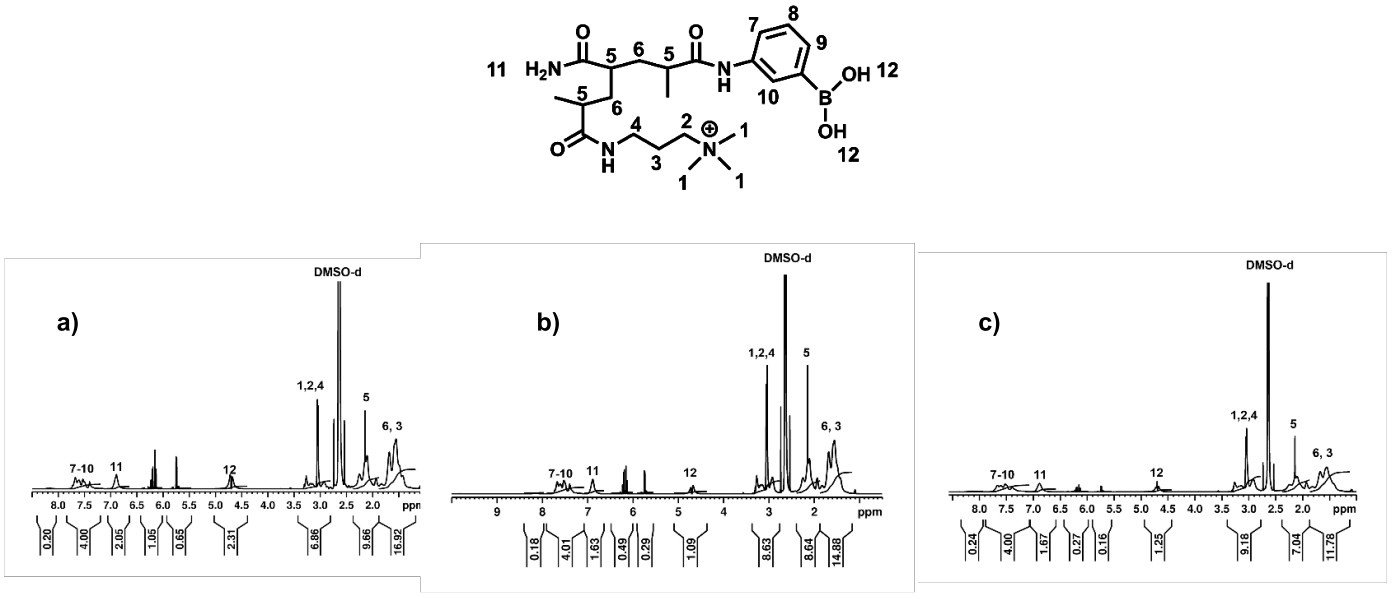


Fig. 16. NMR spectra of Gate 3 at increasing incorporation ratios; a) 90:5:5 mol% Acrylamide: AAPBA: APTAC b) 85:7.5:7.5 mol% Acrylamide:AAPBA:APTAC Acrylamide: APTAC and c) 80:10:10 mol% Acrylamide: AAPBA: APTAC

8.2.3 Incorporation Analysis Across Ratios

By integration in Bruker Topspin, Gate 1 and 2 acrylamide:monomer ratios were as expected: 70:30, 85:15, and 95:5. For Gate 1, this was done by calibrating the aromatic protons (1-4 on Fig. 14) to a value of 4 and comparing to integration of protons 5 and 6, which exist on the polyacrylamide backbone. For Gate 2, this was done by calibrating protons on the carbons adjacent to a nitrogen atom (1, 2, 4 on Fig. 15) to a value of 13 and comparing to integration of protons 5 and 6 once again. Gate 3, however, saw more convoluted incorporation, with AAPBA consistently incorporated at a higher rate than APTAC. The 80:10:10, 85:7.5:7.5, and 90:5:5 ratios are compositionally 53:30:17, 73:17:10, and 85:10:5. Gate 3's aromatic protons were calibrated to a value of 4, similar to Gate 1.

8.3. Electrode Functionalization on Gold Electrodes

8.3.1 Screen-Printed Electrode Functionalization

To coat the working electrodes of the MetrOhm DRP-220AT SPEs, a polyethylenimine (PEI) base layer and glutaraldehyde capping layer, covalently anchoring the recognition elements to the substrate, were chosen. Three different approaches to functionalizing using PEI and glutaraldehyde were considered

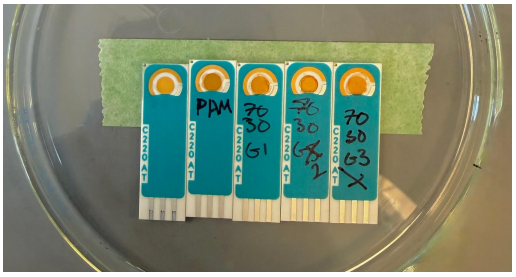


Fig. 17. Representative screen-printed gold electrodes following polymer functionalization.

8.3.2 Electrochemical Confirmation of Deposition

To functionally assess what method of functionalization was most successful, tests were run on electrodes functionalized with gates 1 and 2 using Cyclic Voltammetry (CV), a test that runs anodic sweeps from low to high voltages and cathodic sweeps from high to low voltages continuously for a number of cycles. Three cycles were run from -.6 V to .7 V on each electrode in 5 mM ferrocyanide solution before and after functionalization to assess whether the peak and absolute value of the minimum current decreased significantly, indicating successful functionalization as a lower current indicates more of the gold electrode surface was covered during functionalization.

As shown in Fig. 18, two methods were similarly effective: after a series of rinses with acetone, methanol, isopropyl alcohol, and molecular biology-grade distilled water in that order, first 2 µL of PEI was applied, then 2 µL of polymer, and finally 2 µL of 2% glutaraldehyde; the other method was the same with the polymer and glutaraldehyde switched in order. The former method of functionalization was selected and applied in all subsequent experiments.

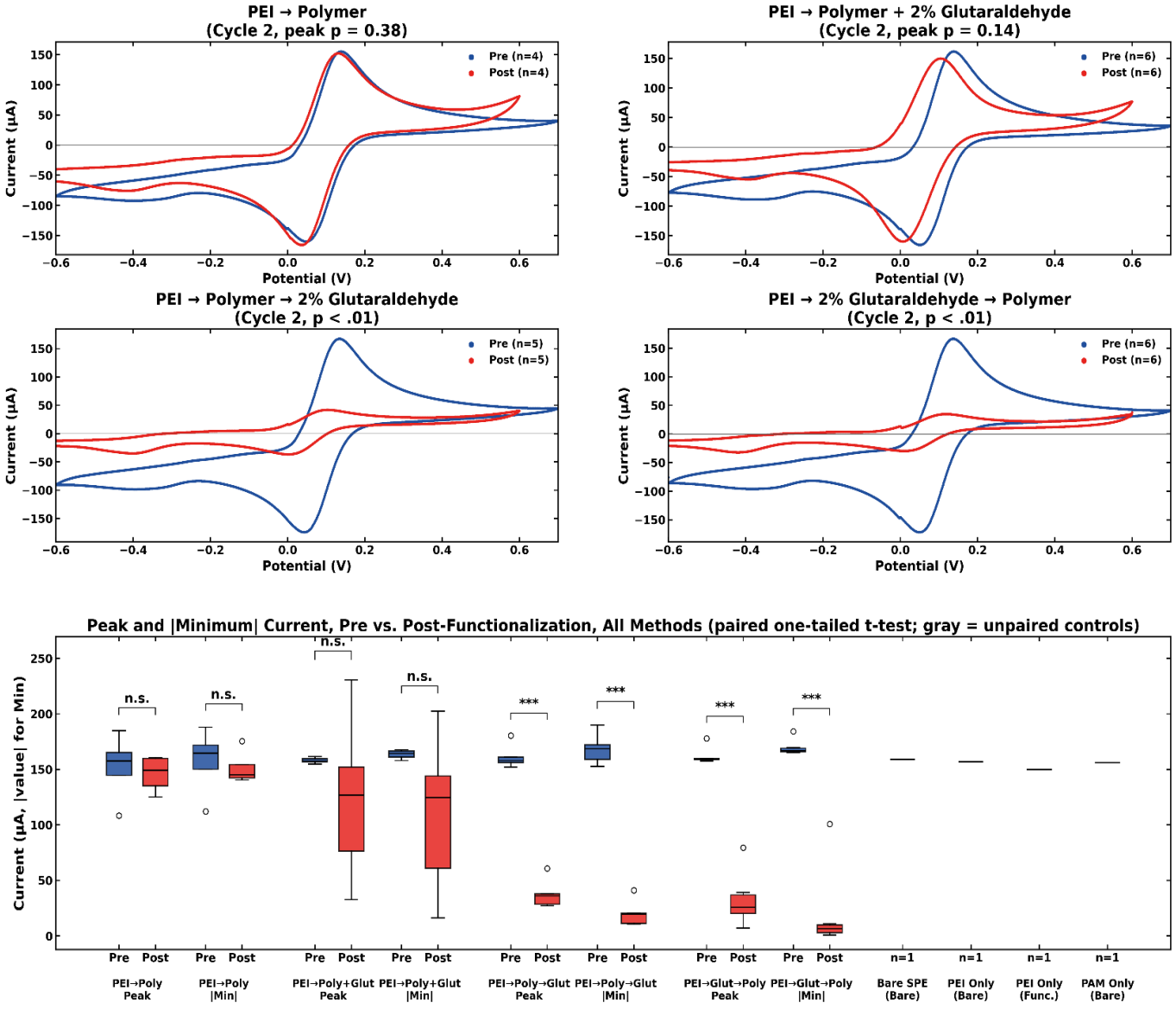


Fig. 18. Python analysis of pre- vs. post-functionalization ferrocyanide cyclic voltammetry across four polymer deposition methods. (Top, 2×2 grid) Averaged ferrocyanide cyclic voltammograms (5 mM $K_3[Fe(CN)_6]$ in 0.1 M KCl, Cycle 2, 50 mV/s) before (blue) and after (red) functionalization for each method: PEI → Polymer (n = 4, no significant change in peak current, 152.1 → 145.9 µA, p = 3.83×10^{-1}, or minimum current, p = 3.78×10^{-1}); PEI → Polymer + 2% Glutaraldehyde (n = 6, no significant change in peak current, 157.9 → 122.9 µA, p = 1.36×10^{-1}, or minimum current, p = 5.18×10^{-2}); PEI → Polymer → 2% Glutaraldehyde (n = 5, significant decrease in both peak current, 161.6 → 38.1 µA, p = 4.25×10^{-5}, and minimum current, 168.5 → 20.7 µA, p = 3.65×10^{-5}); and PEI → 2% Glutaraldehyde → Polymer (n = 6, significant decrease in both peak current, 162.0 → 32.9 µA, p = 6.57×10^{-5}, and minimum current, 169.7 → 21.3 µA, p = 1.71×10^{-4}). (Bottom) Extended boxplot panel showing peak current during anodic sweep and |minimum current| during cathodic sweep before and after functionalization for all four methods, with paired one-tailed t-tests as reported above; gray boxes show unpaired reference measurements from bare SPE, PEI-only, and PAM-only controls.

8.3.3. Gold Wafer Gate Functionalization

The optimized functionalization protocol was adapted for gold wafers designed for integration with the proposed flow cell, although sensing studies have not yet been conducted. To accommodate the larger substrate, the deposition volume was increased from 2 µL to 3 µL. However, the contact angle of PEI on the gold wafer surface was too high, so it would not spread over the surface of the gold wafer, which was solved via a 2 minute treatment of plasma cleaning using a Harrick Plasma cleaner post-rinses and applying PEI within 15 minutes of plasma cleaning.

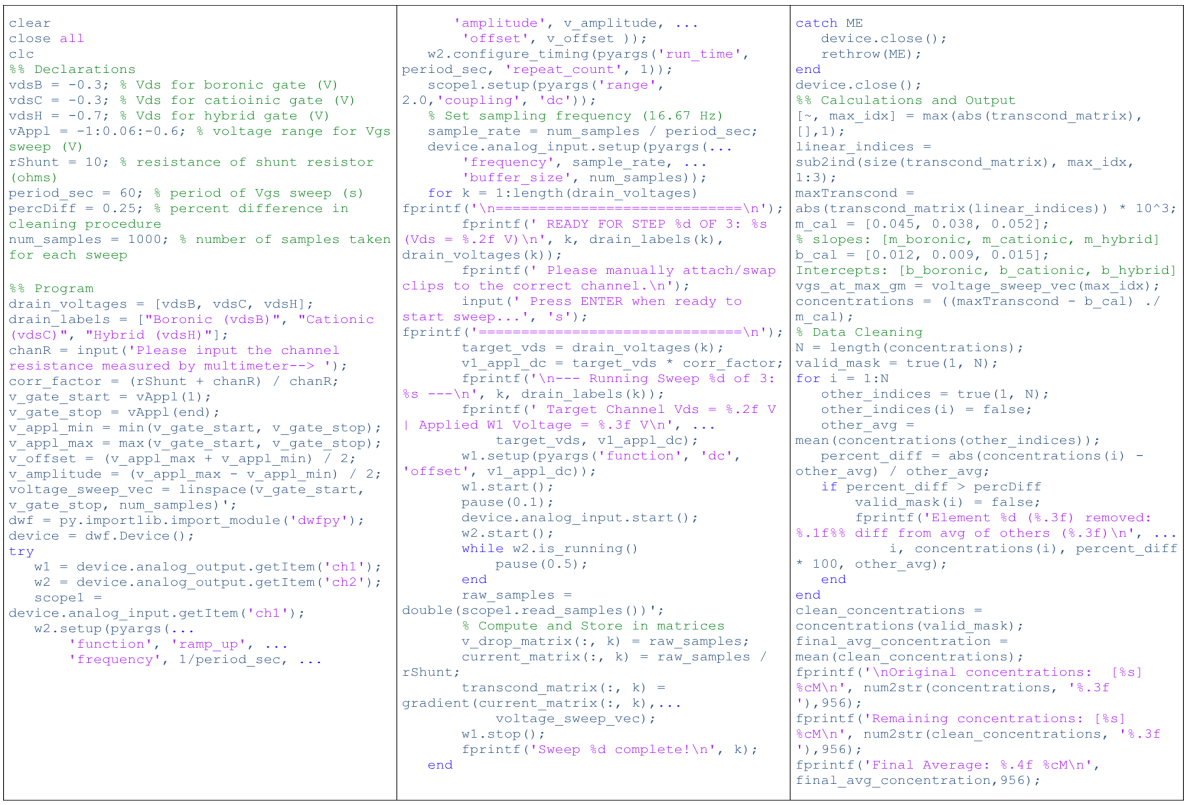


Fig. 19. Functionalized gold wafer samples prepared with PAM and Gates 1-3.

8.4. Algorithm for Eindhoven Testing Event

8.4.1. Current Algorithm to Determine Levodopa Concentration

To calculate levodopa concentrations from OECT data generated using the ETE, a singular MATLAB script that sequentially sweeps V_{GS} from -1 to -0.6 V for each of the gate electrodes. For each V_{GS} sweep, the V_{DS} is biased at a constant voltage described in Section 8.7.4. Oscilloscope measurements from the AD3 determine the voltage drop over the shunt resistor for each transfer sweep, allowing the calculation of I_D via Ohm's Law. The peak transconductance value is extracted by taking the derivative of I_D with respect to V_{GS}, and these values are then mapped through gate-specific calibration equations to identify an independent concentration measurement for each gate. A brief cleaning loop runs to discard any concentration that differs from the other two by a margin of 25%. Remaining concentrations are averaged together, dictating sensor output.



```
clear
close all
clc
%% Declarations
vdsB = -0.3; % Vds for boronic gate (V)
vdsC = -0.3; % Vds for catioinic gate (V)
vdsH = -0.7; % Vds for hybrid gate (V)
vAppl = -1:0.06:-0.6; % voltage range for Vgs
sweep (V)
rShunt = 10; % resistance of shunt resistor
(ohms)
period_sec = 60; % period of Vgs sweep (s)
percDiff = 0.25; % percent difference in
cleaning procedure
num_samples = 1000; % number of samples taken
for each sweep

%% Program
drain_voltages = [vdsB, vdsC, vdsH];
drain_labels = ["Boronic (vdsB)", "Cationic
(vdsC)", "Hybrid (vdsH)"];
chanR = input('Please input the channel
resistance measured by multimeter--> ');
corr_factor = (rShunt + chanR) / chanR;
v_gate_start = vAppl(1);
v_gate_stop = vAppl(end);
v_appl_min = min(v_gate_start, v_gate_stop);
v_appl_max = max(v_gate_start, v_gate_stop);
v_offset = (v_appl_max + v_appl_min) / 2;
v_amplitude = (v_appl_max - v_appl_min) / 2;
voltage_sweep_vec = linspace(v_gate_start,
v_gate_stop, num_samples)';
dwf = py.importlib.import_module('dwfpy');
device = dwf.Device();
try
    w1 = device.analog_output.getItem('ch1');
    w2 = device.analog_output.getItem('ch2');
    scope1 =
device.analog_input.getItem('ch1');
    w2.setup(pyargs(...
        'function', 'ramp_up', ...
        'frequency', 1/period_sec, ...
        'amplitude', v_amplitude, ...
        'offset', v_offset ));
    w2.configure_timing(pyargs('run_time',
period_sec, 'repeat_count', 1));
    scope1.setup(pyargs('range',
2.0,'coupling', 'dc'));
    % Set sampling frequency (16.67 Hz)
    sample_rate = num_samples / period_sec;
    device.analog_input.setup(pyargs(...
        'frequency', sample_rate, ...
        'buffer_size', num_samples));
    for k = 1:length(drain_voltages)
fprintf('\n============================\n');
        fprintf(' READY FOR STEP %d OF 3: %s
(Vds = %.2f V)\n', k, drain_labels(k),
drain_voltages(k));
        fprintf(' Please manually attach/swap
clips to the correct channel.\n');
        input(' Press ENTER when ready to
start sweep...', 's');
fprintf('============================\n');
        target_vds = drain_voltages(k);
        v1_appl_dc = target_vds * corr_factor;
        fprintf('\n--- Running Sweep %d of 3:
%s ---\n', k, drain_labels(k));
        fprintf(' Target Channel Vds = %.2f V
| Applied W1 Voltage = %.3f V\n', ...
            target_vds, v1_appl_dc);
        w1.setup(pyargs('function', 'dc',
'offset', v1_appl_dc));
        w1.start();
        pause(0.1);
        device.analog_input.start();
        w2.start();
        while w2.is_running()
            pause(0.5);
        end
        raw_samples =
double(scope1.read_samples())';
        % Compute and Store in matrices
        v_drop_matrix(:, k) = raw_samples;
        current_matrix(:, k) = raw_samples /
rShunt;
        transcond_matrix(:, k) =
gradient(current_matrix(:, k),...
            voltage_sweep_vec);
        w1.stop();
        fprintf('Sweep %d complete!\n', k);
    end
catch ME
    device.close();
    rethrow(ME);
end
device.close();
%% Calculations and Output
[~, max_idx] = max(abs(transcond_matrix),
[],1);
linear_indices =
sub2ind(size(transcond_matrix), max_idx,
1:3);
maxTranscond =
abs(transcond_matrix(linear_indices)) * 10^3;
m_cal = [0.045, 0.038, 0.052];
% slopes: [m_boronic, m_cationic, m_hybrid]
b_cal = [0.012, 0.009, 0.015];
Intercepts: [b_boronic, b_cationic, b_hybrid]
vgs_at_max_gm = voltage_sweep_vec(max_idx);
concentrations = ((maxTranscond - b_cal) ./
m_cal);
% Data Cleaning
N = length(concentrations);
valid_mask = true(1, N);
for i = 1:N
    other_indices = true(1, N);
    other_indices(i) = false;
    other_avg =
mean(concentrations(other_indices));
    percent_diff = abs(concentrations(i) -
other_avg) / other_avg;
    if percent_diff > percDiff
        valid_mask(i) = false;
        fprintf('Element %d (%.3f) removed:
%.1f%% diff from avg of others (%.3f)\n', ...
            i, concentrations(i), percent_diff
* 100, other_avg);
    end
end
clean_concentrations =
concentrations(valid_mask);
final_avg_concentration =
mean(clean_concentrations);
fprintf('\nOriginal concentrations:  [%s]
%cM\n', num2str(concentrations, '%.3f
'),956);
fprintf('Remaining concentrations: [%s]
%cM\n', num2str(clean_concentrations, '%.3f
'),956);
fprintf('Final Average: %.4f %cM\n',
final_avg_concentration,956);
```

Fig. 20. MATLAB algorithm used during ETE to determine levodopa concentration of unknown samples.

8.4.2. Proposals for Future Algorithm to Determine Levodopa Concentration

Future studies will leverage the triple-gate architecture to generate distinct combinations of binding interactions, enabling the production of a unique fingerprint for each analyte; a real-time deconvolution algorithm would then invert this response vector to recover levodopa concentration alongside interferent concentrations. Multi-gate and array-based OECT architectures for catecholamine discrimination are well-precedented: OECT arrays have been used to map catecholamine neurotransmitter release in vivo with nanomolar sensitivity inaccessible to conventional voltammetry (Xie et al., 2020), and dual-gate OECTs with differentially functionalized gate electrodes have demonstrated simultaneous detection of dopamine and glutamate from a shared PEDOT:PSS channel, establishing the core sequential multiplexing concept the architecture extends (Yao et al., 2025). The fingerprint discrimination strategy is most directly validated for dopaminergic agents by Shahdost-Fard et al., (2021), who developed a cross-reactive fluorescent sensor array that simultaneously detected and discriminated levodopa, carbidopa, and others in human urine through differential response patterns across array elements, demonstrating that pattern-based deconvolution can resolve carbidopa, the only cross-reactant that satisfies all recognition criteria of the gate architecture from levodopa in a biologically relevant matrix. The broader feasibility of machine-learning-assisted multiplex

discrimination of levodopa from structurally related catecholamines including dopamine, epinephrine, and norepinephrine has been further confirmed using gold nanoparticle colorimetric arrays under varying buffer conditions, where unique fingerprint response patterns enabled simultaneous discrimination of all four analytes (Hassani-Marand et al., 2023).

For signal deconvolution, a systematic comparison of preprocessing and modelling strategies for voltammetric electronic tongue arrays, including principal component regression, partial least squares (PLS), multi-way PLS, and artificial neural networks, found PLS consistently competitive for both discrimination and quantification in mixed analyte systems, supporting its selection as the starting point before escalating to nonlinear methods (Cetó et al., 2013). Furthermore, the first oxidation wave of carbidopa, the hardest to resolve of all potential interferences, is separated from levodopa by approximately 50 mV in electrochemical measurements on glassy carbon (Quintino et al., 2006), and a DPV-PLS methodology has been validated for simultaneous determination of levodopa and carbidopa in pharmaceutical mixtures, suggesting linear multivariate discrimination may be sufficient (Cetó et al., 2013). A nonlinear support vector regression or compact neural network would be implemented only if PLS residual error exceeds the clinical tolerance of ±2 µM across the 3–50 µM sensing range.

8.5. Electrochemical Evaluation of Levodopa Response

8.5.1 Differential Pulse Voltammetry and Open-Circuit Potential

To test and verify the electrochemical properties of polymeric recognition elements with levodopa, the MetrOhm DropSens system was used. The primary technique used to assess polymer performance, derived from the literature (Crapnell & Banks, 2023), was Differential Pulse Voltammetry (DPV). DPV is a faradaic mode of sensing which was used to sweep from low to high voltages to induce a surge in current due to the oxidation of Levodopa, reported in the literature to occur above ~0.1 V vs. Ag/AgCl (Probst et al., 2024) and as low as ~0.24 V vs. Ag/AgCl at optimized modified electrodes (State, 2022), with the surge in current increasing as Levodopa concentration was increased. This range reflects the known pH-dependence of levodopa's oxidation potential, consistent with a Nernstian, coupled two-proton, two-electron transfer mechanism (Wang et al., 2024). Although the intended application of the polymer is integration with the OECT for non-Faradaic sensing, this validation was designed to demonstrate polymer-based levodopa detection using well-established electrochemical

methods and to establish a sensitivity benchmark against which OECT performance could subsequently be compared.

The second electrochemical technique employed was open-circuit potential (OCP), which measures the resting potential of the electrodes. OCP served two primary purposes. First, it was used to determine when polymer swelling had reached equilibrium, a process that could not be reliably assessed through visual inspection. A stable resting potential indicated that the polymer had completed swelling and was suitable for subsequent differential pulse voltammetry (DPV) measurements. Second, OCP was used as a preliminary assessment of the polymers' potential for non-Faradaic sensing. The resting potential of the electrodes was expected to decrease with increasing levodopa concentration because levodopa contains a carboxylate group that is deprotonated under the experimental conditions, resulting in a negatively charged species. Observation of this concentration-dependent relationship and the generation of corresponding OCP calibration curves would provide additional support for the proposed non-Faradaic sensing mechanism.

8.5.2 Determination of Polymer Stability During Electrochemical Characterization

Through the process of iteration, though the final procedure was 2.5 hours long, tests could be run for up to 6 hours. Therefore, tests were run on electrodes functionalized with all three gates to assess stability while left soaking in 10uM levodopa solution continuously in an incubator held at 37°C and 5.0% CO_2 to simulate the electrodes soaking in Levodopa solutions of various concentrations while in a Faraday cage. Electrical Impedance Spectroscopy was used to test polymer integrity, resolving changes in interfacial charge-transfer resistance and capacitance across the frequency spectrum as indicators of film coverage and stability. A paired two-tailed t-test run on all electrodes revealed a p-value of .672, indicating no significant degradation of the polymers over 24 hours, substantiating the results.

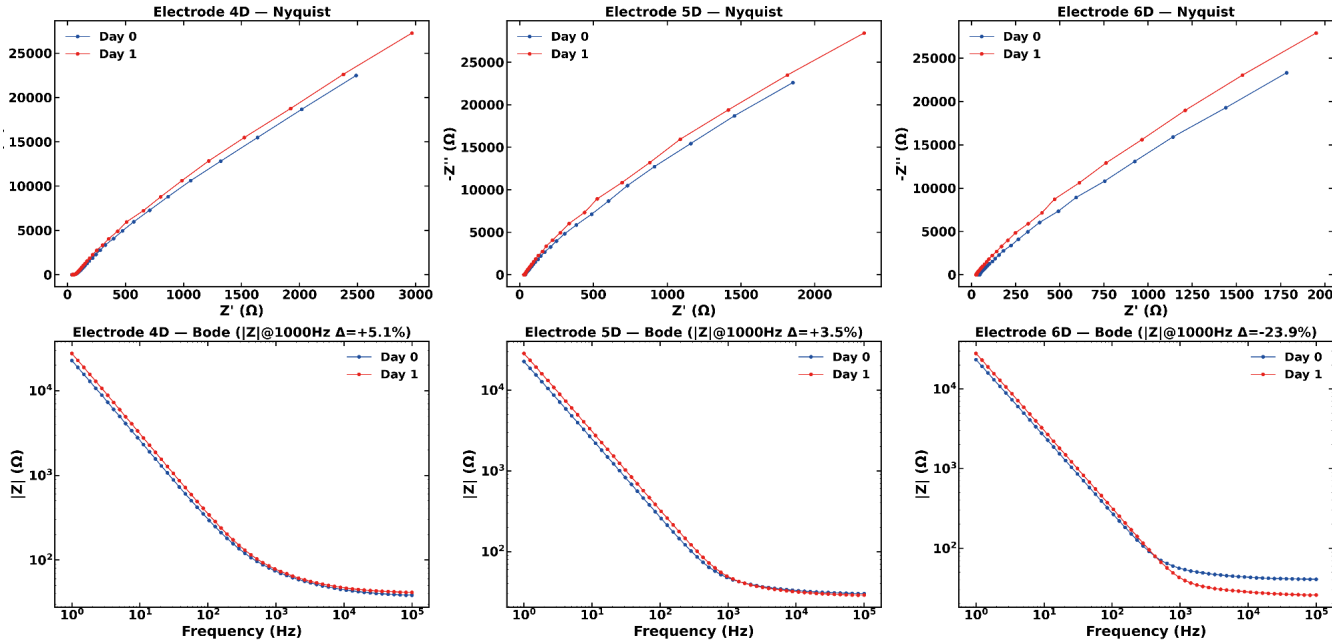


Fig. 21. Nyquist (top row) and Bode (bottom row) plots of electrochemical impedance spectra for electrodes 4D, 5D, 6D (n = 3) at Day 0 and Day 1 of the longevity study. Nyquist plots show Z' (real impedance) vs. -Z'' (negative imaginary impedance); Bode plots show |Z| (impedance magnitude) vs. frequency on a log-log scale, swept from 1 Hz to 100 kHz. A paired two-tailed t-test (n = 3 electrodes, each measured at both time points) comparing Day 0 to Day 1 impedance magnitude |Z| at 1000 Hz showed no statistically significant difference (mean change = −5.1%, p = .672; per-electrode changes: 4D: +5.1%, 5D: +3.5%, 6D: -23.9%).

8.5.3 Reversible Levodopa-Dependent Responses (Ascending vs. Descending)

The final methodology for collecting DPV and OCP data began with a 30-minute soak in 50 µM levodopa solution followed by a 30-minute soak in PBS, establishing a saturated baseline and a washed baseline, respectively. Open-circuit potential (OCP) was then recorded for 1 minute to confirm electrode stability before 2 DPV runs were taken at either the high or low pulse height. Each subsequent ascending and descending concentration was equilibrated under OCP for 15 minutes before DPV was run, ensuring the polymer film had reached a steady interfacial state at each concentration before the measurement was taken.

This sequence was designed to test not only whether the sensor responds to levodopa, but whether that response is reversible, the central requirement for continuous, real-time monitoring. Concentrations were therefore run as a full ascending-then-descending series (0 → 50 → 0 µM) rather than a single ascending sweep, so that each concentration is sampled twice: once while approaching from a lower concentration and once while approaching from a higher one. The 15-minute OCP equilibration preceding each DPV measurement ensures that the recorded signal reflects

the electrode's equilibrium state at that concentration rather than a transient mid-exchange value, allowing the ascending and descending arms to be compared on equal footing. Polymer-film integrity across this extended protocol was independently verified in Section 8.5.2, confirming that any signal changes over the run arise from levodopa binding rather than film degradation.

A 2 mM levodopa stock was diluted in filtered PBS to 3, 10, 25, 40, and 50 µM. DPV traces were smoothed (3-point moving average) and baseline-corrected (linear fit; peak window 0.10-0.25 V), with the blank-subtracted peak current taken as the signal. Calibration used the ascending, nonzero, valid peak-current points, and each electrode is presented as a representative response.

Fig. 22 presents the DPV raw sweeps and resulting calibration curves for all three gates across the ascending/descending series. All three gates produced concentration-dependent peak currents, with the ascending and descending calibration fits closely tracking one another; Gate 2 (R^2 = 0.99 asc, 0.98 des) and Gate 3 (R^2 = 0.96 asc, 0.97 des) in particular show strong linearity and near-overlapping directional fits. The close agreement between ascending and descending curves at matched concentrations indicates that peak current depends on the present levodopa concentration rather than on the electrode's concentration history, confirming that binding and release are reversible and do not suffer from significant hysteresis. Gate 1's run was cut short (data available only through 25 µM descending), so its reversibility is established over a narrower window and its fit is correspondingly weaker (R^2 = 0.88).

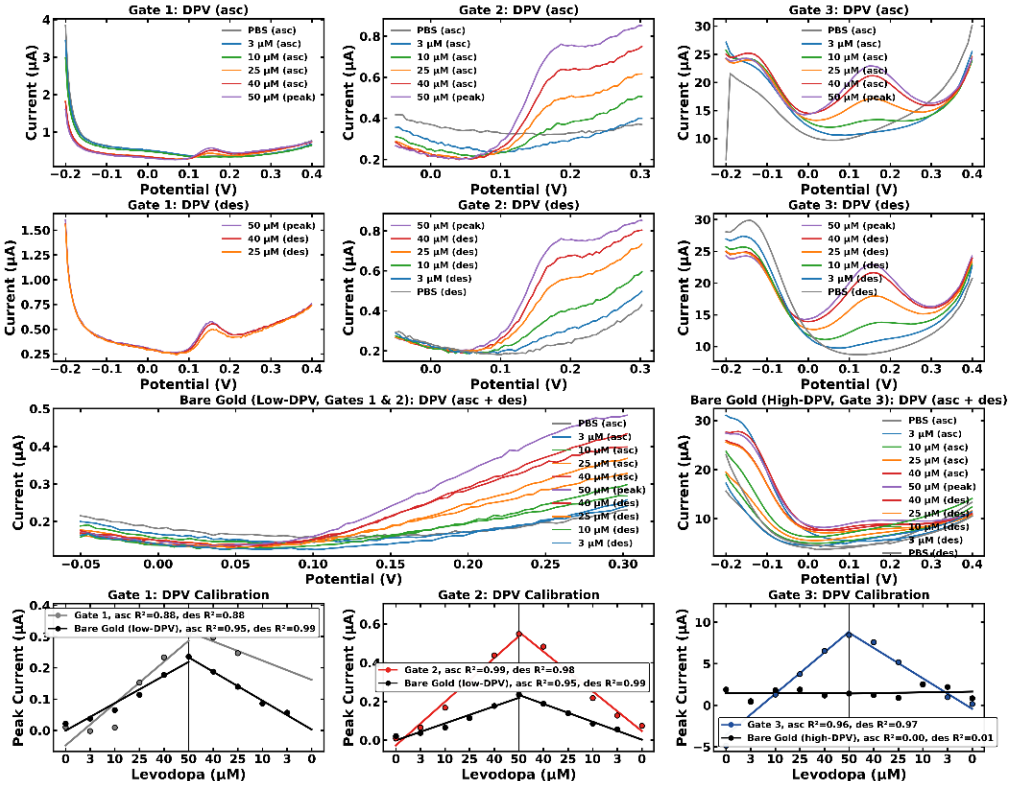


Fig. 22. DPV raw sweep curves (rows 1–2) and bare gold reference raw sweep curves (row 3) for Gates 1, 2, and 3, across an ascending/descending 0–50–0 µM levodopa concentration series. Row 3 bare gold references were run on the same low-DPV (Gates 1 & 2, spanning both columns) and high-DPV (Gate 3) instrument ranges as their respective gates (Section 8.5.4). Row 4 calibration curves show each gate's own data alongside its same-range bare gold reference. DPV calibration currents were extracted via per-curve baseline correction followed by a shared, gate-specific optimized redox potential (averaged from each gate's three highest-concentration curves). Limitation: Gate 1's run was cut short, with data available only through 25 µM des (8 of 11 expected points); remaining concentrations are shown as gaps on a shared axis rather than omitted entirely, for direct visual comparison with the other gates. The descending calibration fit line is extrapolated from the last measured point out to 0 µM using that same fit's slope and intercept, and should not be interpreted as measured data over that extrapolated range.

Fig. 23 presents the corresponding OCP responses, extracted as the final equilibrium potential of each 15-minute period. The OCP data reproduce the same qualitative concentration dependence seen in the DPV results, with potential shifting systematically with levodopa concentration and following the same ascending/descending trend, independently corroborating that the recognition chemistry is responding to levodopa at the polymer–electrolyte interface. However, the OCP calibration fits are markedly weaker and noisier than the DPV fits (R^2 ranging from ~0.55 to ~0.79 across gates), reflecting the lower signal-to-noise and limited amplification inherent to a passive potentiometric readout. The OCP results therefore serve as a proof of

concept, confirming that the binding event produces a measurable interfacial potential change, but are not sufficient for standalone sensing at the required sensitivity. This limitation motivates the transduction step of the final device: coupling the recognition chemistry to an organic electrochemical transistor (OECT), whose intrinsic gain amplifies these interfacial potential shifts into a robust, continuously readable signal.

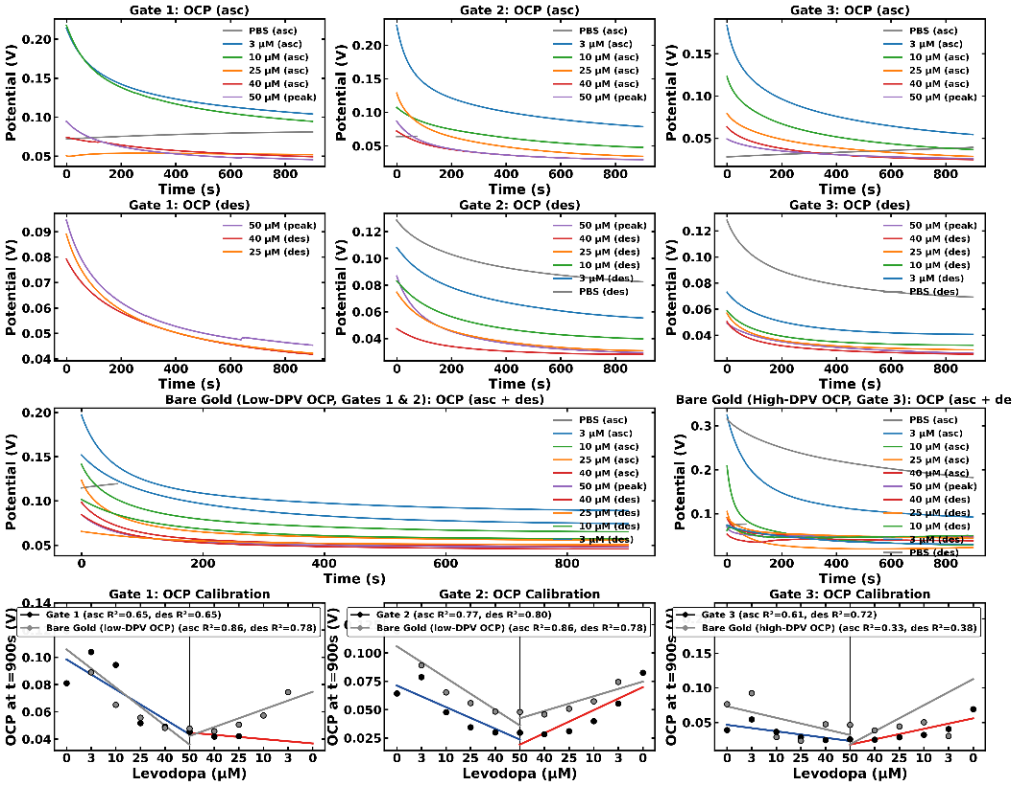


Fig. 23. OCP raw sweep curves (rows 1–2) and bare gold reference raw decay curves (row 3) for Gates 1, 2, and 3, across an ascending/descending 0–50–0 µM levodopa concentration series. Row 3 bare gold references were run on the same low-DPV (Gates 1 & 2, spanning both columns) and high-DPV (Gate 3) instrument ranges as their respective gates (Section 8.5.4). Row 4 calibration curves show each gate's own data alongside its same-range bare gold reference. OCP calibration voltages were extracted via a shared, gate-specific optimized reference time (the minimum of the three highest-concentration curves' own last recorded times), with every curve's voltage read at that same shared time via interpolation rather than each curve's own independent endpoint. Limitation: Gate 1's run was cut short, with data available only through 25 µM des (8 of 11 expected points); remaining concentrations are shown as gaps on a shared axis rather than omitted entirely, for direct visual comparison with the other gates. The descending calibration fit line is extrapolated from the last measured point out to 0 µM using that same fit's slope and intercept, and should not be interpreted as measured data over that extrapolated range.

8.5.4 DPV low & high settings

To balance sensitivity against dynamic range across the three recognition chemistries, differential pulse voltammetry (DPV) was run under two pulse-amplitude

settings: a low-sensitivity setting (LDPV) and a high-sensitivity setting (HDPV). The LDPV setting used a pulse amplitude of 0.025 V and was applied to Gates 1 and 2 (boronic AAPBA and cationic APTAC), where it preserved peak resolution across the expected levodopa range and avoided premature signal saturation. The HDPV setting used a pulse amplitude of 0.2 V and was applied to Gate 3 (hybrid AAPBA + APTAC), amplifying the signal-to-noise ratio to resolve the weaker, more complex binding response of the dual-chemistry gate. Assigning each gate the pulse amplitude matched to its binding behavior ensured that every chemistry operated within its optimal electrochemical window, enabling accurate, chemistry-resolved levodopa detection across the tested concentration range.

Table A4.

Pretreatment Settings Applied to all Gates Prior to DPV Measurement

Setting	Value
E Condition	-0.05 V
t Condition	5 s
E Deposition	0.0 V
t Deposition	0 s

Table A5.

Differential Pulse Voltammetry Parameters for the Low- (LDPV) and High-Sensitivity (HDPV) Settings

Setting	LDPV (Gates 1, 2)	HDPV (Gate 3)
t Equilibrium	0 s	0 s
E Begin	-0.05 V	-0.2 V
E End	0.30 V	0.40 V
E Step	0.005 V	0.01 V
E Pulse	0.025 V	0.2 V
t Pulse	0.05 s	0.02 s
Scan Rate	0.025 V/s	0.05 V/s

Note. Pulse amplitude (E pulse) is the only parameter that differs between the two protocols.

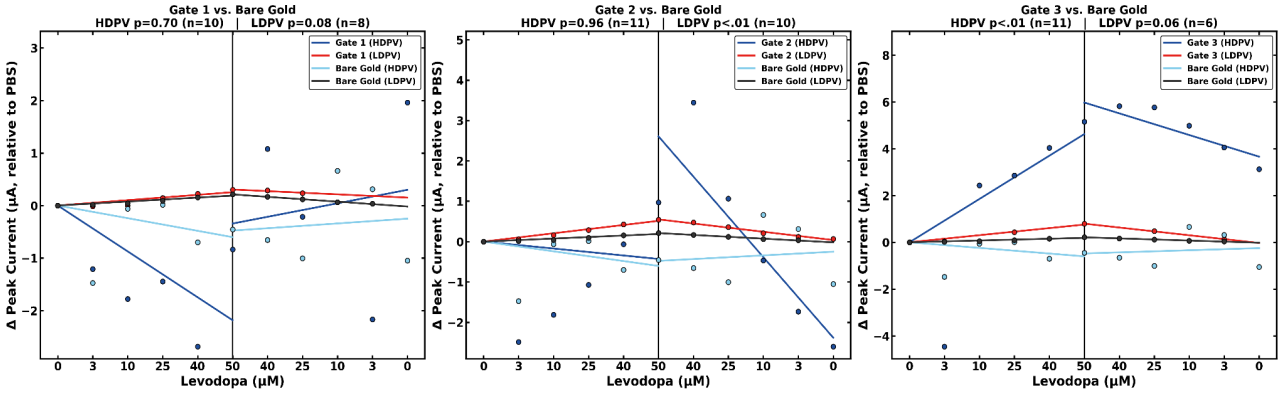


Fig. 24. DPV calibration curves for each gate compared against bare gold on the same instrument range (high- and low-DPV), with paired two-tailed t-tests (paired across matched ascending/descending concentration points) assessing whether each gate's response differs significantly from bare gold on that range. Each series is normalized to its own PBS (0 µM, ascending) value, so every curve starts at 0 and subsequent points reflect the change in peak current relative to that sample's own PBS baseline; this removes baseline current offset differences between samples before comparing their responses, both visually and in the significance test: Gate 1 vs. bare gold: HDPV t=-0.40, p=0.70 (n=10); LDPV t=2.03, p=0.08 (n=8). Gate 2 vs. bare gold: HDPV t=-0.05, p=0.96 (n=11); LDPV t=4.81, p=9.55e-04 (n=10). Gate 3 vs. bare gold: HDPV t=4.01, p=2.48e-03 (n=11); LDPV t=2.48, p=0.06 (n=6).

8.5.5 Specificity Control: Levodopa vs. PBS Soak

To confirm that the DPV response arises specifically from levodopa binding to the recognition chemistry, two negative controls were performed using the soak protocol described in Section 8.5.3. First, Gate 3 was tested under a PBS-only soak in place of the levodopa soak. As shown in Fig. 25, the PBS-soak condition produced no concentration-dependent peak current, confirming that the signal is driven by the presence of levodopa rather than by soaking, incubation time, or handling artifacts. Second, a non-functional polyacrylamide (PAM) electrode was tested under identical levodopa and PBS conditions. PAM shares the same polymer backbone as the three recognition elements but lacks the boronic and cationic binding groups, and showed no concentration-dependent DPV response. Together, these controls establish that the sensor response is specific both to the presence of levodopa (PBS control) and to the engineered recognition groups (PAM control), rather than to the polymer backbone or the measurement conditions themselves.

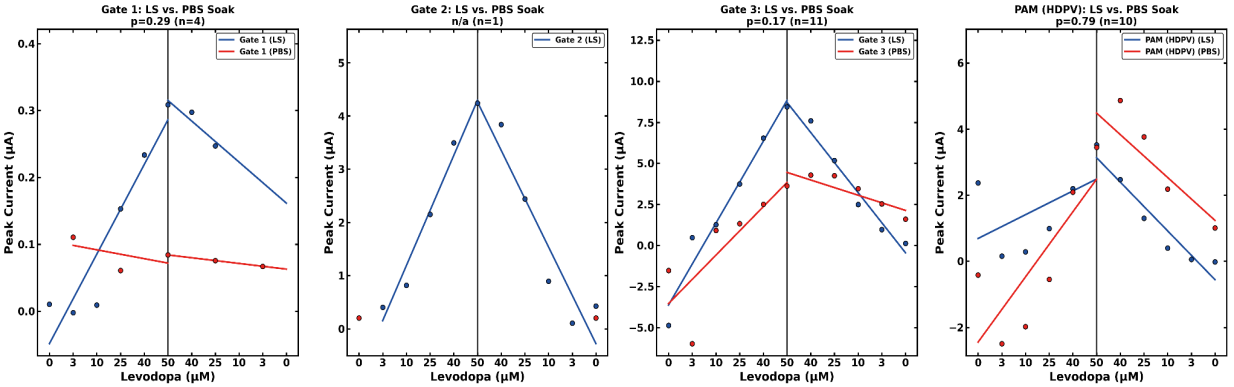


Fig. 25. DPV calibration curves for Gate 1, Gate 2, Gate 3, PAM (HDPV) comparing levodopa-soak (LS) to PBS-only-soak conditions, with paired two-tailed t-tests (paired across matched ascending/descending concentration points) testing whether LS and PBS soak differ significantly for each sample: Gate 1: p=0.29 (n=4). Gate 2: n/a (n=1). Gate 3: p=0.17 (n=11). PAM (HDPV): p=0.79 (n=10). PAM, a non-specific-binding control, is included to test whether any LS-vs-PBS difference observed for Gates 1-3 reflects genuine levodopa-specific recognition beyond simple non-specific entanglement in the polyacrylamide matrix: an insignificant (or comparatively weaker) LS-vs-PBS difference for PAM alongside a significant (or comparatively stronger) difference for Gates 1-3 would support specific binding at the gates.

8.5.6 Long-Term Shelf Stability Testing

During the process of electrochemical validation, electrodes were made in batches of 10–30 electrodes at a time, and anywhere from 2–5 electrodes would be tested in a day, so multiple electrodes were used weeks after their production. Furthermore, in the long term, the polymer must be able to withstand storage under room-temperature conditions for extended periods, one of the primary advantages of an inorganic recognition element and a key factor informing its implementation. Hence, to assess the effects of long-term storage on the electrodes as validation for both the results obtained from older electrodes and the claim that an inorganic polymer remains more stable over time, DPV and OCP were run on a previously fabricated APTAC-functionalized electrode that was tracked after 21 days to quantify drift in baseline signal, peak position, and sensitivity relative to an identically prepared electrode immediately after its production.

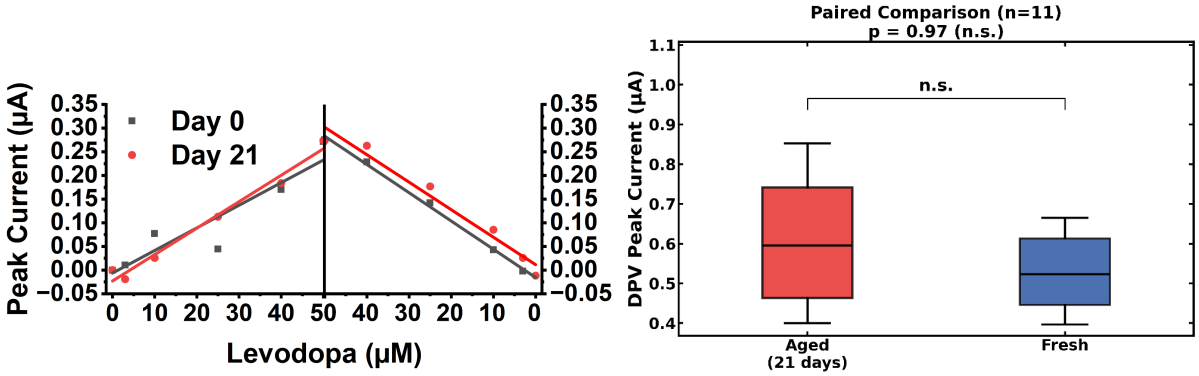


Fig. 26. DPV peak current comparison between an aged Gate 2 electrode (21 days old) and a fresh Gate 2 electrode, evaluated across a matched ascending/descending levodopa concentration series (n = 11 matched concentration/direction points; PBS, 3, 10, 25, 40, 50 uM). (Left) Peak DPV current across the full concentration series for both electrodes. (Right) Paired comparison of peak currents across all matched points. A one-tailed paired t-test (testing whether aged electrode peak current is lower than fresh electrode peak current) showed no statistically significant difference (mean change = +13.1%, p = .969).

8.6. OECT Device Fabrication

8.6.1. Synthesis of PEDOT:PSS Channel

Poly(3,4-ethylenedioxythiophene):poly(styrene sulfonate) (PEDOT:PSS) is a conducting polymer complex comprising two components. PEDOT is a conjugated polymer that becomes electrically conductive upon oxidation: removal of electrons from the polymer backbone generates positive charge carriers, or "holes," which hop along and between polymer chains to produce hole current. PSS serves as the counter-ion, electrostatically compensating these positive charges along the PEDOT backbone. In an

organic electrochemical transistor (OECT) configuration, where the PEDOT:PSS channel is in direct contact with an electrolyte, application of a positive gate voltage drives cations from the electrolyte into the polymer film. These cations pair with PSS sites, compensating the positive polarons on PEDOT, thereby reducing the density of mobile hole carriers throughout the film volume and decreasing channel conductivity (Rivnay et al., 2018).

Because PSS is water-soluble, 3-glycidoxypropyltrimethoxysilane (GOPS) is commonly incorporated as a crosslinker to render PEDOT:PSS films insoluble and mechanically stable in aqueous environments. This crosslinking process, however, tends to reduce film conductivity, an effect that can be offset by incorporating ethylene glycol (EG) as a secondary dopant. A surfactant such as dodecylbenzenesulfonic acid (DBSA) is also commonly added to improve film spreadability and wetting during processing (Tumová et al., 2023).

To prepare the channel formulation, PEDOT:PSS (Ossila PH1000) was stirred at 100 rpm while EG, DBSA, and GOPS were added sequentially in specified proportions. Following 30 minutes of mixing, the solution was transferred to a conical tube and sonicated for 15 minutes to ensure homogeneous dispersion, then filtered to remove residual aggregates.

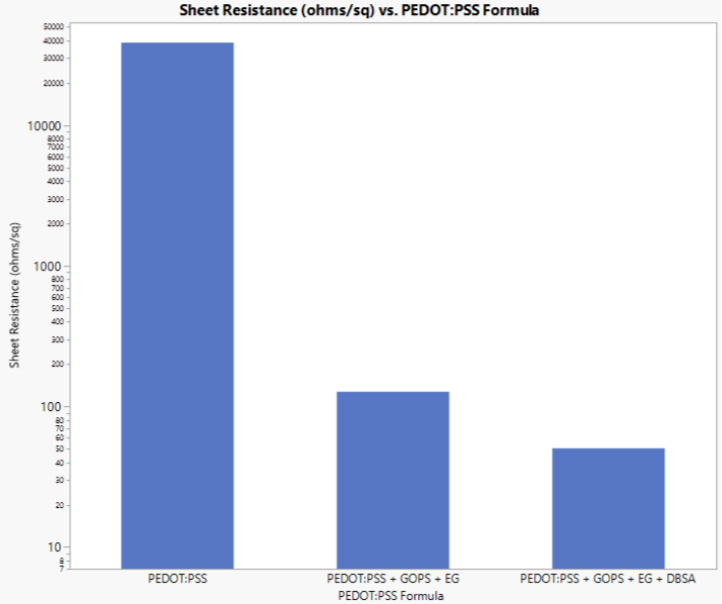


Fig. 27. Sheet resistance of PEDOT:PSS (PH1000) films with varying additive formulations. Films were spin-coated at 4000 rpm onto glass slides from three formulations: (1) unmodified PEDOT:PSS, (2) PEDOT:PSS + EG + GOPS, and (3) PEDOT:PSS + EG + GOPS + DBSA. Sheet resistance was measured using a four-point probe.

As shown in Fig. 27, incorporation of EG and GOPS substantially reduced the sheet resistance of the resulting PEDOT:PSS films, indicating a corresponding increase in conductivity. Among the formulations tested, a composition of 93.82% PEDOT:PSS, 4.94% EG, 0.99% GOPS, and 0.25% DBSA was selected for OECT fabrication, as the inclusion of DBSA improved film spreadability during processing while preserving high conductivity.

8.6.2. Deposition of PEDOT:PSS Channel

Rather than employing lithographic patterning and electrodeposition to fabricate custom OECT geometries, commercially available electrodes (Metrohm C220-AT) were utilized as the device substrate. These electrodes, designed for electrochemical testing, comprise a gold working electrode, a gold counter electrode, and a silver pseudo-reference electrode. In this configuration, the gold working and counter electrodes serve as the source and drain contacts, respectively, while the pseudo-reference electrode is either employed as a gate (Section 8.7.1) or, more commonly, passivated and excluded from the circuit.

To establish electrical continuity between the source and drain electrodes via a PEDOT:PSS channel, an acrylic passivation layer was deposited over all exposed gold not intended for coating, defining a confined well between the two electrodes. This well was patterned using a laser-cut vinyl mask, 1 mm in width, which constrained the PEDOT:PSS during deposition and ensured consistent channel spacing and coverage across samples, yielding a nominal 1 mm × 1 mm channel geometry. Samples were spin-coated to achieve uniform film thickness across devices, corresponding to an estimated 120 nm based on manufacturer specifications (Ossila, 2026).

Prior to masking and passivation, electrodes were sequentially rinsed in acetone, isopropyl alcohol (IPA), and deionized (DI) water, then dried under a nitrogen stream. Following masking, passivation, and mask removal, samples were plasma-cleaned for 2 minutes to eliminate residual organic contaminants and enhance surface wettability.

To deposit the channel film, the electrode substrate was affixed to a flat chuck and secured on a spin coater under vacuum. Three microliters of the PEDOT:PSS formulation were drop-cast into the patterned well and spin-coated at 500 rpm for 45 seconds. The resulting film was subsequently cured on a hot plate at 140°C for 1 hour.

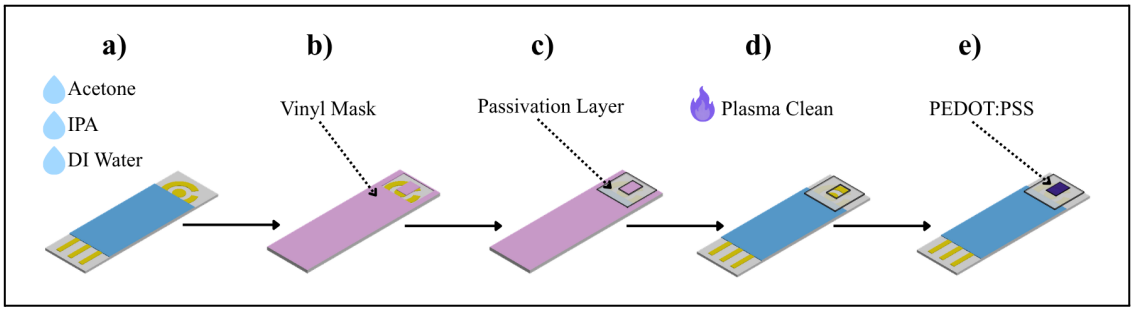


Fig. 28. OECT fabrication process. (a) Electrodes (Metrohm C220-AT) are sequentially rinsed with acetone, isopropyl alcohol (IPA), and deionized (DI) water for 30 seconds each. (b) A laser-cut vinyl mask is applied to define the channel region. (c) A passivation layer is deposited over the unmasked region. (d) The electrode is plasma-treated for 2 minutes. (e) PEDOT:PSS is drop-cast into the well left by mask removal and spin-coated to achieve consistent channel thickness. The electrode is then cured at 140°C for 1 hour to complete PEDOT:PSS crosslinking.

8.7 Experimental Setup(s) of OECT Devices

8.7.1. Silver Gate Electrode

Preliminary OECT characterization employed a silver gate electrode, corresponding to the pseudo-reference electrode integrated into the commercially available Metrohm substrate. During device fabrication, the masking process was applied to both the channel region and the pseudo-reference electrode, preserving each from passivation. Utilizing this pre-existing electrode as the gate offered the advantage of a fixed, planar geometry relative to the channel, ensuring consistent gate-to-channel spacing and exposed surface area across devices.

To characterize OECT performance with an unfunctionalized silver gate, 20 µL of NaCl solution at a specified concentration was applied dropwise across the gate and channel, forming a continuous droplet to bridge both electrodes for testing. Transfer sweeps were performed across a gate-source voltage (V_{GS}) range of -0.6 to 0.6 V at drain-source voltage (V_{DS}) biases of -0.1, -0.3, -0.5, and -0.7 V. Transconductance curves were extracted from the resulting transfer curves, and calibration curves were derived from the drain current response at a V_{GS} of -0.5 V (Fig. 29). Reported curves were truncated at ±0.5 V to exclude edge effects observed near the sweep limits, likely attributable to insufficient equilibration time between successive V_{DS} bias steps.

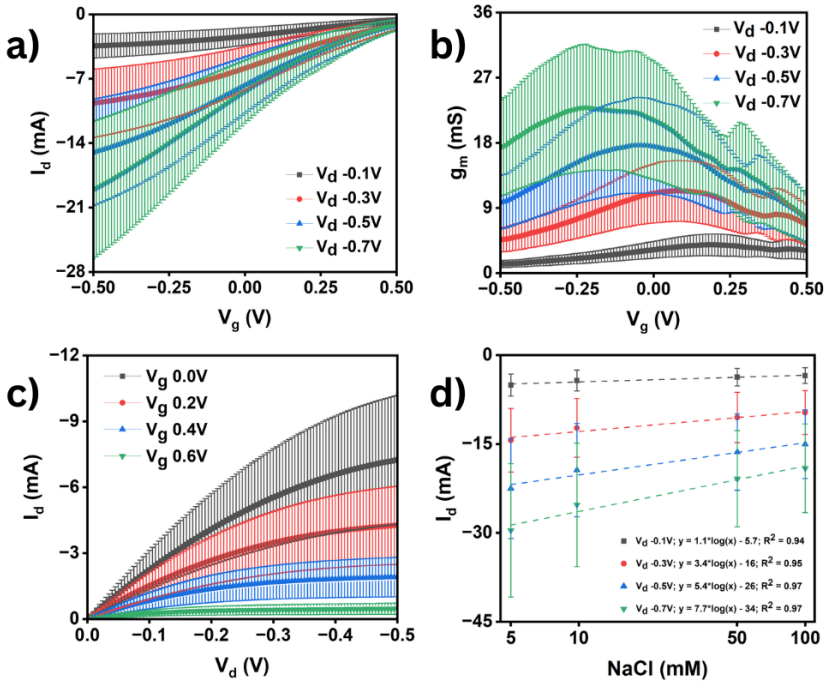


Fig. 29. Characterization of OECT devices with a silver gate (n = 3). (*a*) Transfer curves in 100mM NaCl, (*b*) Transconductance curves extracted from the derivative of *a*, (*c*) Output curves in 100mM NaCl, (*d*) Transfer response over NaCl concentrations at a gate voltage of -0.5V. R^2 values are 0.94, 0.95, 0.97, and 0.97 for V_{DS} values of -0.1, -0.3, -0.5, and -0.7V, respectively. Error bars portray standard deviation from mean response.

These preliminary measurements exhibited larger error bars relative to subsequent experiments, primarily due to fabrication methodology: channel masking in this dataset was performed by hand rather than by the laser-cut masking process adopted in later experiments, resulting in channel width variations on the order of several hundred micrometers across devices. Because transconductance and drain current are highly sensitive to channel geometry, this variability introduced substantial measurement scatter. Despite this, strong R^2 values were obtained across replicates, indicating that device response remained consistent once channel width variation was accounted for.

Notably, visual inspection revealed the gradual formation of a surface layer on the silver gate electrode over the course of testing, suggesting an undesired electrochemical side reaction at the gate, potentially involving chloride-mediated corrosion or oxidative film formation on the silver surface. This behavior indicates that silver is not a suitable candidate for functionalized gate electrode use in this system, as faradaic signals attributed to gate-analyte interactions could instead arise from this parasitic surface reaction rather than from binding events at a functionalized recognition layer. This finding directly informed the subsequent transition to gold gate electrodes (Section 8.7.3), which offer superior electrochemical inertness for functionalization.

8.7.2. Ag/AgCl Gate

To validate the use of a Digilent Analog Discovery 3 (AD3) unit as an alternative to the Keithley dual source meter employed in all other OECT experiments (Sections 8.7.1, 8.7.3, and 8.7.4), a single OECT device was characterized using a chlorinated silver wire gate electrode. Because the AD3 does not directly measure current, drain current values are instead computed from measured voltage and known resistance, introducing additional measurement noise relative to direct current sensing.

Without applying signal smoothing, transfer sweeps were performed from 0 to 1 V under V_{DS} biases of -0.1, -0.3, and -0.5 V, and output sweeps were performed from 0.1 to -0.7 V under V_{GS} biases of 0.2, 0.4, and 0.6 V. The resulting current noise propagated into the derived transconductance curves, substantially complicating extraction of peak transconductance values. Calibration curves were instead generated from the output response at a fixed drain voltage of -0.7 V (Fig. 29), circumventing the need for transconductance extraction from noisy transfer data.

Despite this measurement noise, strong R^2 fits across replicates indicate that the underlying transistor behavior remained consistent, suggesting that the observed variability arises primarily from the AD3's indirect current-sensing method rather than

from device-to-device inconsistency. Future work will incorporate signal smoothing and filtering methods to improve transfer curve resolution and enable more reliable transconductance extraction, further validating the AD3 as a viable low-cost alternative to bench-top source meters for field-deployable OECT readout.

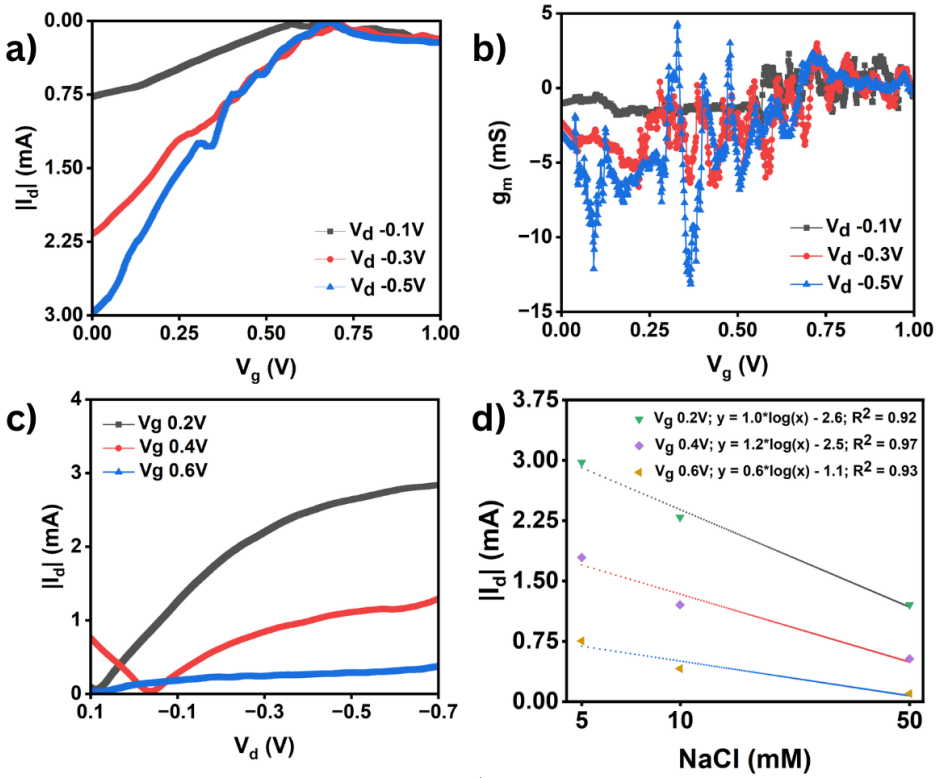


Fig. 30. Characterization of OECT devices with a Ag/AgCl gate (n = 1). (*a*) Transfer curves in 5mM NaCl, (*b*) Transconductance curves extracted from the derivative of *a*, (*c*) Output curves in 5mM NaCl, (*d*) Output response over NaCl concentrations at a drain voltage of -0.7V. R^2 values are 0.92, 0.97, and 0.93, for V_g values of 0.2, 0.4, and 0.6V, respectively.

8.7.3. Gold Wire Gate

Gold wire gate electrodes (0.005-inch diameter) were selected following comparative characterization against alternative gate materials, owing to their ease of functionalization via thiol-based surface chemistry and their electrochemical inertness relative to silver-based alternatives (Sections 8.7.1, 8.7.2). Prior to testing, gold wire electrodes were cleaned by sequential rinsing in acetone, isopropyl alcohol (IPA), and deionized (DI) water, followed by nitrogen drying, to remove surface contaminants prior to droplet-based electrolyte contact.

To increase exposed surface area relative to a straight wire geometry, each gold wire gate was coiled into a spiral configuration prior to testing. Gate electrode placement relative to the channel was maintained at an approximate 1 mm standoff distance, held consistent across trials through the use of a fixed probe station setup. As with the silver

gate configuration (Section 8.7.1), a 20 µL droplet of NaCl solution was applied across the gate and channel to establish electrolytic contact for each measurement, with concentrations spanning 5–50 mM NaCl tested to characterize baseline OECT response across a physiologically-relevant ionic strength range prior to recognition-layer functionalization. Three replicate trials were performed using independently fabricated OECT devices to assess device-to-device reproducibility (Fig. 4).

Unlike the silver gate electrode (Section 8.7.1), no visible surface film formation was observed on the gold wire gate over repeated measurement cycles, supporting its selection as an electrochemically stable platform for subsequent recognition layer functionalization. Notably, the spiral geometry adopted here increases exposed gate surface area in a manner not directly comparable to the planar gold wafer electrodes used in later, functionalized-gate experiments (Section 3.2.2; Section 8.7.4), as immersion depth for the wire gate was not precisely controlled. One possible explanation for the comparable transconductance values observed between the unfunctionalized wire gate and the functionalized wafer gates is the increased surface area of the wafer, which could offset the reduction in effective binding-site density expected from polymer-layer blocking effects on the functionalized wafer surface.

8.7.4. Gold Wafer Gate

Planar gold wafer electrodes (5.6 mm × 10 mm) were subsequently adopted as the gate substrate to increase exposed surface area and thereby improve system sensitivity. This geometry also offers more precise, reproducible placement within the completed flow cell architecture, although the flow cell design had not yet been finalized at the time of these experiments. Critically, the planar wafer geometry closely resembles that of the gold screen-printed electrodes previously functionalized and validated through electrochemical testing (Section 3.2.1), enabling more direct comparison between electrochemical characterization and OECT-based transduction than was possible with the spiraled wire gate configuration (Section 8.7.3).

To ensure consistent gate placement, a probe station setup analogous to that used in Section 8.7.3 was employed, maintaining an approximate 1 mm gate-to-channel distance. Each measurement utilized 40 µL of 1x phosphate-buffered saline (PBS) containing the appropriate levodopa concentration. A single OECT device was used across all experiments (n = 1 per electrode condition), with only the gate electrode exchanged between trials. Four gate conditions were evaluated: PAM (unfunctionalized control), AAPBA-functionalized, APTAC-functionalized, and AAPBA-APTAC hybrid-functionalized

gold wafer electrodes. Each electrode was tested across a series of increasing levodopa concentrations, immediately followed by a series of decreasing concentrations, to assess both response magnitude and reversibility.

Transfer sweeps were performed from -1 to 0 V under VDS biases of -0.3, -0.5, and -0.7 V. Reported curves were truncated at -0.9 V to exclude unwanted edge effects near the sweep limit. Peak transconductance values were extracted for each gate condition, including the PAM control, and used to generate calibration curves under both increasing and decreasing concentration conditions (Fig. 31).

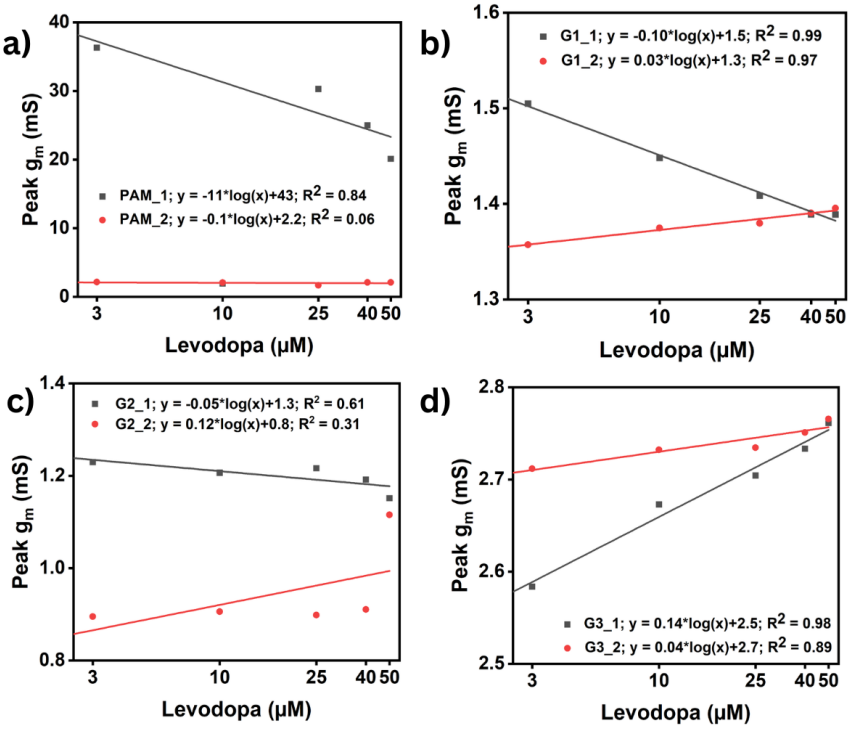


Fig. 31. OECT calibration curves generated for each gate using a gold wafer electrode in increasing and decreasing levodopa concentrations, denoted by X_1 and X_2, respectively (n = 1). (*a*) Calibration curves generated from peak transconductances for a PAM-functionalized gate under V_d bias of -0.7V. (*b*) Calibration curves generated from peak transconductance for Gate 1 under V_d bias of -0.3V. (*c*) Calibration curves generated from peak transconductance for Gate 2 under V_d bias of -0.3V. (*d*) Calibration curves generated from peak transconductance for Gate 3 under V_d bias of -0.7V.

These calibration curves demonstrate strong fits overall, particularly for the increasing-concentration series measured first. Reversibility upon subsequent concentration decrease was comparatively weaker, though the response trends observed still suggest potential for reliable gate performance with further protocol refinement. This limited reversibility is likely attributable to inconsistent flushing procedures during experimental setup. While the experimental design intended to flush each concentration with the subsequent target concentration to simulate continuous sensing, the flow configuration permitted flushing of the channel but not of the gate electrode itself. This likely allowed residual fluid and previously bound levodopa molecules to persist at the

gate surface, producing a progressive decline in transconductance response across the decreasing-concentration series. Future experiments will employ the completed flow cell to ensure consistent gate electrode placement, uniform exposed gate surface area, and effective flushing at both the channel and gate. Given that polymer reversibility was independently confirmed via differential pulse voltammetry (DPV) (Section 3.2.1), Once flushing limitations are addressed, comparable reversibility is expected within the OECT platform.

The unfunctionalized PAM control exhibited high conductance during the increasing-concentration series but showed minimal response change during the subsequent decreasing-concentration series, suggesting that high levodopa concentrations may have saturated or otherwise blocked the polymer surface, forming an effectively insulating barrier for the remainder of the experiment. This behavior will be further investigated in future trials. The 10 µM data point for the increasing PAM series was identified as an outlier and excluded from best-fit calculations.

Calibration curves were additionally generated from raw drain current responses, yielding improved fits across all gate conditions, though with potentially reduced consistency across independent devices (Fig. 33). Future work will therefore include expanded device-to-device variability testing, as well as assessment of signal retention from a single OECT device over extended operation.

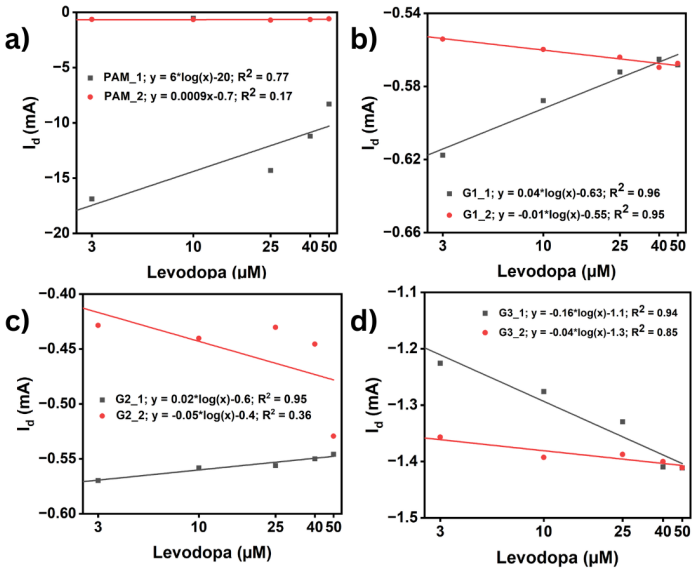


Fig. 32. OECT calibration curves generated for each gate using a gold wafer electrode in increasing and decreasing levodopa concentrations, denoted by X_1 and X_2, respectively (n = 1). (*a*) Calibration curves generated from drain current response for a PAM-functionalized gate under V_{GS} bias of -0.9V and V_{DS} bias of -0.7V. (*b*) Calibration curves generated from drain current response for Gate 1 under V_{GS} bias of -0.7V and V_{DS} bias of -0.3V. (*c*) Calibration curves generated from drain current response for Gate 2 under V_{GS} bias of -0.7V and V_{DS} bias of -0.5V. (*d*) Calibration curves generated from drain current response for Gate 3 under V_{GS} bias of -0.9V and V_{DS} bias of -0.7V.

8.7.5. Sensitivity and Limit of Detection Calculations

For field-effect biosensors (FETs/OECTs) evaluated across logarithmic concentration ranges, logarithmic sensitivity is defined as the absolute value of the slope of the calibration response curve, expressed as the change in transconductance per decade change in logarithmic concentration, in units of mS/decade (Ceccardi et al., 2025).

Because each gate condition was evaluated using a single run (n = 1) without multiple independent zero-concentration replicates, a direct blank-standard-deviation noise estimate was not available. IUPAC standards specify that, in such cases, the standard error of the regression residuals be used as the baseline noise estimate instead. This value is calculated as the square root of the sum of squared differences between each measured response and its corresponding regression-predicted value, divided by the number of calibration points minus two. For each gate, this calculation was based on five non-zero calibration concentrations (3, 10, 25, 40, and 50 µM) (Ceccardi et al., 2025).

Limit of detection (LOD) was calculated using the standard regression-noise method, in which the minimum detectable concentration corresponds to the point at which the signal change exceeds three times the regression noise floor. In practice, this is determined by dividing three times the residual standard error by the absolute sensitivity (slope) of the calibration curve, then raising 10 to that resulting power to convert from a logarithmic value back to a concentration in µM. This method was selected as it does not depend on the specific magnitude of the blank response and is therefore less sensitive to potential baseline drift between the blank measurement and the calibration series.

Table A6.

Sensitivity and LOD Calculations Disaggregated based on Gate

Gate	VDS	R^2	Sensitivity	Standard Error	LOD
G1	−0.3 V	0.9922	0.09807 mS/decade	0.00504 mS	1.426 µM
G2	−0.3 V	0.6056	0.04675 mS/decade	0.02185 mS	25.234 µM
G3	−0.7 V	0.9789	0.13503 mS/decade	0.01147 mS	1.799 µM

8.8 Stakeholder Interviews

8.8.1. Patient-Centered Questions

1. How long have you been diagnosed with Parkinson's Disease, and when did you first begin to notice the symptoms?
2. What are some of the biggest challenges of Parkinson's, and how have you faced them?
    a. What medications, if any, have helped you face them? (unless previously addressed)
3. When do you normally take your medication? Are there consistent periods where you can feel it wear off?
    a. What signs tell you to take your medication? (unless previously addressed)
    b. Would you wear a device that monitors your day-to-day medication fluctuations and alerts you when to take the next dose? (unless previously addressed)
4. Do you currently track your symptoms or manage Parkinson's by using an app or smart device?
    a. What is your biggest challenge in tracking/reporting symptoms? (unless previously addressed)
5. What symptoms or issues do you think researchers should focus on to improve quality of life for individuals with Parkinson's Disease?

8.8.2. Caregiver-Centered Questions

1. How long has your {patient/family member} been diagnosed with Parkinson's Disease, and when did you first begin to notice their symptoms?
2. What do you believe to be the biggest challenges of Parkinson's for both caregivers and patients, and what has your role been in facing them?
    a. What medications, if any, have appeared to be the most effective for the treatment of Parkinson's Disease? (unless previously addressed)
3. When does your {patient/family member} normally take their medication? Are there consistent periods where you can tell that it is wearing off?
    a. What signs tell you that it is time for your patient/family member to take their medication? (unless previously addressed)
    b. Would you recommend your patient/family member wear a device that monitors their day-to-day medication fluctuations and provides an alert when it is time to take the next dose? (unless previously addressed)

4. Do you currently track your {patient's / family member's} symptoms or manage Parkinson's by using an app or smart device?
    a. What is your biggest challenge in tracking/reporting symptoms? (unless previously addressed)
5. What symptoms or issues do you think researchers should focus on to improve quality of life for individuals with Parkinson's Disease?

8.8.3. Physician-Centered Questions

1. What is your role in the {hospital/clinic}, and how do you engage with Parkinson's patients?
2. What are some of the biggest challenges you see {patients/caregivers} face?
3. What does a typical treatment plan for Parkinson's Disease look like and how do you modify it for each patient?
    a. Any other treatments? Dosing? Diagnosis? (unless previously addressed)
4. How many clinical visits does each Parkinson patient usually need, and what usually occurs during those visits?
5. What additional data or procedures would boost your confidence in medication adjustments?
    a. Follow up: What type of data would be ideal for treatment progression?
    b. Follow up: For real-time/continuous levodopa sensing, how would the ideal presentation of data for interpretation look like?
    c. Do you see yourself using something like this in your standard of care practice?

8.8.4. Industry Professional-Centered Questions

1. Do you have 3-5 pieces of general advice regarding communicating the intricacies of our sensor to {consumers/judges/others} who may not have the same scientific background?
    a. What mistakes do academic teams most often make when trying to translate medical sensors from lab use to clinical use? (unless previously addressed)
2. What barriers do you see to patient adherence or usability with continuous monitoring technologies?
3. Are there other emerging technologies (nanomaterials, microfluidics, AI-driven dosing algorithms) that you believe could reshape Parkinson's treatment?

4. Do you have any advice on how to respond to questions of scaling capabilities regarding the complex nature of our device?
5. If you were evaluating this technology internally, what criteria would determine whether it's worth pursuing? What milestones would you want to see before industry investment becomes realistic?
    a. What are 3-5 things that we, as a team, should be doing now to better polish our business model, given that a prototype is still in the works? (unless previously addressed)

8.8.5. Clinical Researcher-Centered Questions

1. How does your research address the unresolved challenges in levodopa-based Parkinson's treatment?
    a. How is your training optimized to solve these challenges, and what skillsets outside of your present experience do you think are most needed to resolve said challenges? (unless previously addressed)
2. How do you approach the issue of plasma levodopa levels not necessarily corresponding with clinical response?
    a. How do you evaluate whether a new delivery technology meaningfully improves therapeutic consistency? (unless previously addressed)
3. Are there other emerging technologies (nanomaterials, microfluidics, AI-driven dosing algorithms) that you believe could reshape Parkinson's treatment?
    a. What technical or regulatory hurdles do you anticipate for a levodopa-monitoring biosensor paired with a therapeutic? (unless previously addressed)
4. What unanswered questions about levodopa pharmacology or patient response remain most pressing for industry?
5. If you were evaluating this technology internally, what criteria would determine whether it's worth pursuing? What milestones would you want to see before industry investment becomes realistic?

8.8.6. Interviewee Demographics

Table A7.

Overview of Interviewed Stakeholders

Interviewee Code	Description	Company
P01	P01 was diagnosed with a tremor-dominant subtype of PD in 2018. Having found levodopa to be largely ineffective before obtaining relief through deep-brain stimulation (DBS), their experiences provided valuable perspective on surgical interventions.	[redacted]
P02	P02 was diagnosed with PD in 2019 after noticing a persistent right-side tremor. They actively take six carbidopa-levodopa tablets daily but emphasized that non-motor challenges impact quality of life to a greater extent than tremors.	
P03	Managing motor symptoms through a frequent six-dose carbidopa-levodopa regimen, P03 struggles with apathy, and severe fatigue as their medicine wears off frequently. Diagnosed with PD in 2021, P03 favors a non-invasive continuous biosensor to maintain steady medication levels and prevent off periods.	
P04	P04, diagnosed within the last year, provided a unique perspective on early-stage disease management. Their input highlighted the challenges of newly navigating life with PD, offering key insights into the clinical support needs of recent diagnoses.	
P05	Diagnosed with PD in 2019, P05 manages mild motor symptoms using a daily carbidopa-levodopa and rasagiline regimen alongside regular exercise. Leading a local support group, they emphasized the social and financial burdens of the disease.	
P06	Diagnosed with PD in 2022, since diagnosis has taken carbidopa-levodopa. P06 highlighted short-term memory loss being the their greatest struggle with PD, otherwise, finds it manageable.	

P07	P07 was diagnosed in 2012, but had been experiencing symptoms long before, but was unable to receive an official diagnosis until 2012. They have been taking carbidopa-levodopa since diagnosis but have recently switched formulas to Crexont. P07 provided unique insight into barriers to access to care and treatment, and other valuable information on daily struggles, confounding factors, and coping strategies.	[redacted]
P08	They were initially diagnosed in January 2021 and started taking carbidopa-levodopa in May 2021. P08 introduced environmental factors that led to PD, such as Agent Orange and pesticides used in golf course management. They highlighted the burden placed on daily life due to PD. From their background in academia, P08 emphasizes the need for continuous biosensing for research in PD.	[redacted]
P09	Diagnosed with PD in 2021 after noticing a combination of non-motor symptoms, P09 manages their condition through intensive daily exercise as well as a carbidopa-levodopa regimen. Drawing on their background as a nurse, P09 stressed the variability of patient symptoms and the need for individualized treatment.	[redacted]
P10	Diagnosed with PD in 2012, P10 manages unpredictable motor off times and balance issues while relying on a non-strict carbidopa-levodopa schedule. Their experience validates the clinical need for a continuous biosensor to track medication levels in real time.	[redacted]
P11	Diagnosed with PD after experiencing a variety of motor and non-motor symptoms, PD12 was largely unable to tolerate oral carbidopa-levodopa and successfully underwent DBS. Drawing on their 40-year career as a nurse, they maintain a positive outlook and stress the value of a continuous levodopa biosensor and integrated digital dashboard.	[redacted]

C01	C01 is the primary caregiver for their husband, who has navigated complex PD therapies including oral carbidopa-levodopa, enteral pumps, and subcutaneous infusions. Throughout their journey, C01 has faced significant friction with device maintenance and administrative barriers.	[redacted]
C02	Speaking as the primary caregiver for their wife, C02 highlighted the complex daily logistics of managing a strict four-dose carbidopa-levodopa schedule alongside competing health conditions like chronic back pain.	
C03	As Executive Director of Partnerships with Rock Steady Boxing — The Carolinas and a columnist for *Parkinson's News Today*, C03 navigates the realities of managing her husband's advanced PD through her writing and advocacy.	
D01	A movement disorder specialist, D01 explained that treatment decisions rely heavily on patient self-reporting, as clinical exams capture only a brief snapshot of fluctuating symptoms.	Atypical Parkinsonism Center at UNC Hospitals
D02	A movement disorder specialist who focuses on DBS for advanced PD, D02 relies on structured patient self-reporting to guide clinical decision-making. While acknowledging the value of closed-loop systems, they noted that a major barrier to continuous levodopa sensing is the challenge of modeling how peripheral ISF levels correlate with central nervous system drug concentrations.	Neurology at UNC Hospitals
D03	As a clinical speech-language pathologist within a multidisciplinary care team, D03 evaluates and treats PD patients for speech, swallowing, and cognitive-communication challenges. They highlighted how PD's depletion of dopamine heavily impairs a patient's intrinsic motivation, validating the clinical need for automated monitoring.	Speech Pathology at Duke Hospital
D04	D04 is a primary care geriatrician who co-manages PD patients alongside neurologists, with a clinical focus on the holistic management of advanced disease progression. Drawing from their	UNC Hospitals

	experiences, D04 emphasized the importance of conservative dosing strategies.	
D05	D05 is a professor in Clinical Neurology and works as a movement disorder specialist, serving individuals with PD. Her holistic approach to treatment fostered conversations regarding diet and mental health support when considering PD management.	Movement Disorder Clinic at UM Hospital
D06	A primary care physician, D06 co-manages PD patients with Neurology, focusing on monitoring disease progression, medication side effects, and comorbidities. He expressed a strong interest in objective monitoring tools for patient mobility and mood.	Geriatrics at UF Hospital
D07	D07 is a clinical and movement disorder specialist with decades of experience in diagnosing PD through standardized assessments like the UPDRS, a 50-question tool used to measure the severity and progression of PD, alongside participating in Phase 2 and 3 clinical trials for emerging therapeutics. D07 indicated that continuous sensing technology would be more impactful for pharmaceutical research and clinical trials than for standard care.	Neurology at Duke Hospital
I01	An electrical engineer, I01 provided targeted technical feedback on device setup, advising a simplified electrical design as well as the analysis of both Faradaic and non-Faradaic behavior. His recommendations established a clear path forward to correct the remaining technical challenges.	PalmSens
I02	A systems engineer, I02 provided technical and strategic guidance on bridging the gap between academic biosensor research and commercial manufacturing. They emphasized optimizing microfluidic design for scalable production and maintaining rigid risk management frameworks for regulatory approval.	Demcon
I03	Heavily involved with strategy, quality, regulatory, clinical research, and global commercial marketing, I03 advised	Medtronic

	refining the business plan by establishing realistic market penetration, accounting for insurance reimbursement, and structuring pitches around a strong narrative hook.	
I04	I04 is an industrial engineering and finance professional with expertise in direct investments, biotech acquisitions, and startup valuation. They provided advice regarding our market segmentation and suggested restructuring conversations with businesses around engaging storytelling and product differentiation.	Cemvita Inc
I05	I05 serves as an analytical developer at UCB, and they highlighted that PD clinical trials are severely hampered by subjective, inconsistent patient-reported data. They emphasized that continuous wearable sensors would dramatically streamline trials and accelerate regular approvals.	UCB Pharma
R01	R01, a UNC researcher, leverages the continuous glucose monitor framework to develop an enzyme-based levodopa sensor for PD management. They emphasized that clinical adoption depends on calibrating ISF measurements directly to patient symptoms rather than raw brain concentrations.	Sode Lab at UNC-Chapel Hill

Note. Given that all interviews were anonymized prior to analysis, each individual was assigned a unique interviewee code. The first letter corresponds to the position or title of the interviewee and aligns with the following key: C = Caregiver; D = Physician; I = Industry Professional; P = Patient; R = Clinical Researcher.

8.8.7. Identified Stakeholders and Adoption Factors

Table A8.

Value, Opportunity, Risk, and Adoption Barrier Associated with a Wearable and Continuous Levodopa Biosensor Disaggregated by Stakeholder

Stakeholder	Value	Adoption Barrier	Opportunity	Risk
Patients	Improves self-management; reduces complex dosing regimens; maximizes "on time"	Social stigma of wearing medical device; lack of actionable benefit	Motivated patients could become product advocates, working seamlessly with our KOLs	Data pipeline vanishes if patients abandon the device
Caregivers	Improves patient management, even when patient struggles to verbalize their condition	Increased level of involvement due to software analysis may lead to technical burnout	Able to ensure appropriate device function while using output to optimize individualized care	Patient may lack independence to leverage the technology on their own
Physicians	Replaces subjective and unreliable patient journals and self-reporting with objective, continuous data	Data fatigue when exposed to continuous data streams; PK data only relevant when compiled into concise reports	Allows for rapid medication adjustments in order to optimize individualized dosing regimens in an efficient manner	Comprehensive output data may be unnecessary or difficult to interpret
Researchers	Replaces limited data provided by UPDRS; continuous and objective metrics to evaluate emerging therapies	Extensive cross-validation against HPLC standards are necessary; strict data integrity requirements	Early use in clinical trials establishes device as a standard within the realm of academic literature, moving toward broader clinical use	Sensor will initially lack peer-reviewed backing and scientific validation
Pharma	Validates the therapeutic stability of levodopa-based drugs in real time; useful in clinical trial validation	Accurate data on effectiveness of levodopa-based drug and any unideal characteristics	Bundling biosensor alongside medication would greatly expedite clinical trials by providing a wealth of relevant data	Large pharma companies could back other digital diagnostic tools

MedTech	Allows company to expand existing line of PD-related products (mainly pumps) into the expanding data-driven neurology market	Disputes over IP; concerns regarding scaling/manufacturing capabilities	Rapid scaling from manufacturing plants and global supply chains; could integrated with pump as closed-loop solution	Development of competing biosensors or other rival technologies

Note. HPLC = High-Performance Liquid Chromatography; KOLs = Key Opinion Leaders; MedTech = Medical Technology Companies; Pharma = Pharmaceutical Companies; PK = Pharmacokinetic.

8.8.8. Qualitative Inductive Coding Findings

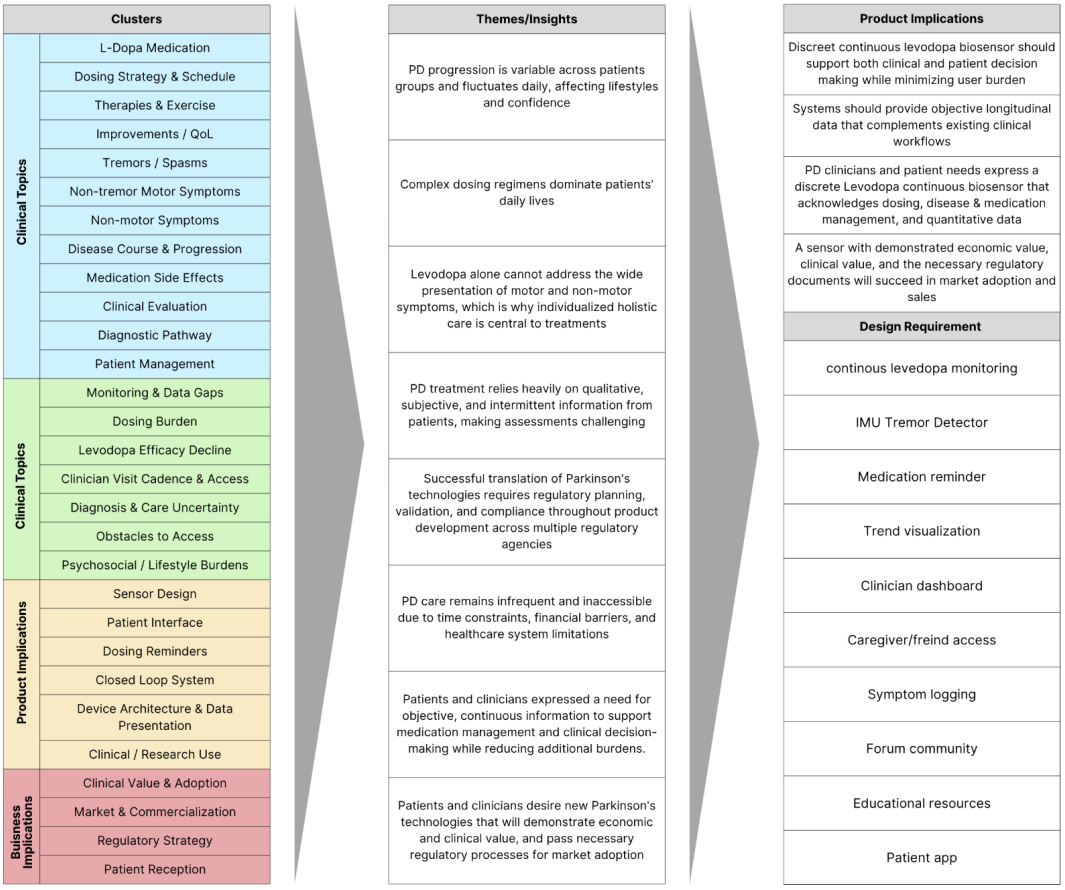


Fig. 33. Findings from Qualitative Inductive Coding Process

8.9. Market Analysis

The Parkinson's monitoring landscape can be broadly divided into three non-overlapping sectors. Motion-only wearables quantify symptoms continuously but provide no drug-level data. Chemistry-only research prototypes (microneedle and OECT

levodopa sensors from academic labs) detect levodopa but provide no symptom context. Subjective diary-based methods (the Hauser diary and its app variants) serve only as recall-dependent snapshots. There is currently no commercial product that combines continuous levodopa measurement with continuous motor monitoring. AbbVie's Vyalev pump is an adjacent therapeutic product commercialized in 2024; however, it is not a monitoring device. Vyalev is designed to deliver levodopa subcutaneously, but it does not measure drug concentration in ISF. Our device is situated within this well-defined gap as the first continuous monitoring system that combines biochemical levodopa measurement with continuous motor-state tracking.

Translating this patient-centered system into a viable commercial venture begins in the clinical trial pipeline, where continuous and objective biomarker data is in high demand. With approximately 540 active clinical trials worldwide for novel, medication-based PD treatments and the average global pharmaceutical contract for a Phase III trial utilizing continuous biomarker monitoring being $2.5 million per program, the total accessible market (TAM) is $1.25 billion (National Library of Medicine, 2026). Ultimately, only the sector of the market within the United States is serviceable during the early stages of business development. When narrowing the scope to the 140 active Phase III clinical trials in the US market, the serviceable addressable market (SAM) is $350 million. During the first 36 months following regulatory clearance through the FDA De Novo pathway, 10 clinical trial contracts with mid-sized biotechnology companies and specialized neuropharmaceutical innovators are projected to be secured. Based on these assumptions, the serviceable obtainable market (SOM) is projected to be $25 million, capturing approximately 7% of the SAM and 2% of the TAM. The relatively small opportunity within the SOM is justifiable by setting high gross margins. Selling data, subscriptions, and single-use disposable microneedle patches makes it reasonable to set the gross margin at 70%, ensuring that the inherent sensor value is reflected in economic outcomes.

8.10. Companion Software

The Dopametric companion application supports both patients and industry stakeholders through real-time levodopa and symptom monitoring. Designed specifically for users who may experience motor impairment or lower digital literacy, the patient interface utilizes large buttons, simple visual designs, and simplified data trend analyses. A built-in alert system proactively notifies patients when levodopa levels approach therapeutic off periods. Additionally, the platform provides dose timing schedules, a peer

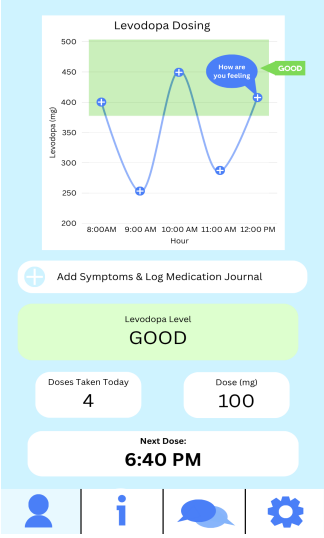


Fig. 34 Landing page for patient software.

community forum, and answers to frequently asked questions. Fig. 33 illustrates the primary features of the landing page in a portrait layout that is optimized for mobile devices.

The portal designed for clinical researchers and biopharmaceutical stakeholders provides a more comprehensive overview of biosensor data. Industry professionals can simultaneously monitor cohort data (Fig. 34) with automated alerts flagging critical levodopa fluctuations, medication regimen changes, or shifts in reported symptoms. Key interface components include detailed levodopa kinetic graphs, customizable data filters for cohort stratification, and direct pathways to patient histories. Quick-access tools enable rapid export of clinical reports, while the underlying architecture ensures that the software operates seamlessly with existing Electronic Health Record systems, minimizing onboarding training.

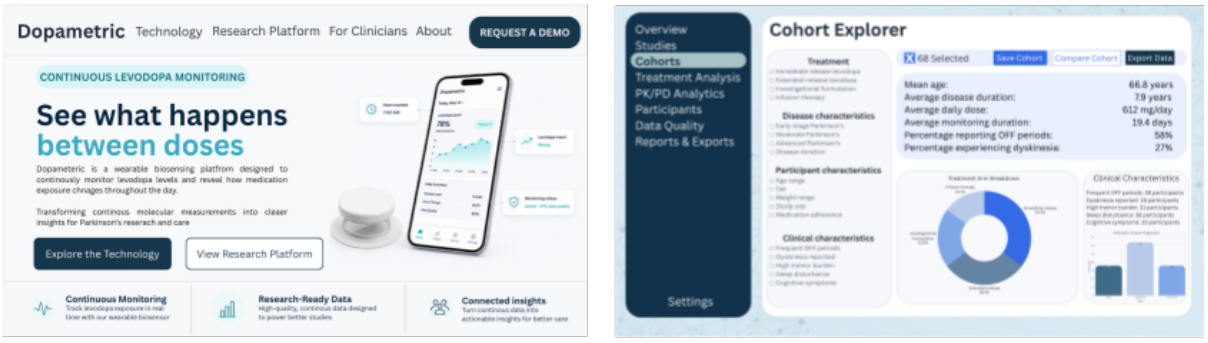


Fig. 35. Mockup of Clinician Dashboard with the landing page (left) and cohorts with patient summaries (right).

8.11. Validation Survey

8.11.1. Survey Questions

The SenseNC Stakeholder Validation Survey was designed as a formative pre-validation tool within the human-centered design framework. Built to capture quantitative feedback subsequent to the initial qualitative interviews, the survey branches into distinct pathways depending on the respondent's role.

Section 1: Demographics

1. Full Name (please note that all results will be anonymized)
2. Contact Information (email address is preferred)

3. The following survey will be catered to your personal experience. Please select the option below that most closely relates to your role
    a. Patient
    b. Caregiver / Family of a Patient
    c. Allied Health (Physician, Clinician, etc.)
    d. MedTech Professional
    e. Pharmaceutical Industry Professional

Section 2: Patient Questions

Responses evaluated on a 5-point Likert Scale: (1) Strongly Disagree, (2) Disagree, (3) Neutral / No Change, (4) Agree, (5) Strongly Agree.

1. *Feature Matrix Ratings* (Evaluated across: Improve PD Management | Be Easy to Use | Easily Integrate into Daily Life | Provide Greater Peace of Mind | Likely Be Used if Available):
    - Continuous Levodopa Monitoring
    - Tremor Detection (IMU Sensor Integration)
    - Medication Reminders or Notifications
    - Sharing Information with Clinician
    - Providing Notification Access to Friend/Caregiver
    - Symptom Logging and Journaling
    - User Forum Community
    - Educational Resources & FAQ
2. *Software Usability & Aesthetics* (Evaluated across Appearance | Color Scheme | Button Size | Text Size):
    - I am satisfied with the _____ of the software.
3. Do you have any remaining questions, feedback, or comments about the device and software?

Section 3: Caregiver Questions

Responses evaluated on a 5-point Likert Scale: (1) Strongly Disagree, (2) Disagree, (3) Neutral / No Change, (4) Agree, (5) Strongly Agree.

1. *Feature Matrix Ratings* (Evaluated across: Improve PD Management | Be Easy to Use | Easily Integrate into Patient's Daily Life | Provide Greater Peace of Mind | Likely Be Used if Available):
    - Continuous Levodopa Monitoring
    - Tremor Detection (IMU Sensor Integration)
    - Medication Reminders or Notifications
    - Sharing Information with Clinician
    - Patient Notification Access to Caregiver
    - Access to Symptom Logging and Journaling
    - Patient Forum Community
    - Educational Resources & FAQ
2. *Software Usability & Aesthetics* (Evaluated across Appearance | Color Scheme | Button Size | Text Size):
    - I am satisfied with the _____ of the software.
3. Do you have any remaining questions, feedback, or comments about the device and software?

Section 4: Allied Health Questions

Responses evaluated on a 5-point Likert Scale: (1) Strongly Disagree, (2) Disagree, (3) Neutral / No Change, (4) Agree, (5) Strongly Agree.

4. *Feature Matrix Ratings* (Evaluated across: Improve PD Care | Be Easy to Implement | Likely Be Used if Available):
    - Continuous Levodopa Monitoring (Biosensor Hardware + Software)
    - IMU Sensor Integration (Tremor Detection)
    - Patient Portal
    - Medication Provider / Pharmacist Portal
    - Data Summary of All Patients (Medication Overview)
    - Data Summary of Individual Patients
5. *Clinical Workflow Confidence*
    - I would be confident in my ability to interpret a patient's 24-hour levodopa trend profile within a standard consultation window.
    - The presence of continuous levodopa data improves my confidence in making specific adjustments to a patient's medication timing or dosage (if ISF and brain levels are correlated)

- The data format, analysis and summary provided align with how I want the data presented and analyzed to improve patient treatment.

6. Do you have any remaining questions, feedback, or comments about the device and software?

Section 5: Pharmaceutical Questions

Responses evaluated on a 5-point Likert Scale: (1) Strongly Disagree, (2) Disagree, (3) Neutral / No Change, (4) Agree, (5) Strongly Agree.

1. Company Name
2. Formal Title
3. *Feature Matrix Ratings* (Evaluated across: Be Easy to Implement | Likely Be Used if Available | Be Worth Investment):
    - Continuous Levodopa Monitoring (Biosensor Hardware + Software)
    - IMU Sensor Integration (Tremor Detection)
    - Clinician Portal
4. *Dashboard Module Utility* (Perceived benefit across Study Search & Comparison | Cohort Explorer | Treatment Analysis | PK/PD Analytics | Participant Profile | Data Quality & Sensor Performance | Reports & Export):.
5. *Commercial & Strategic Alignment*
    - Possessing high-resolution levodopa PD/PK data is highly important for clinical trial analysis.
    - Possessing high-resolution levodopa PD/PK data is highly important for post-market analysis.
    - I can envision a joint venture with a company specializing in continuous levodopa monitoring technology.

Section 6: MedTech Questions

Responses evaluated on a 5-point Likert Scale: (1) Strongly Disagree, (2) Disagree, (3) Neutral / No Change, (4) Agree, (5) Strongly Agree.

1. Company Name
2. Formal Title

3. *Feature Matrix Ratings* (Evaluated across: Be Easy to Implement | Likely Be Used if Available | Be Worth Investment):
    - Continuous Levodopa Monitoring (Biosensor Hardware + Software)
    - IMU Sensor Integration (Tremor Detection)
6. *Dashboard Module Utility* (Perceived benefit across Study Search & Comparison | Cohort Explorer | Treatment Analysis | PK/PD Analytics | Participant Profile | Data Quality & Sensor Performance | Reports & Export):.
7. *Commercial & Strategic Alignment*
    - Possessing high-resolution levodopa PD/PK data is highly important for clinical trial analysis.
    - Possessing high-resolution levodopa PD/PK data is highly important for post-market analysis.
    - I can envision a joint venture with a company specializing in continuous levodopa monitoring technology.

8.11.2. Raw Data from Patients and Caregivers

Survey evaluations from individuals with Parkinson's disease and caregivers demonstrated broad acceptability and strong perceived utility across all evaluated biosensor and software features.

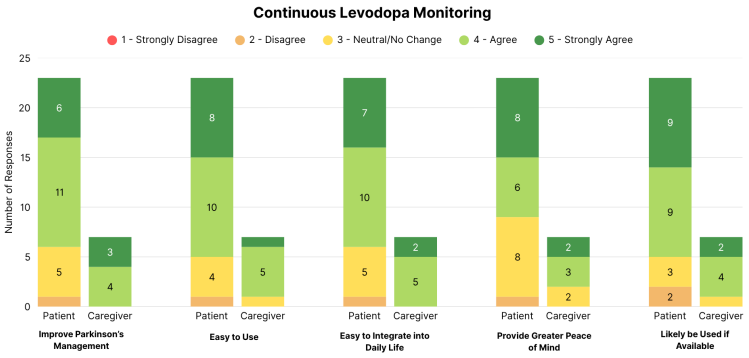


Fig. 36. Distribution of responses from patients and caregivers evaluating continuous levodopa monitoring in a proposed biosensor

Most patients and caregivers agreed or strongly agreed on the utility and ease of use of continuous levodopa monitoring. Disagreement was virtually non-existent, highlighting strong confidence in integrating this feature into routine care.

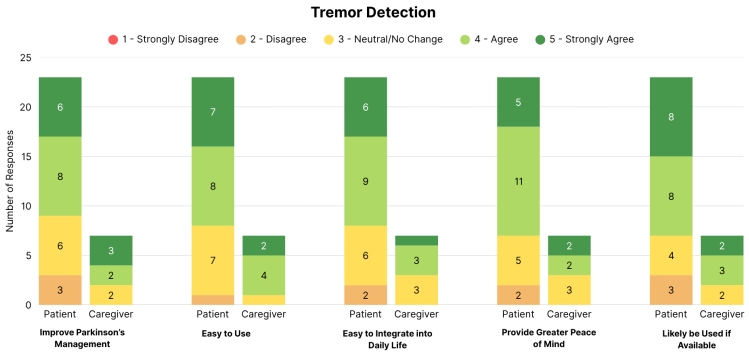


Fig 37. Distribution of responses from patients and caregivers evaluating tremor detection in a proposed biosensor

Feedback on tremor detection was predominantly positive across all metrics, though neutral responses were more frequent than for medication features. Disagreement

remained low, indicating acceptance of tremor tracking as a complementary monitoring tool.

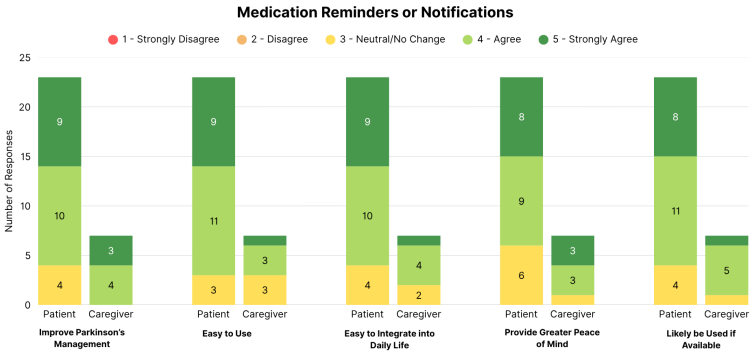


Fig 38. Distribution of responses from patients and caregivers evaluating notifications and reminders to take medications from a proposed software and biosensor.

Medication reminders received exceptionally favorable evaluations, with zero disagreement recorded across both groups. High agreement on ease of use and integration demonstrates that participants found automated notifications intuitive and practical.

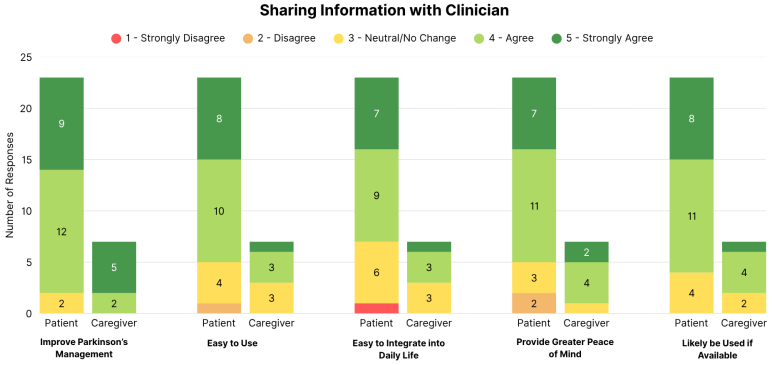


Fig 39. Distribution of responses from patients and caregivers evaluating sharing patient inputted data and biosensor readings to clinicians

Sharing biosensor data directly with clinicians garnered widespread positive support, particularly for improving disease management and providing peace of mind. Disagreement was rare, reflecting strong endorsement of clinician access to longitudinal health data.

Sharing notifications with support networks received mostly positive feedback, driven by high agreement regarding future use and care coordination. Despite minor neutrality and disagreement around ease of use, overall consensus favored shared alerts.

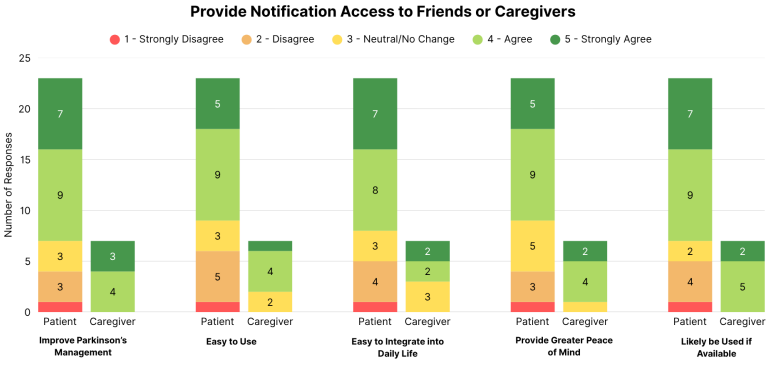


Fig 40. Distribution of responses from patients and caregivers evaluating providing notifications to caregiver or friends pertaining to patient's health and PD management.

Symptom logging achieved consistently high approval, with peak agreement centered on disease management and peace of mind. Negative ratings were minimal, confirming the value of structured tracking for self-management and clinical discussions.

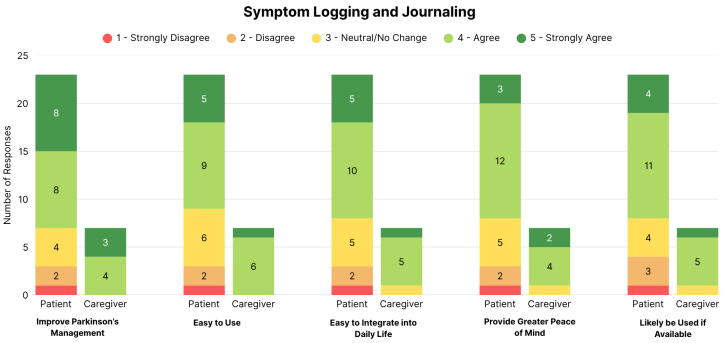


Fig. 41. Distribution of responses from patients and caregivers evaluating in-app software allowing for symptom logging and journaling.

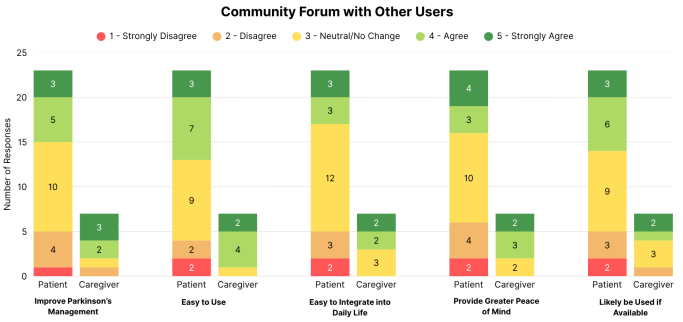


Fig. 42. Distribution of responses from patients and caregivers evaluating an in-app discussion forum feature.

The community forum produced the most varied distribution, marked by a substantial proportion of neutral ratings across criteria. While positive responses remained the largest category, the neutrality suggests peer support was viewed as supplementary rather than essential.

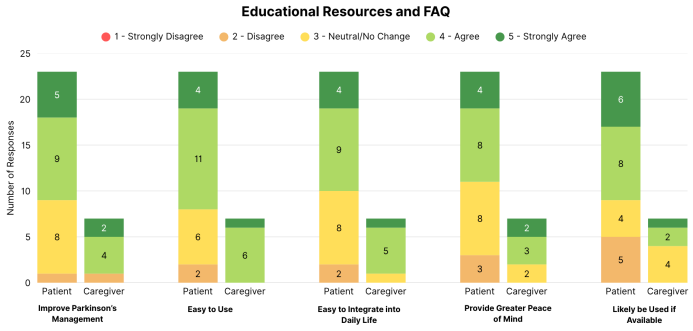


Fig 43. Distribution of responses from patients and caregivers evaluating an in-app educational section and FAQ.

Educational materials and FAQs were well received, earning high marks for ease of use and management utility. Moderate neutral responses appeared regarding peace of mind, but overall sentiment supported access to educational content.

Software design parameters were generally well received, with positive ratings forming the largest response category for button size and text size. While neutral ratings were frequent across visual aspects like color scheme, minor patient disagreement highlighted opportunities for interface customization.

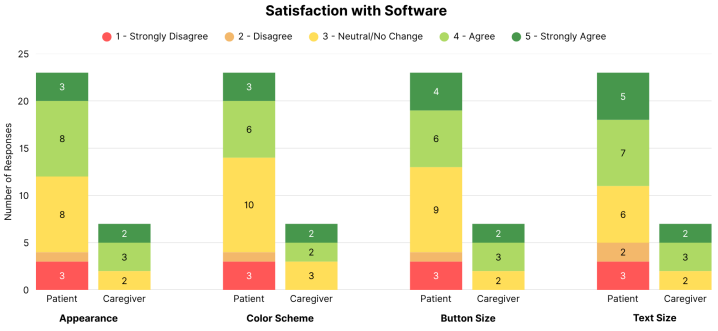


Fig. 44. Distribution of responses from patients and caregivers evaluating visual aspects of the software.

8.11.3. Raw Data from Allied Health Professionals

Clinicians strongly agreed that continuous levodopa monitoring improves Parkinson's care and indicated high likelihood of adoption. However, implementation ease saw predominant neutrality, pointing to potential concerns regarding integration into existing clinical routines, and demonstrates the need for well synthesized data.

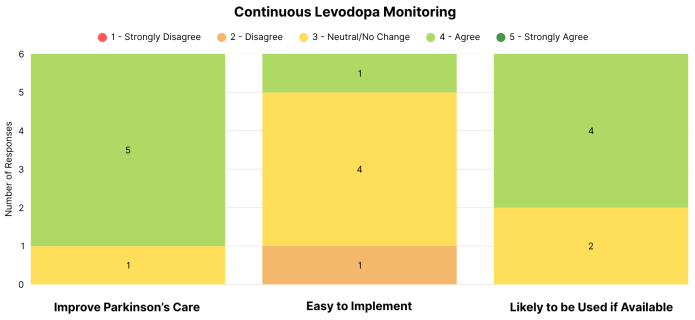


Fig 45. Distribution of responses from allied health professionals evaluating continuous levodopa monitoring.

Providers unanimously agreed that IMU-based tremor detection improves Parkinson's care, with a majority intending to use the capability. Implementation ease drew mostly neutral feedback, reflecting uncertainty around routine setup and operational overhead.

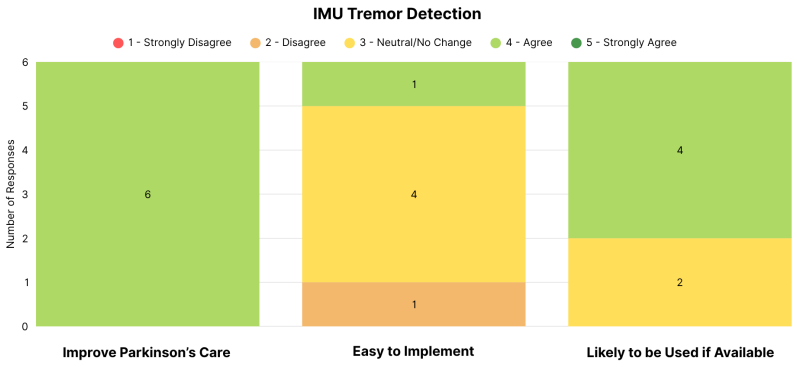


Fig. 46. Distribution of responses from allied health professionals evaluating an IMU based tremor detector.

The patient portal was perceived positively for enhancing patient care, though anticipated adoption was primarily neutral. Implementation ease received mixed feedback, including isolated strong disagreement regarding practical feasibility.

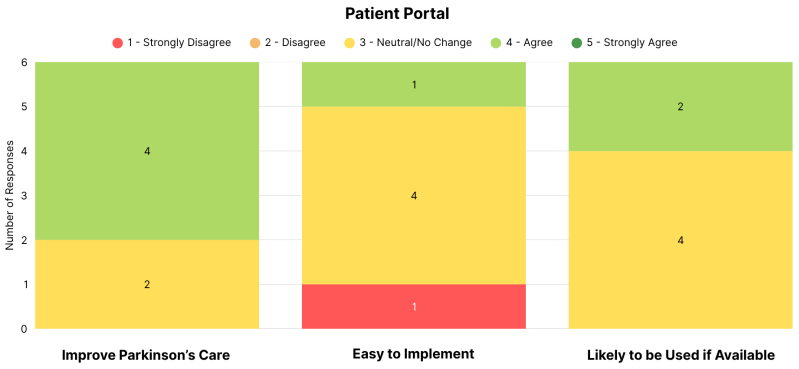


Fig 47. Distribution of responses from allied health professionals evaluating the patient portal.

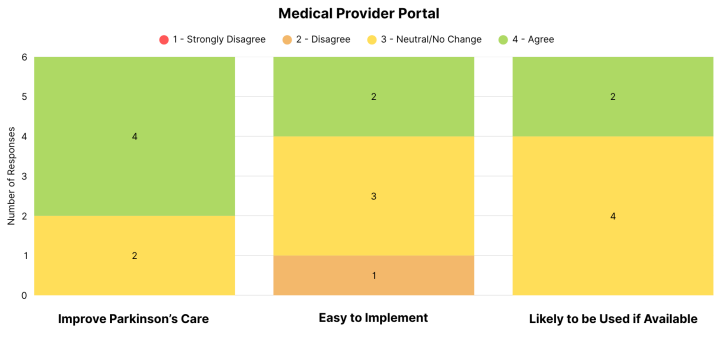


Fig. 48. Distribution of responses from allied health professionals evaluating the medical provider portal.

Clinicians generally acknowledged the provider portal's potential to improve care delivery. Ratings for ease of implementation and future

use slanted neutral, indicating that adoption depends on demonstrating seamless clinical utility.

Aggregate patient summaries generated mostly neutral feedback across care improvement, implementation, and future use. These results suggest providers see less immediate utility in population-level data compared to patient-specific metrics.

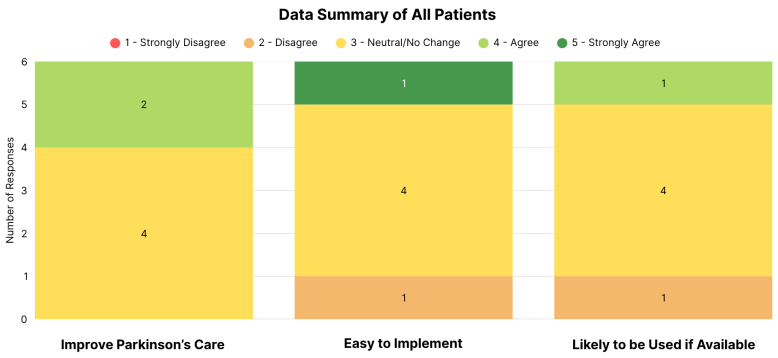


Fig. 49. Distribution of responses from allied health professionals evaluating a synthesized data summary for all patients

Synthesized individual patient summaries received broad endorsement, with nearly all clinicians agreeing on care improvements and expressing high intent to utilize the feature. Implementation ease was balanced between neutral and positive ratings, demonstrating favorable overall clinical feasibility. Further emphasizing how individualized PD care is, a key insight found during the qualitative interview process.

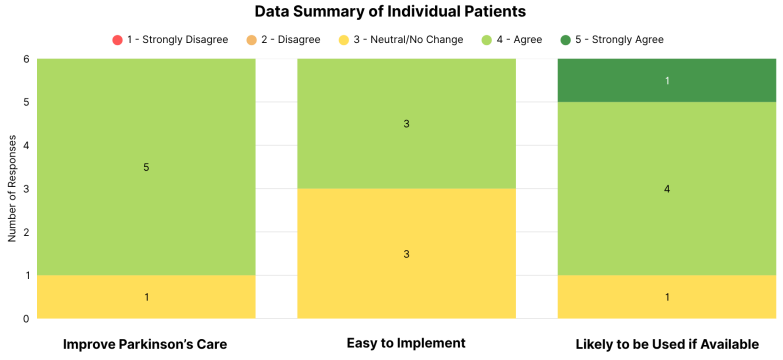


Fig. 50. Distribution of responses from allied health professionals evaluating a synthesized data summary for individual patients.

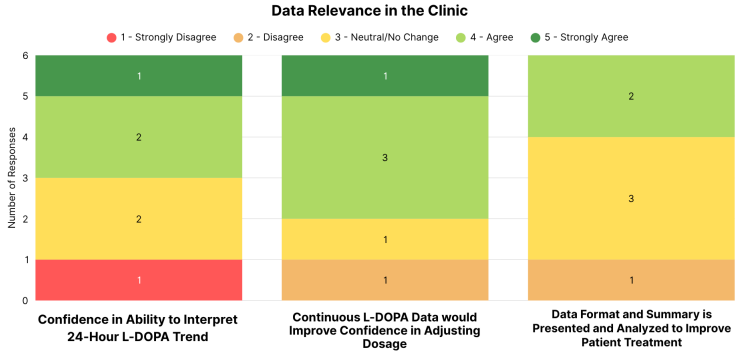


Fig 51. Distribution of responses from allied health professionals evaluating how data will be used in a clinical setting.

Most respondents expressed confidence in interpreting continuous trends and using levodopa data to adjust medication dosages. Sentiment regarding data presentation formats was more reserved, highlighting opportunities to refine analytical summaries for point-of-care decision-making

8.11.3. Raw Data from Pharmaceutical and Medical Technology Industry Professionals

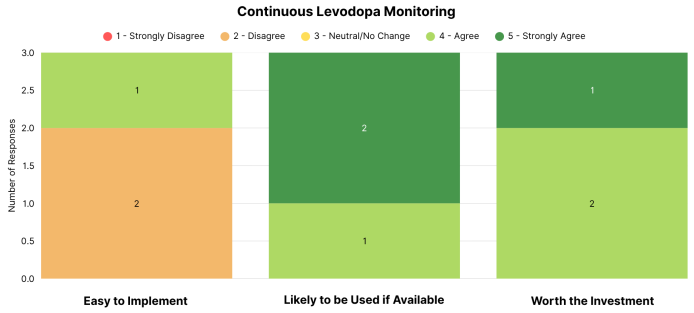


Fig. 52. Distribution of responses from pharmaceutical and medtech professionals evaluating a synthesized data summary for individual patients.

All respondents agreed that continuous levodopa monitoring is worth the investment and highly likely to be used if available. However, execution concerns were evident, with most respondents expressing disagreement regarding ease of implementation. Responses to IMU tremor detection leaned positive regarding future adoption and implementation feasibility. Views on overall investment value were more reserved, with most respondents taking a neutral position on financial return.

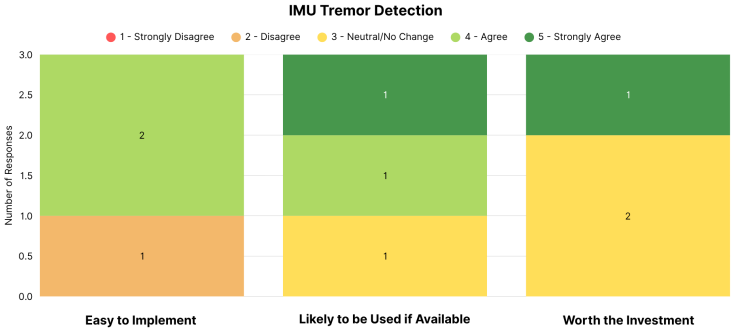


Fig. 53. Distribution of responses from pharmaceutical and medtech professionals evaluating an IMU based tremor detector.

Analytical, PK/PD, participant profile, and reporting pages achieved strong positive ratings across the board for trial management. By contrast, the cohort explorer page recorded the most variable feedback, including both neutral and negative ratings.

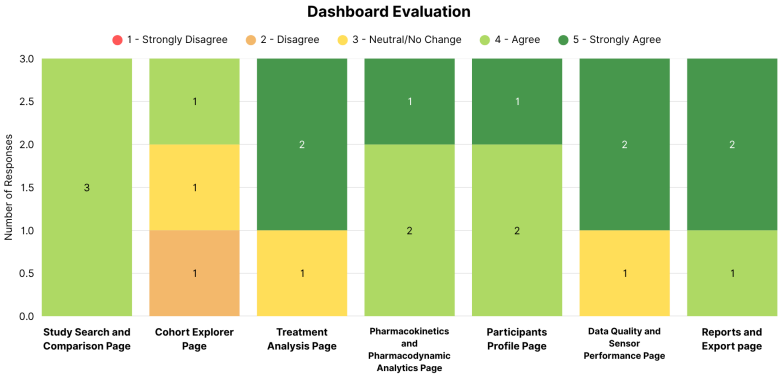


Fig. 54. Distribution of responses from pharmaceutical and medtech professionals evaluating the importances of various dashboard pages.

Stakeholders unanimously affirmed the critical importance of high-resolution PK/PD data for clinical trial analysis. Positive sentiment also extended to post-market surveillance and joint venture opportunities,

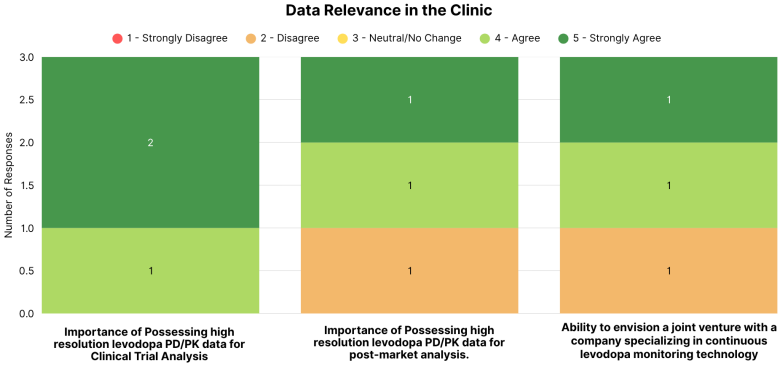


Fig 55. Distribution of responses from pharmaceutical and medtech professionals evaluating the importance of high resolution levodopa PD/PK data in real world scenarios.

despite some disagreement on commercialization approaches.

8.11.4. Statistical Analyses of Responses

To evaluate stakeholder prioritization of the platform's core tracking capabilities, independent Kruskal-Wallis H tests were performed for Continuous Monitoring and Tremor Detection across Patients (PT), Caregivers (CG), Allied Health Professionals (AH), and Industry Professionals (IP). Each feature was evaluated as an independent hypothesis using a significance threshold of $\alpha = 0.05$. The results of these tests are housed in Table A9 along with basic descriptive statistics. When considering descriptive statistics, literature confirms that parametric statistical assessments remain appropriate means of analysis, even when analyzing ordinal data (Norman, 2010; Sullivan & Artino, 2013).

Table A9.

Statistical Analysis Evaluated across Patients (n = 23), Caregivers (n = 7), Allied Health (n = 6), and Industry (n = 3) via Kruskal-Wallis H

Feature	Stakeholder	Median	IQR	Mean (SD)	*H*	df	p-value
Continuous Monitoring	Patient	4	2	4.01 (0.87)	8.73	3	0.032
	Caregiver	4	1	4.17 (0.62)			
	Allied Health	4	1	3.50 (0.62)			
	Industry	4	1	4.00 (1.00)			
Tremor Detection	Patient	4	2	3.84 (0.94)	2.97	3	0.396
	Caregiver	4	2	3.97 (0.79)			
	Allied Health	4	1	3.56 (0.62)			
	Industry	4	2	4.00 (0.87)			

A statistically significant difference in stakeholder ratings was observed for Continuous Monitoring ($\chi^2(3) = 8.78$, $p = .032$). Consequently, post hoc pairwise comparisons were conducted using Dunn's test with a Bonferroni-adjusted significance threshold ($\alpha = .0083$) to control for multiple comparisons. The adjusted analyses

demonstrated that Patients (Mean Rank = 90.73) and Caregivers (Mean Rank = 98.11) rated Continuous Monitoring significantly higher than Allied Health Professionals (Mean Rank = 58.53). No other pairwise comparisons reached statistical significance, with Industry Professionals exhibiting a comparable mean rank (92.39).

In contrast, Tremor Detection demonstrated no statistically significant difference across stakeholder groups ($\chi^2(3) = 2.97$, $p = .396$). Therefore, the null hypothesis was not rejected, indicating that the perceived importance of Tremor Detection was comparable among Patients, Caregivers, Allied Health Professionals, and Industry Professionals. All stakeholder groups reported a median rating of 4.0, with mean ranks of 86.64, 88.86, 69.33, and 92.83 for Patients, Caregivers, Allied Health Professionals, and Industry Professionals, respectively. Although Allied Health Professionals exhibited a descriptively lower mean rank, these differences were not statistically significant, and no post hoc analyses were performed.

These statistical findings demonstrate robust, widespread cross-stakeholder alignment regarding the platform's core functional capabilities, supporting its viability for future clinical deployment. However, the independent analysis uncovers a critical operational outlier that must be addressed prior to deployment: the Allied Health Professional cohort.While Patients, Caregivers, and Industry Professionals uniformly advocate for continuous tracking, Allied Health Professionals scored this capability significantly lower. The statistical drop in their mean rank points directly to practical barriers highlighted in their qualitative comments, specifically concerning escalating workload burnout, acute alarm fatigue, and a lack of seamless clinical workflow integration. Because Allied Health staff are the frontline users often tasked with managing real-time data streams, their lower prioritization reflects valid operational anxiety regarding data triage burdens rather than a rejection of the technology's clinical value. In contrast, the uniform cross-cohort consensus surrounding Tremor Detection highlights a universally accepted, low-friction feature. Because tremor tracking represents an objective diagnostic metric that does not demand constant passive monitoring or trigger continuous alert cycles, it faces relatively low stakeholder resistance. Moving forward, the platform architecture should leverage this overwhelming support for tremor detection as an onboarding wedge, while simultaneously redesigning the Continuous Monitoring dashboard to directly address allied health concerns through automated data filtering and minimized alert frequencies.

As depicted in Table AX, only features requiring direct interaction between Patients and Caregivers were analyzed using Mann-Whitney U tests. These included

Medication Reminders, Clinician Sharing, Caregiver Notifications, Symptom Journaling, Community Forums, Educational Resources, and Software Appearance. Each feature represented an independent hypothesis evaluated at $\alpha = 0.05$. No statistically significant differences were observed for Medication Reminders ($U = 1798.5$, $p = .304$), Clinician Sharing ($U = 1868.5$, $p = 0.492$), Caregiver Notifications ($U = 1660.0$, $p = 0.099$), or Educational Resources ($U = 1694.0$, $p = 0.134$), indicating comparable prioritization of these platform functionalities between stakeholder groups. Statistically significant differences were identified for Community Forums ($U = 1270.0$, $p < 0.001$), Software Appearance ($U = 900.0$, $p = 0.012$), and Symptom Journaling ($U = 1561.0$, $p = 0.031$). Across these features, caregivers consistently assigned higher importance ratings than patients, although the observed effect sizes were small, suggesting modest but reliable differences in stakeholder priorities.

Table A10.

Statistical Analysis Evaluated Between Patients (n = 23) and Caregivers (n=7) via Mann-Whitney U

Feature	Patient Mean (SD)	Caregiver Mean (SD)	Mann-Whitney U	p-value
Medication Reminders	4.19 (0.72)	4.06 (0.63)	1798.5	0.3036
Clinician Sharing	4.09 (0.83)	4.03 (0.75)	1868.5	0.4921
Caregiver Notifications	3.67 (1.17)	4.11 (0.68)	1660	0.0993
Symptom Journaling	3.69 (1.05)	4.14 (0.68)	1561	0.031
Forum	3.19 (1.09)	3.91 (0.92)	1270	0.0005651
Educational Resource	3.68 (0.92)	3.94 (0.73)	1694	0.1341
Software Appearance	3.30 (1.20)	3.96 (0.79)	900	0.0121

Collectively, these findings suggest that patients and caregivers share similar expectations regarding the platform's core clinical support functions while differing in features that facilitate long-term caregiving and user engagement. Caregivers placed greater emphasis on symptom journaling, community forums, and software appearance,

indicating increased value for tools that support longitudinal disease management, peer support, and an intuitive user experience. Although these differences reached statistical significance, their small effect sizes indicate that the overall preferences of patients and caregivers remain broadly aligned.

8.11.5. Hazard Matrix

To ensure patient safety and compliance with the required risk management standards (ISO 14971), a Failure Mode and Effects Analysis was conducted for our levodopa sensor. Potential Hazards spanning physical insertion, electronic operation, and biosensor signal were evaluated based on Occurrence (O), Severity (S), and Detectability (D) to calculate a Risk Priority Number (RPN). As shown in Figure 56, accurate sensing capabilities represent the highest risk, with these false readings posing the greatest threat to clinical outcomes. Much of the technical validation required for

Hazard	Description	O	S	D	RPN
Mechanical Injury	Microneedle array is inserted into a sensitive region or is forcefully removed.	3	5	2	30
Infection	A breach in the sterile field, incomplete sterilization, or contaminated instruments introduce bacteria to the ISF upon insertion.	3	8	6	144
Thermal Injury	Reusable electronic module or battery overheats, causing local epidermal discomfort or tissue burns.	2	7	5	70
Material-Related Complications	Patient experiences localized epidermal irritation or allergic reaction from the adhesive patch.	5	3	2	30
Delayed ISF Concentration Readings	Biosensor latency or biofouling delays levodopa concentration updates, causing clinical misalignment.	5	5	5	125
False Low Levodopa Reading	Biofouling, polymer degradation, or calibration error causes biosensor to report artificially low concentrations, risking patient over-medication.	5	8	8	320
False High Levodopa Reading	Electrochemical interference or signal drift causes sensor to report artificially high concentrations, risking under-medication.	5	8	8	320
Exposure to Polymeric Recognition	Chemical leaching or structural breakdown leads to localized cytotoxic effects or tissue inflammation.	2	8	5	80
Early Detachment	Premature adhesive loss leads to incomplete wear cycles and data loss.	6	4	4	96
Calibration Algorithm Corruption	Corrupted software or telemtry packet results in inaccurate pharmacokinetic trend plotting.	3	7	6	126
Reuse of Single-Use Component	Paitent attempts to reapply disposable sensing module multiple times.	2	8	8	128
Delayed Data Transfer	Trend data transmission is delayed from the wearable patch to the companion software.	5	4	6	120

Fig. 56 Hazard traceability matrix with color-coded (values from 1-10) Occurrence (O), Severity (S), and Detectability (D) levels, based on defined risk ranges.

8.12 Regulatory Pathway

The transition from the current stage of development to commercial deployment is organized into three sequential phases, each building upon the preceding stage. Because commercialization is planned within the United States, regulatory approval from

the U.S. Food and Drug Administration (FDA) will be required prior to market entry, establishing the regulatory pathway described below. (FDA, Premarket Approval (PMA), 2025)

Stage 1: The intellectual property surrounding the novel algorithm developed to correlate compartmental levodopa levels with clinical presentation will be protected via a utility patent, given that this documentation protects how the invention works as well as its usage for a specific purpose (PMC6139778). Because premature public disclosure may limit patent eligibility in many jurisdictions, the United States one-year grace period following public disclosure will be utilized (Bennett E. Kuhar, 2026). Accordingly, a utility patent application will be filed within one year of public disclosure at the SensUs International Student Competition, providing approximately 20 years of intellectual property protection at an estimated total cost of $25,000 (University of Notre Dame, 2026). While patent examination proceeds over the next two to three years, bench and preclinical work runs in parallel: interference validation against the full ISF catecholamine panel, stability testing across a fourteen-day continuous wear period (preliminary results shown in Section 8.5.6), ethylene oxide sterilization process validation (per ISO 11135 / ISO 11137), and first-in-animal pharmacokinetic studies in a rodent Parkinson's model to generate the ISF-to-blood levodopa correlation data that no published group has yet produced. That dataset is the foundation on which the clinical program is built.

Stage 2: The Phase I feasibility study enrolls ten to twenty patients at a single site, using intravenous levodopa administration with simultaneous ISF sensing and liquid chromatography-tandem mass spectroscopy blood reference to confirm pharmacokinetic curve is tracked with sufficient accuracy to justify a pivotal trial. A successful Phase I supports the Phase II pivotal study, which enrolls eighty to one hundred twenty patients across multiple sites on oral levodopa, with structured motor assessments correlated to sensor output and mean absolute relative difference as the primary accuracy endpoint. The data package from Phase II supports the PMA submission under 21 U.S.C. 360e, reviewed by CDRH's Office of In Vitro Diagnostics under 21 CFR Part 862, using the Senseonics Eversense PMA (P160048) as the direct submission template. Upon approval, the PMA would authorize commercialization of the system as a clinician-facing adjunctive continuous levodopa monitoring platform. The device would provide pharmacokinetic trend information to clinicians to support therapeutic decision-making while maintaining physician-directed treatment. Interference testing follows CLSI EP7 guidelines and biocompatibility testing follows ISO 10993 for all skin- and ISF-contacting materials.

Stage 3: Following commercial deployment and accumulation of real-world evidence, two parallel regulatory pathways are anticipated. The expanding pharmacokinetic dataset will continuously validate and refine the prediction algorithm, enabling improved identification of levodopa concentration thresholds and rate-of-change signatures associated with OFF symptom onset. Synchronously, the clinical evidence base supports a De Novo request under 21 U.S.C. 360c(f)(2) to establish a new device classification, the Continuous Levodopa Monitoring System, with tailored special controls under 21 CFR 862. This replicates the 2018 De Novo that created the designation at 21 CFR 862.1355 for integrated CGM systems, causing the device to become a regulatory benchmark that competitors must reference. Non-adjunctive status is the milestone that closes the loop on patient autonomy. A patient sees levodopa levels declining on their device, receives an alert that concentrations are approaching the threshold historically associated with symptom onset for them specifically, and takes a rescue dose proactively. The algorithm driving that alert is reviewed as a Medical Device under FDA's Digital Health Center of Excellence framework, authorized independently from the sensor itself.

8.13 Financial Projections

A cost-of-goods (COGS) analysis was conducted to estimate the manufacturing expenses associated with commercial production of the biosensor platform. The estimated short-term manufacturing cost was $180 per biosensor, consisting of approximately $140 in electrical components, $21 in chemical reagents, and $19 allocated toward packaging and marketing. Based on these production costs, a commercial selling price of $540 per biosensor was selected, providing an approximate three-fold markup to support manufacturing, operational expenses, future development, and profitability.

To evaluate commercial feasibility at different production scales, both short-term and long-term manufacturing models were assessed. The short-term model assumed fixed startup costs of $150,000 with variable manufacturing costs of $180 per biosensor, whereas the long-term model incorporated increased capital investment ($500,000) to represent expanded manufacturing infrastructure while reducing variable production costs to $105 per biosensor through economies of scale.

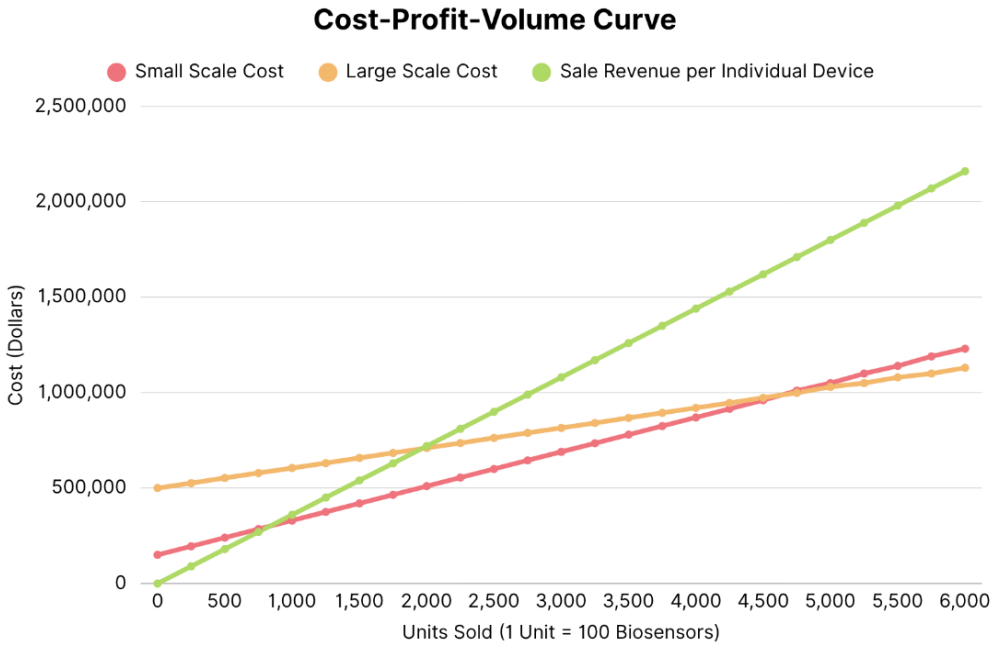


Fig. 57. Cost-Profit-Volume Curve. Relationship between cumulative sales revenue and total production costs under short-term and long-term manufacturing scenarios. Break-even points identify the number of biosensors required for cumulative revenue to equal total costs.

The cost-profit-volume analysis demonstrates the economic advantages of scaling production. Under the short-term model, the projected break-even point occurs at approximately 834 biosensors sold, whereas the long-term manufacturing model reaches break-even at approximately 1,961 biosensors sold because of the substantially larger initial capital investment. Although long-term commercialization requires greater upfront expenditure, reduced manufacturing costs result in improved profitability as production volume increases, supporting large-scale deployment

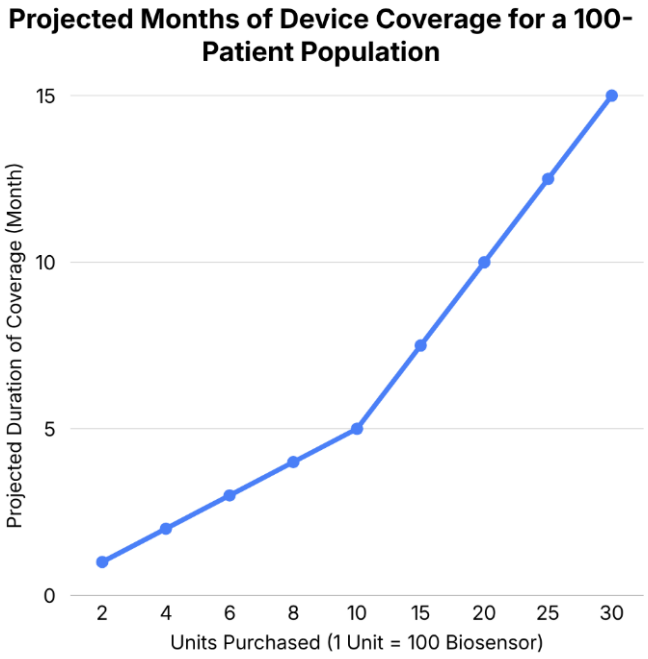


Fig 58. Projected Months of Device Coverage for a 100-Patient Population. Relationship between the number of commercial units purchased (100 biosensors per unit) and the projected duration of continuous monitoring coverage for a healthcare system serving approximately 100 patients.

To facilitate institutional purchasing, biosensors will be distributed in standardized commercial units, with each unit containing 100 biosensors. Assuming continuous monitoring for a healthcare system managing approximately 100 patients, the quantity of units

purchased directly determines the projected duration of monitoring coverage.

For example, purchasing 2 commercial units provides approximately 1 month of continuous monitoring, whereas 10 units provide approximately 5 months of coverage. Larger institutional purchases proportionally extend monitoring duration, with 30 units supporting approximately 15 months of continuous use. This purchasing structure allows hospitals and healthcare systems to align procurement decisions with anticipated patient volume, monitoring duration, and budgetary planning. To further encourage larger institutional purchases, volume discounts are introduced beginning at 15 units, with progressively larger discounts applied at higher purchasing thresholds.

The relationship shown in Fig 58 demonstrates a nearly linear increase between commercial units purchased and projected monitoring duration. This predictable scaling enables healthcare institutions to estimate inventory requirements and financial commitments while supporting flexible procurement strategies for healthcare systems of varying sizes.

To evaluate the long-term financial sustainability of commercialization, a 36-month cash flow projection was developed following market entry. The financial model incorporated an initial investment of $1.5 million, projected manufacturing costs (COGS), monthly operating expenses, anticipated hospital adoption rates, and recurring product revenue.

During the first six months, the company operates without commercial sales while regulatory preparation, manufacturing scale-up, and customer acquisition activities are completed. Consequently, monthly operating expenses exceed incoming revenue, resulting in an expected negative monthly cash flow during the pre-commercialization period. Commercial sales begin in Month 7, generating recurring institutional revenue as hospitals adopt the platform.

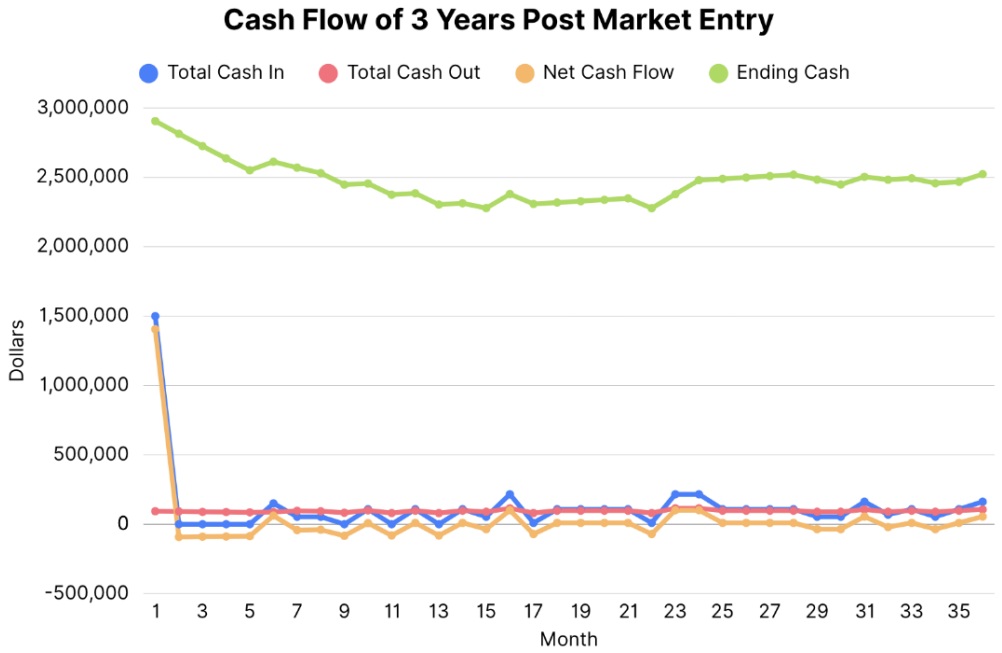


Fig. 59. Three-Year Cash Flow Projection Following Commercialization. Monthly projected total cash inflow, total cash outflow, net cash flow, and ending cash balance over a 36-month commercialization period based on projected hospital adoption, manufacturing costs, and operating expenses.

Following commercialization, increasing hospital adoption progressively offsets manufacturing and operating expenses. Although several months exhibit temporary negative net cash flow because of fluctuations in customer acquisition, these short-term deficits do not compromise overall financial stability. Throughout the projection period, the company maintains a positive ending cash balance supported by the initial investment and steadily increasing institutional revenue.

By the end of the 36-month projection, the model estimates 51 active hospital customers and an ending cash balance of approximately $2.52 million, representing an increase of approximately 21.5% relative to the initial investment. These findings suggest that the proposed commercialization strategy remains financially sustainable throughout early market entry while maintaining sufficient liquidity to support continued expansion.

Collectively, the financial analyses indicate that the proposed commercialization strategy is economically viable under the stated assumptions. The cost-profit-volume analysis demonstrates achievable break-even thresholds and increasing profitability with manufacturing scale. The commercial packaging strategy provides a flexible purchasing model that accommodates healthcare systems with varying patient populations and monitoring durations. Finally, the 36-month cash flow projection indicates that, despite expected short-term operating losses during early commercialization, sustained

institutional adoption supports positive long-term liquidity and continued business growth.

8.14 European Market Expansion

Initial commercialization is planned for the United States, followed by strategic expansion into the European Union to increase market penetration and capture a larger proportion of the total addressable market (TAM). The In Vitro Diagnostic Regulation (IVDR) establishes the regulatory framework governing the development, manufacture, and commercialization of in vitro diagnostic medical devices within the European Union (European Parliament and the Council of the European Union, 2017). Because the proposed biosensor analyzes interstitial fluid (ISF) to quantify levodopa concentrations, it falls within the scope of Regulation (EU) 2017/746. Accordingly, commercialization within the European Union requires classification of the device under the IVDR and completion of the appropriate conformity assessment pathway prior to market entry (European Commission, 2026).

Phase 1: Device Classification According to Article 47 of Regulation (EU) 2017/46, all in vitro diagnostic medical devices must be classified in accordance with Annex VIII, which defines a risk-based classification system (Classes A through D). Our wearable, continuous levodopa sensor would be considered a Class C device, specifically under Rule 3(j): “Devices intended for monitoring levels of substances or biological components, where erroneous results could lead to a patient management decision with significant risk to the patient” (European Parliament and the Council of the European Union, 2017). This aligns with the classification for a CGM meant for diagnostic use. Classification under the IVDR determines the level of regulatory oversight required throughout the conformity assessment process, with Class C devices requiring extensive review by a designated Notified Body prior to commercialization (European Commission, 2026). Parallel to classification, initial compliance activities include establishing key economic operators in accordance with Articles 10-14. These economic operators, including the manufacturer, authorized representative, importer, and distributor, are collectively responsible for maintaining regulatory compliance and ensuring device traceability throughout the European supply chain (European Commission, 2026). The device will ultimately be intended for near-patient testing (NPT), as clinicians will implement and calibrate the sensor to track levodopa levels in Parkinson’s patients, ensuring optimal therapeutic dosing.

Phase 2: Conformity Assessment The conformity assessment verifies whether the device meets the specific standards or requirements established by the EU, and this process commonly consists of groups reviewing the device documentation, safety standards, labeling, and risk management procedures. Successful completion of the conformity assessment is required before a CE marking may be affixed, demonstrating that the device satisfies all applicable European regulatory requirements for commercialization (European Commission, 2026). For Class C devices, the involvement of a Notified Body, organizations appointed by the EU to assess whether a device complies with IVDR regulations, is required. The Notified Body will evaluate whether additional clinical data, corrective actions, or approvals are required for further approval.

Given that the device falls under Class C, the traditional conformity assessment route includes an analysis of the Quality Management System (QMS) as well as a Technical Documentation Assessment. The QMS is meant to ensure compliance with regulatory, safety and performance requirements throughout the lifecycle of the IVD device. In accordance with Annex IX, this system oversees design, manufacturing, clinical performance evaluation, vigilance, corrective and preventive actions, and post-market surveillance. Throughout the Technical Documentation Assessment, the designated Notified Body reviews the complete device documentation to verify that the IVD device meets the appropriate safety and regulatory requirements. In accordance with Annex II, the assessment should not be conducted via sampling due to the NPT nature of the device; rather, evaluation should only involve a thorough investigation of the technical documentationConsistent with the post-market surveillance requirements outlined in Annex III, a Periodic Safety Update Report (PSUR) will be prepared and updated annually following the device's first year on the market. The required Summary of Safety and Performance document will also be drafted and reviewed by the designated Notified Body.

Phase 3: Obtaining a UDI and registering the Medical Device in the European Database on Medical Devices To ensure traceability of the device, a Unique Device Identification (UDI) comprised of a sequence of alphanumerical characters serves as the primary access key for regulatory databases. This code is also included on the packaging of the device to ensure authenticity and supply chain visibility. In accordance with Articles 24 and 27 of Regulation (EU) 2017/746, the manufacturer assigns the UDI and uploads the required device data to the European Database on Medical Devices (EUDAMED), making important safety and performance information accessible to the public. EUDAMED promotes regulatory transparency by centralizing information related to device

registration, clinical investigations, market surveillance, and vigilance activities (European Commission, 2026).

Phase 4: Notified Body Final Review & EU Declaration of Conformity The designated Notified Body will review the QMS and comprehensive technical documentation. Following successful review, an EU Declaration of Conformity will be prepared, certifying that the device complies with all applicable European regulations and formally accepting legal responsibility for its safety and performance. Upon completing these requirements, the device will be legally authorized for placement on the EU market. An EU Authorized Representative will be designated to satisfy the regulatory requirements applicable to manufacturers established outside the European Union. As the IVDR represents a rigorous framework that fully replaced the In Vitro Diagnostic Directive (IVDD) in May 2022, the team remains committed to monitoring regulatory developments to ensure continued compliance.